CHARACTERIZATION OF GAS DISPERSION IN INDUSTRIAL FLOTATION MACHINES

Jason S. Doucet

Department of Mining, Metals and Materials Engineering

McGill University

Montreal, Canada

A thesis submitted to McGill University

in partial fulfillment of the requirements of the degree of

Master of Engineering

Your file Votre référence
ISBN: 978-0-494-28592-3
Our file Notre référence
ISBN: 978-0-494-28592-3

Abstract

The flotation process is designed to collect hydrophobic particles by attachment on to bubbles dispersed in slurry. The effectiveness of the flotation process depends on the properties of the bubble dispersion. For example, the ability of a machine to form small bubbles at a given flow rate of air will control the quantity of surface area available for bubble-particle collision.

The gas dispersion, defined for the purposes of this thesis as bubbles suspended in slurry, is quantified by a group of "so-called" gas dispersion parameters including: superficial gas velocity (gas rate, J_g), gas holdup (ε_g), bubble size (D_b) and bubble surface area flux (S_b).

Cell characterization is a commonly used term in the study of gas dispersion parameters referring to any test designed specifically to increase understanding of the gas dispersion inside a particular machine, including how the dispersion can be manipulated by adjusting the operating variables and how the dispersion parameters vary with location inside a machine.

Industrial tests were done to study mechanisms of manipulating the gas dispersion in forced air and self-aerated mechanical flotation machines, demonstrating that gas rate can be used to manipulate the gas dispersion in forced air machines, while froth depth, impeller speed and impeller submergence can be used to manipulate the dispersion in self-aerated machines.

Facilitated by the development of the multi-Jg sensor, a technique based on gas rate

mapping was developed for down-the-bank sample point selection. Experience using the sensor is described. Based on industrial tests, recommendations regarding sample point selection for down-the-bank optimization are offered.

The development of an axial pressure profile sensor is described, facilitating axial investigation of variation in gas dispersion parameters. The proposed technique can be used to evaluate machine operating conditions and to resolve previously unexplained results.

Résumé

Le procédé de flottation est conceptualisé pour recueillir des particules hydrophobes par l'attachement, au moyen de gaz dispersée dans la pulpe. L'efficacité du processus de flottation dépend sur les propriétés de la dispersion de la bulle. Par exemple, la capacité d'une machine de former des petites bulles à un débit réglé d'air contrôlera la quantité de surface disponible pour des collisions entre la bulle et la particule.

La dispersion de gaz est quantifiée par les paramètres de dispersion de gaz incluant: superficial gas velocity (gas rate, J_g), gas holdup (ε_g), taille de bulle (D_b) et bubble surface area flux (S_b).

La caractérisation de cellule est une phrase ordinairement utilisée dans l'étude des paramètres de dispersion de gaz. Cette phrase se réfère à n'importe quel test conçu avec but d'augmenter la compréhension de la dispersion de gaz dans une machine particulière. Ceci compris l'hypothèse que la dispersion peut être manipulée par les variables opérationnelles de la machine, et que la dispersion change selon l'emplacement dans une

machine.

Des tests industriels pour étudier des mécanismes pour manipuler la dispersion de gaz dans des machines d'air forcé et des machines naturellement aspirées ont démontré que "gas rate" pourrait être utilisé pour manipuler la dispersion de gaz dans les machines d'air forcées. Cependant, la profondeur de mousse, la vitesse de l'agitateur et la plongé de l'agitateur peut être utilisée pour manipuler la dispersion dans une machine d'air aspiré naturellement.

Facilité par le développement d'une sonde "multi-Jg", une technique fournit la cartographie de "gas rate" pour la sélection de point d'échantillon dans une bande de cuves de flottation. Basé sur les tests industriels, des recommandations de sélection d'un point d'échantillon pour l'optimisation de banc sont offertes.

Le développement d'une sonde de profil de pression dans la direction de l'axe permet l'investigation des variations des paramètres de dispersion de gaz avec la profondeur. La technique proposée peut être utilisée pour évaluer les conditions d'opération de machine et pour résoudre des résultats inexpliqués.

Contribution of the Authors

This thesis was prepared in accordance with article C of the Guidelines Concerning Thesis Preparation of McGill University. This article reads as follows:

1. Candidates have the option of including, as part of the thesis, the text of one or more papers submitted, or to be submitted, for publication, or the clearly-duplicated text (not the reprints) of one or more published papers. These texts must conform to the "Guidelines for Thesis Preparation" with respect to font size, line spacing and margin sizes and must be bound together as an integral part of the thesis. (Reprints of published papers can be included in the appendices at the end of the thesis.)

2. The thesis must be more than a collection of manuscripts. All components must be integrated into a cohesive unit with a logical progression from one chapter to the next. In order to ensure that the thesis has continuity, connecting texts that provide logical bridges proceeding and following each manuscript are mandatory.

3. The thesis must conform to all other requirements of the "Guidelines for Thesis Preparation" in addition to the manuscripts. The thesis must include the following: a table of contents; a brief abstract in both English and French; an introduction which clearly states the rational and objectives of the research; a comprehensive review of the literature (in addition to that covered in the introduction to each paper); a final conclusion and summary; a thorough bibliography; Appendix containing an ethics certificate in the case of research involving human or animal subjects, microorganisms, living cells, other biohazards and/or radioactive material.

4. As manuscripts for publication are frequently very concise documents, where appropriate, additional material must be provided (e.g., in appendices) in sufficient detail to allow a clear and precise judgement to be made of the importance and originality of the research reported in the thesis.

5. In general, when co-authored papers are included in a thesis the candidate must have

made a substantial contribution to all papers included in the thesis. In addition, the candidate is required to make an explicit statement in the thesis as to who contributed to such work and to what extent. This statement should appear in a single section entitled "Contributions of Authors" as a preface to the thesis. The supervisor must attest to the accuracy of this statement at the doctoral oral defence. Since the task of the examiners is made more difficult in these cases, it is in the candidate's interest to clearly specify the responsibilities of all the authors of the co-authored papers.

The following are the co-authored manuscripts used in preparation of this thesis. Manuscript 1, 2 and 3 correspond to Chapters 3, 4 and 5.

All the manuscripts are co-authored by Prof. James A. Finch in his capacity as research supervisor. All the manuscripts are co-authored by Dr. Cesar O. Gomez in his capacity as senior research associate. All the experiments were conducted by the candidate. The candidate is the primary author of all manuscripts. Manuscript 1 includes contribution from Mr. Davin Knuutila who helped during the data acquisition process and provided valuable input regarding interpretation of the data. Manuscript 2 includes contribution from Mr. Willy Kracht who measured and processed the bubble size data that is incorporated into the manuscript. Manuscript 3 includes contribution from Mr. Claudio Acuña and Mr. Jarrett Quinn. These students provided critical input towards the development of a model to predict axial pressure profiles using the drift flux equations, Microsoft Excel and Microsoft Visual Basic.

Acknowledgements

Thanks to Lindsay and family for support of my studies.

Thanks to all those who make up the Mineral Processing Group at McGill University. I was fortunate to be a part of such a strong, intelligent and talented group of individuals. Particular thanks to my friends, Jarrett Quinn, Mustafa Tarkan, Vera Gella for their encouragement and laughter and to Davin Knutilla, Helin Girgin, Willy Kracht for their support of my experiments.

Funding for this work is from two grants under the Collaborative Research and Development program of the Natural Sciences and Engineering Research Council of Canada, one sponsored by Inco, Falconbridge, Teck-Cominco, Corem and SGS Lakefield Research, and the second sponsored by the North American partners in the AMIRA P9 project.

Particular thanks to plant personnel who allowed me to use their facilities for experiments or photographs presented within this thesis. These are, in order of appearance: Laronde (Agnico-Eagle), Brunswick Mine (Falconbridge), Leinster (BHP Billiton), Los Colorados and Laguna Seca (Escondida – BHP Billiton), El-Salvador (Codelco), Waterval (Anglo-Platinum), Troilus (Inmet), Mount Keith (BHP Billiton), Kennecott (Rio Tinto).

During my work, I was exposed to three individuals of incredible knowledge and experience who were always willing to lend their advice. These unofficial supervisors of my project were Dr. Cesar Gomez, who is recognized around the world as the leading expert in industrial gas dispersion measurement, Mr. Jan Nesset, who with many years of

engineering and management experience has given me a lifetime of valuable lessons and Mr. Claudio Acuña, who's endless dedication to teaching and problem solving has enriched the research of every mineral processing graduate student.

Finally, most sincere thanks go to my supervisor, Professor J.A. Finch. His calm, focussed management style is the reason so many chose to study under him. His greatest asset however, is his unique teaching ability. Michael Faraday wrote that a teacher "should give the audience full reason to believe that all his powers have been exerted for their pleasure and instruction". In spite of his busy schedule, through 4 years as an undergraduate, and 2 years as a master's student, Prof. Finch was always ready to dedicate his effort towards my learning. For this, I consider myself fortunate, and am grateful.

Table of Contents

List of Figures

Chapter 1 - Introduction

1.1 Background

Metals, used throughout the world for countless applications, all originate from minerals in the earth's crust. But even mineral reserves considered "rich" have low valuable metal content (1-2 %). The task of upgrading and transforming these resources into useful products falls to minerals, metals and materials engineers.

The first stage in the upgrading process, mineral processing, involves the separation of target minerals ('pay minerals') from the bulk by exploiting specific mineral properties. Flotation is a widely used separation technique that takes advantage of differences in particle surface properties. In this process, air is dispersed as bubbles into a tank (cell or machine) containing slurry (a mixture of particles and water). Hydrophobic particles in the slurry selectively attach to the bubbles and rise to the surface where they are recovered, while hydrophilic particles remain in the slurry and exit through the bottom of the flotation machine.

1.2 Role of Gas Dispersion in Flotation

A key aspect controlling the kinetics of flotation is the efficiency of collision between gas (air) bubbles and particles in the flotation slurry (Finch and Dobby, 1990). The efficiency of collision is largely dependant on the properties of bubbles in the flotation machine (Jameson et al., 1977).

Given the importance of the gas phase, measurement tools have been developed to quantify gas dispersion in industrial machines. Starting with Jameson and Allum (1984),

the tools have been evolving simultaneously among several research groups (Yianatos et al., 2001; Gomez and Finch, 2002; Grau and Heiskanen, 2003; Schwarz and Alexander, 2005). The sensors employed by each group are designed to measure so-called gas dispersion parameters, which characterize the behaviour of bubbles inside a flotation machine. The various sensors are described and reviewed in some detail in Chapter 2. The objective of this thesis is to continue the development of these sensors, and to extend their use in cell characterization.

1.2.1 Definition of Gas Dispersion Parameters

The term "gas dispersion" or "air dispersion" has been used commonly in recent literature, but is rarely given an explicit definition. In some cases, "gas dispersion" is used to describe the ability of a machine to disburse gas bubbles throughout the flotation slurry (Gorain et al., 1996; Deglon et al., 2000). In other cases "gas dispersion" is used to describe the act of separating a continuous stream of air into bubbles in slurry (Gomez and Finch, 2002). The noun "gas dispersion" has been used to refer to the suspension of fine bubbles in slurry (Harris et al., 2005). In the majority of cases however, "gas dispersion" is not defined but linked to a set of measurable parameters (gas dispersion parameters), each having a precise definition (Grau and Heiskanen, 2003; Kracht et al., 2005; Nesset et al., 2005). The commonly referenced set of gas dispersion parameters introduced by Xu et al. (1991) include superficial gas rate (gas rate, J_g), gas holdup (ε_g), bubble diameter (D_b) and superficial bubble surface rate (bubble surface area flux, S_b).

The gas rate is the volumetric flow-rate of gas (Q_g) rising in the flotation machine divided by the cross section area (CSA) through which the gas is passing (Eq (1.1)).

$$J_g = \frac{Q_g}{CSA} \tag{1.1}$$

The gas rate is a commonly used parameter for flotation machine scale up (Harris, 1974) and has recently been identified as a key parameter in flotation bank optimization (Cooper et al., 2004; Gorain, 2005).

Gas holdup is defined as the volume fraction of gas in the slurry and is usually expressed as a percentage (Eq. (1.2)). For a given gas rate, gas holdup is determined by bubble rise velocity. For typically sized bubbles in flotation (< 2 mm) in a given reagent (surfactant) scheme, rise velocity tends to be a function of size (smaller bubbles rising more slowly) (Clift et al., 1978). Therefore, ε_g can be used as an indirect measure of bubble size.

$$\varepsilon_g = \frac{V_g}{V_{g+s+l}} \tag{1.2}$$

The size of bubbles produced inside a flotation machine is not uniform. The reported single value of D_b is typically one of several average diameters. The most commonly quoted averages are the arithmetic mean diameter (D_{10}) and the Sauter mean diameter (D_{32}). The D_{10} is the summation of all the bubble diameters measured, divided by the number of bubbles. The D_{32} represents the size of bubble with the same ratio of volume to surface as the total distribution. The D_{32} is a particularly useful number for flotation as kinetic models often incorporate bubble surface area flux as a function of the input volumetric airflow.

The bubble surface area flux is a calculated parameter that quantifies the rate of bubble surface area generation. Bubble surface area flux is the flow rate of bubble surface area

per unit cross sectional area of cell through which the bubbles are passing. It has been observed that this parameter tends to govern the rate of recovery (Gorain et al., 1998; Hernandez et al., 2003; Hernandez-Aguilar et al., 2005). Surface area flux is calculated by Eq. (1.3),

$$S_b = \frac{6J_g}{D_{32}} \tag{1.3}$$

For the purposes of this thesis, gas dispersion is used as a noun referring to the suspension of air bubbles in slurry. The justification for the selection of this definition is that "the gas dispersion" is then quantified using the above set of parameters.

1.2.2 Definition of Cell Characterization

The ultimate goal of research into gas dispersion in flotation is to develop an understanding of the links between the gas dispersion and metallurgical performance (or even better, financial return) of a process. A necessary precursor to this "long-term" goal is to develop an understanding of how various machines generate a gas dispersion. Cell characterization is the term used by researchers in the AMIRA P9 project[1] to describe a group of tests that investigate the gas dispersion within a flotation machine (tests not concerned with metallurgical performance). The main goals of cell characterization are increased understanding of: a) relationships between operational variables and gas dispersion parameters, and b) variation in gas dispersion parameters with location in a machine. Characterization also includes the establishment of typical ranges in gas

---

[1] AMIRA P9 project is an international collaborative research group developing measurements and simulations for mineral processing operations.

dispersion parameters in industrial flotation machines (Schwarz and Alexander, 2005).

1.3 Flotation Machines

A wide variety of machine designs are available for flotation. The variables available for manipulation of gas dispersion parameters depend on the type of flotation machine. For the purpose of this thesis, it is convenient to group the machines into the following four categories: forced air / mechanically agitated, self-aerated / mechanically agitated, forced air / self-agitated, self-aerated / self-agitated. As implied by the names, the categories are formed by two key features of the flotation machines, the source of aeration and the mechanism of slurry and slurry/air mixing. The properties of these categories of machine are reviewed briefly. This thesis will focus on the mechanically agitated flotation machines.

1.3.1 Forced Air / Mechanically Agitated Machines

Forced air / mechanically agitated flotation machines are used in almost every Canadian flotation operation (Figure 1.1a). The term 'forced air' derives from air being delivered in a controllable manner from a compressor through a rotating impeller (Figure 1.1b) and 'mechanical' derives from the driven impeller used to suspend solids and disperse air into bubbles. The shear induced by the impeller forms small bubbles and spreads them throughout the machine, creating the gas dispersion. In these machines, gas rate can be manipulated through the plant control system (or manually using local valves in older plants). By varying gas rate, other properties of the gas dispersion are manipulated (Gorain et al., 1996). It should be noted that in addition to changing gas dispersion

parameters, changes in gas rate will have an impact on froth behaviour. In these machines, there is potential for manipulation of gas dispersion parameters via impeller speed, however, at an industrial scale, this is rarely done.

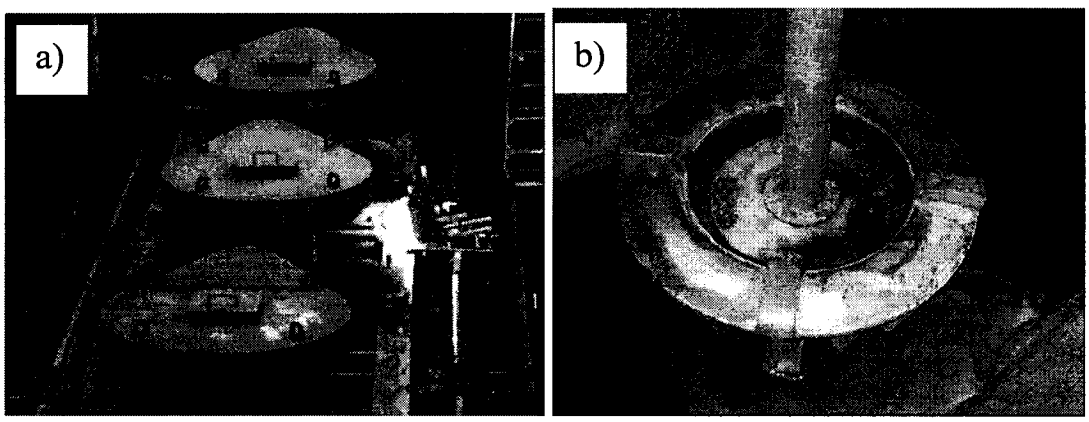

Figure 1.1 – picture of a) a top view of operating machines and b) a rotor/stator mechanism from Agnico Eagle's Laronde concentrator.

1.3.2 Self-Aerated / Mechanically Agitated Machines

Less commonly found in Canada, self-aerated / mechanically agitated flotation machines are widespread throughout world. The most popular example is the Wemco machine (Figure 1.2). In these, the rotation of the impeller aspirates air into the machine, eliminating the need for a compressor/blower. Air drawn in to the centre of the rotor forms a 'pocket' and the shear at the surface of the pocket forms small bubbles. Without an independent blower, manipulation of operating variables is difficult. Gas rate, and therefore the gas dispersion, in self-aerated machines depends on an interaction of several factors, e.g., froth depth, slurry density, impeller speed, impeller submergence (Weber et al., 2005). However, manipulation of these parameters impacts more than just the gas dispersion, e.g., froth behaviour and retention time are also influenced.

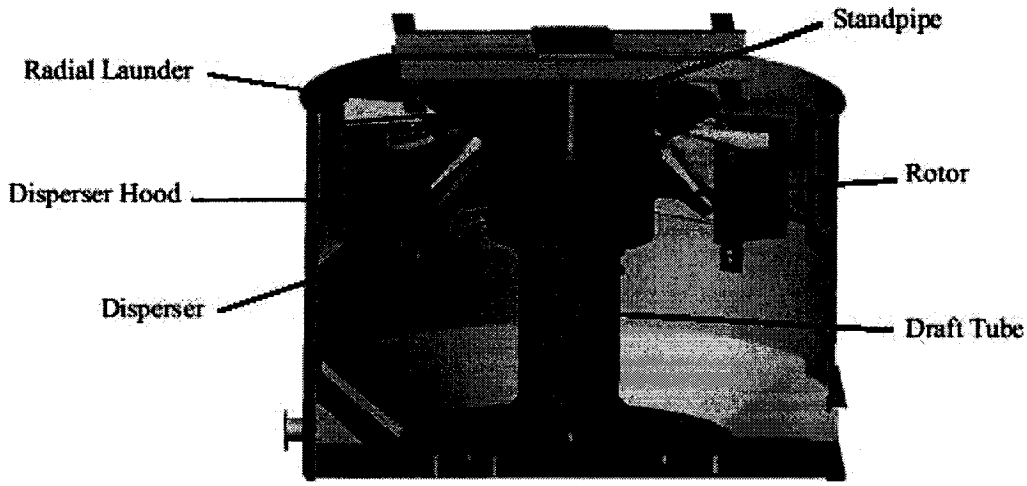

Figure 1.2 – Cut-away of a Wemco self-aerated flotation machine. (Weber et al., 2005)

1.3.3 Forced Air / Self Agitated Machines

Another group of flotation machines commonly used in Canada are designed for gas delivery from a compressor, while the agitation takes place through interaction of the air and liquid flows. This class of flotation machine includes flotation columns and contact cells. In these examples, bubbles are generated by a variety of mechanisms including MinnovEx Jetting Spargers (Figure 1.3) and Metso's Microcel.

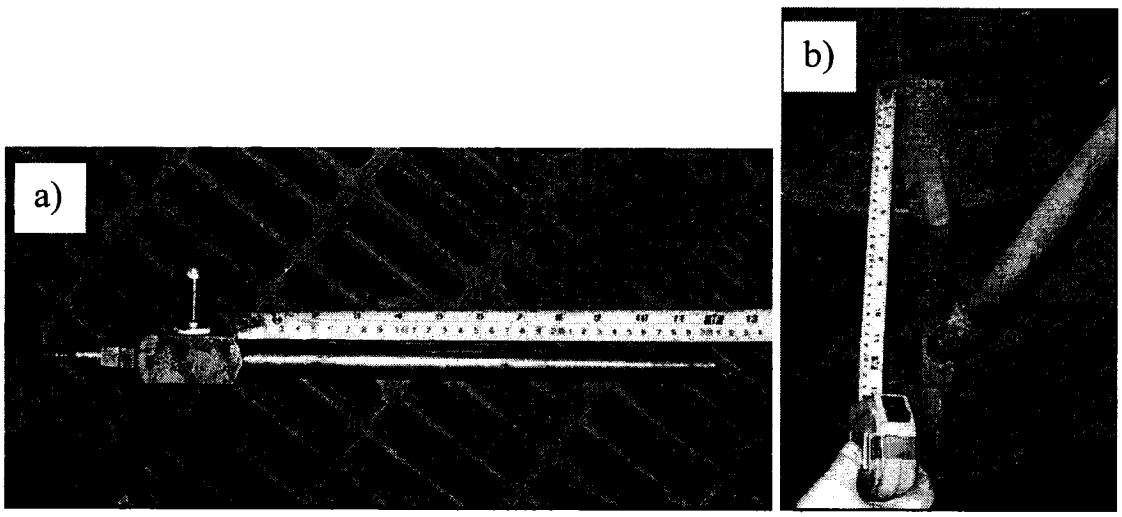

Figure 1.3 – A MinnovEx jetting sparger a) during cleaning and b) installed in a column.

Typically, bubbles enter the machine towards the bottom, while slurry is introduced in the upper portion. The slurry flows downward, counter current to the bubbles, inducing bubble-particle collisions. The gas dispersion can be manipulated by varying gas rate and, depending on the method of bubble generation, other variables can be used to manipulate the gas dispersion (e.g., gap size in the jetting sparger).

1.3.4 Self-Aerated / Self Agitated Machines

The final class of flotation machine requires neither air blower nor impeller. In these machines (e.g., Jameson Cells), air is entrained into a plunging slurry jet in a downcomer. The resulting high gas holdups in the downcomer facilitate bubble / particle collisions, eliminating the need for mechanical mixing. However, manipulation of gas dispersion parameters is difficult given the sensitivity to changes in operating variables (Summers, 1995).

1.4 Role of Frothers for Control of Gas Dispersion Parameters

In flotation plant practice, a class of chemical reagents known as frothers provide the most important control over bubble size, and hence surface area flux. The role of frother has yet to be completely understood (Laskowski et al., 2003). Evidence has shown that one of the actions is, for a given gas rate, to produce a finer, narrower bubble size distribution (Klassen and Mokrousov, 1963; Harris, 1976; O'Connor et al., 1990; Grau et al., 2005). Up to a certain concentration (critical coalescence concentration, CCC), frothers reduce bubble size. Above this concentration, the addition of frother has only a small impact on bubble size (Klassen and Mokrousov, 1963; Finch and Dobby, 1990; Cho and Laskowski, 2002; Grau et al., 2005; Azgomi, 2006).

It has been shown that salts can also be used to control the bubble size distribution and that in these cases, flotation can be effective without frother (Quinn et al., 2006).

1.5 Research Objectives

The research objectives of the masters project can be broken into two categories. The first is the development of tools to advance current techniques for measurement of gas dispersion parameters in industrial machines. This includes the development of a standard method for simultaneous measurement of gas rate at multiple locations and development of a pressure sensor for axial bulk density profiling. The second is to develop experimental protocols by which gas dispersion sensors can be used for cell characterization. In particular, these protocols should facilitate the selection of a sample point for down-the-bank gas dispersion parameter determination and should aid in the establishment of relationships between operational variables and gas dispersion parameters.

1.6 Structure of the Thesis

Chapter 1 – The concept and importance of the gas dispersion in flotation is introduced. The variables available for manipulation of gas dispersion parameters as a function of machine type are presented.

Chapter 2 – Instruments available for measurement of gas dispersion parameters are reviewed. Advantages and weaknesses of the selected tools are discussed. Objectives for sensor development are proposed.

Chapter 3 – In-plant control of gas dispersion parameters by manipulation of operating variables is discussed. This control is achieved in both forced air and self-aerated

machines, however in the latter, there are more interactions.

Chapter 4 –The motivation for, and development of a multi-Jg sensor is described. Industrial trials using the multi-Jg sensor are reported. The impact of the new procedures on subsequent optimization exercises is discussed with emphasis on sample point selection.

Chapter 5 – Development and application of an axial pressure profile sensor is described. Case studies are presented in which the sensor is used to evaluate axial variations in gas and solid holdup in large tank cells.

Chapter 6 – The conclusions reached in each of the chapters are summarized.

1.7 References

Azgomi, F., "Characterizing frothers by their bubble size control properties"; Masters Thesis, McGill University, Montreal, Quebec, Canada, 2006.

Cho, Y.S., Laskowski, J.S., "Effect of flotation frothers on bubble size and foam stability"; International Journal of Mineral Processing, 64, pp. 69 – 80, 2002.

Clift, R., Grace, J.R., Weber, M.E., Bubbles, Drops and Particles; Academic Press, 1978.

Cooper, M., Scott, D., Dahlke, R., Gomez, C.O., Finch, J.A., "Impact of air distribution profile on banks in a Zn cleaning circuit"; CIM Bulletin, 97, 1083, pp. 73 – 78, October, 2004.

Deglon, D.A., Egya-Mensah, D., Franzidis, J.P., "Review of hydrodynamics and gas dispersion in flotation cells on South African platinum concentrators"; Minerals Engineering, 13, 3, pp. 235 – 244, 2000.

Finch, J.A., Dobby, G.S., Column Flotation; Pergamon Press, 180 p., 1990.

Gomez, C.O., Finch, J.A., "Gas dispersion measurements in flotation machines"; CIM Bulletin, 95, N° 1066, pp. 73 – 78, November/December, 2002.

Gorain, B.K., Franzidis, J.P., Manlapig, E.V., "Studies on impeller type, impeller speed and air flow rate in an industrial scale flotation cell. Part 3: effect on superficial gas velocity"; Minerals Engineering, 9, 6, pp. 639 – 654, 1996.

Gorain, B.K., Napier-Munn, T.J., Franzidis, J.P., Manlapig, E.V., "Studies on impeller type, impeller speed and air flow rate in an industrial scale flotation cell. Part 5: validation of k-Sb relationship and effect of froth depth"; Minerals Engineering, 11, 7, pp. 615 – 262, 1998.

Gorain, B. K., "Optimization of flotation circuits with large flotation cells"; Centenary of Flotation Symposium, Ed. G.J. Jameson, AusIMM, Brisbane, Qld, June 6 – 9, pp. 843 – 851, 2005.

Grau, R.A., Heiskanen, K., "Gas dispersion measurements in a flotation cell"; Minerals Engineering, 16, pp. 1081 – 1089, 2003.

Grau, R.A., Laskowski, J.S., Heiskanen, K., "Effect of frothers on bubble size"; International Journal of Mineral Processing, 76, pp. 225 – 233, 2005.

Harris, C.C., "Impeller speed, air and power requirements in flotation machine scaleup"; International Journal of Mineral Processing, 1, pp. 51 – 64, 1974.

Harris, C.C., "Flotation machines"; in Flotation, A.M. Gaudin Memoprial Volume, Vol. 2, e.d. M.C. Fuerstenau, AIME, New York, pp. 753 – 815, 1976.

Harris, R., Ng, K.W., Wraith, A.E., "Spargers for controlled bubble size by means of the multiple slot disperser"; Chemical Engineering Science, 60, pp. 3111 – 3115, 2005.

Hernandez, H., Gomez, C.O., Finch, J.A., "Gas dispersion and de-inking in a flotation column"; Minerals Engineering, 16, 6, pp. 739 – 744, 2003.

Hernandez-Aguilar, J.R., Rao, S.R., Finch, J.A., "Testing the k-Sb relationship at the microscale"; Minerals Engineering, 18, pp. 591 – 598, 2005.

Jameson, G.J., Allum, P., "A survey of bubble sizes in industrial flotation cells"; Report to AMIRA Ltd., 1984.

Jameson, G.J., Nam, S., and Young, M, "Physical factors affecting recovery rates in flotation"; Mineral Science Engineering, 9, 3, 103 – 118, 1977.

Klassen, V.I., Mokrousov, V.A., An Introduction to the Theory of Flotation; Eng. Transl. By J. Leja and G.W. Poling, Butterworths, London, 1963.

Kracht, W., Vallebuona, G., Casali, A., "Rate constant modelling for batch flotation as a function of gas dispersion properties"; Minerals Engineering, 18, pp. 1067 – 1076, 2005.

Laskowski, J.S., Tlhone, T., Williams, P., Ding, K., "Fundamental properties of the polyoxypropylene alkyl ether flotation frothers"; International Journal of Mineral Processing, 72, pp. 289 – 299, 2003.

Nesset, J.E., Hernandez-Aguilar, J.R., Acuña, C.A., Gomez, C.O., Finch, J.A., "Some gas dispersion characteristics of mechanical flotation machines"; Centenary of Flotation Symposium, Ed. G.J. Jameson, AusIMM, Brisbane, Qld, pp. 243 – 249, 2005.

O'Connor, C.T., Randall, E.W., Goodall, C.M., "Measurement of the effects of physical and chemical variables on bubble size"; International Journal of Mineral Processing, 28, pp. 129 – 139, 1990.

Quinn, J.J., Gomez, C.O., Finch, J.A., "Exploring the effects of salts on gas dispersion in flotation systems"; proceedings of the JKMRC International Student Conference II, Brisbane, Qld, pp. 59 – 70, 2006.

Schwarz, S., Alexander, D., "Gas dispersion measurements in industrial flotation cells"; Centenary of Flotation Symposium, Ed. G.J. Jameson, AusIMM, Brisbane, Qld, June 6 – 9, pp. 265 - 269, 2005.

Summers, J.A., "A study of the operating variables of the Jameson Cell"; Master's Thesis, McGill University, Montreal, Quebec, Canada, 1995.

Weber, A., Meadows, D., Villanueva, F., Polamo, R., Prado, S., "Development of the world's largest flotation machine"; Centenary of Flotation Symposium, Ed. G.J. Jameson, AusIMM, Brisbane, Qld, pp. 285 - 291, 2005.

Xu, M., Finch, J.A., Uribe-Salas, A., "Maximum gas and bubble surface rates in flotation columns"; International Journal of Mineral Processing, 32, 233 – 250, 1991.

Yianatos, J.B., Bergh, L., Condori, P., Aguilera, J., "Hydrodynamic and metallurgical

characterization of industrial flotation banks for control purposes"; Minerals Engineering, 14, 9, pp. 1033 – 1046, 2001.

Chapter 2 - Review of Gas Dispersion Measurements

Many research groups have undertaken the measurement of gas dispersion parameters in flotation environments. The details vary because of differences in both instruments and methodology. This chapter reviews the instruments and methodologies of the various groups. Advantages and weaknesses of the various sensors are discussed. Objectives for sensor development are proposed.

2.1 Gas Dispersion Measurement Tools

2.1.1 Gas Rate (J_g) sensors

The first estimates of gas rate were made by dividing the input airflow rate (AFR) by the cross sectional area. Many modern flotation machines (e.g., tank cells) include a measure of AFR (Burgess, 1997), i.e., an average or global J_g. However, many cells remain with no AFR measurement. When available, the global measurement does not indicate how well the air is dispersed, for which a local J_g is required. The first J_g measurements reported were by Jameson and Allum (1984). These measurements were accomplished by submerging an inverted cylinder full of water into the pulp zone of a flotation machine. Bubbles enter the cylinder, thus lowering the water level. The rate of water level descent was then related to J_g.

A modification reported by Gorain et al. (1996) and in more detail by Savassi et al. (1999) builds on the Jameson and Allum (1984) device by incorporating a pneumatic pinch valve at the bottom of the cylindrical tube and a water inlet / air outlet combination at the top. The pneumatic valve is used to initiate bubble sampling; the water inlet is

used to set the starting water level in the sensor. The air outlet prevents pressure build-up as the sensor is filled with water. When full, the inlet and outlet at the top of the sensor are sealed and the pinch valve at the bottom of the sensor is opened. As bubbles from the pulp enter the probe, the water level is pushed down. The time for the water level to descend a known distance is recorded using a stopwatch and the average rate of descent is the estimate of J_g.

Falutsu (1994) proposed a method of measuring J_g in flotation machines, still using a submerged sampling probe, but employing a pumping system to extract gas and liquid from the flotation machine. By determining the rate at which air and liquid (or slurry) were pumped through the sampling probe, the gas rate could be calculated based upon a pump calibration equation. This measurement technique depends on cell and slurry characteristics, e.g., corrections are required depending on slurry percent solids.

Yianatos et al. (2001) proposed a method of continuous gas rate measurement in flotation machines using a probe attached to a peristaltic pump. A novel aspect of this device was the inclusion of a vacuum gage, measuring pressure inside the sampling probe. The pumping rate was controlled to maintain a constant pressure in the tube, ensuring that the rate of gas entering the probe was equal to the rate of gas being pumped from the probe. The gas flow pumped out of the probe was measured using a standard flow meter. A similar concept was proposed by Grau and Heiskanen (2003) incorporating a gas drying column, particle filter and mass flow meter to achieve online measurement of gas rate in laboratory flotation machines. Further developments made to this sensor were reported by Rudolphy et al. (2005) including a tube diameter expansion designed to prevent froth build up, proven effective in two-phase systems with large frother dosages, facilitating

long term continuous measurement.

An alternative continuous gas rate measurement was reported by Torrealba-Vargas et al. (2004), again using a submerged sampling probe, in this case with a calibrated orifice attached to the top. Under steady state conditions, air expels at the same rate that it enters the probe. The pressure required to discharge air at this rate is measured and J_g subsequently calculated from the prior orifice calibration.

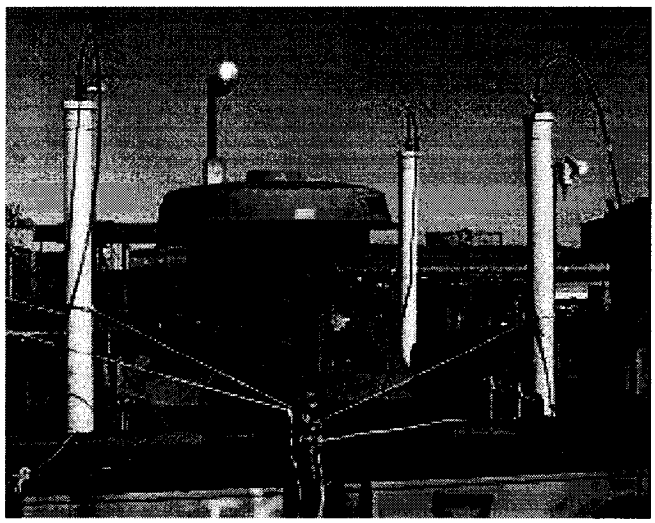

Figure 2.1 – Three gas rate sensors being used for cell mapping.

The gas rate sensor used for the experiments described in this thesis (Figure 2.1), described by Gomez et al. (2003a), builds on the original concept reported by Jameson and Allum (1984) whereby incoming bubbles displace slurry height inside a sampling probe. The novel aspect of this sensor is that rather than tracking slurry level, the pressure change as gas accumulates is monitored. This facilitates electronic data storage, processing and analysis. The major drawback is that it gives a discrete measurement. To obtain a single value of J_g, the probe (tube) must be given time to fill with air. Before a

second value of J_g can be measured, the air in the probe must be released and the filling process re-initiated. In general, it takes 1 to 2 minutes for each measurement of J_g. A second drawback is the requirement for a bulk density measurement. By incorporating a second tube, the pressure difference when both tubes are full of air can be related to bulk density. An advantage of the technique is that it has proven capable of measuring gas rate in practically any type of flotation machine.

The fundamentals of the relationship between rate of pressure increase and J_g were derived by Torrealba-Vargas (2004), yielding Eq. (2.1) where P_{atm} is atmospheric pressure, ρ_b is bulk density, g is the gravitational constant, H_l is the length of the sensor tube, H_p is the length of sensor above the froth and dP/dt is the rate of pressure increase. This particular equation produces a value of J_g corrected to the pressure at the bubble sampling location.

$$J_g = \frac{P_{atm} + \rho_b g H_l}{\left(P_{atm} + \rho_b g (H_l - H_p)\right)\rho_b g} \frac{dP}{dt} \tag{2.1}$$

It is noted that the term in the denominator ($P_{atm} + \rho_b g(H_l - H_p)$) is used to approximate the pressure at the bubble sampling location. Given that standard practice is to measure this pressure, this term in Eq. (2.1) can be replaced with the measured value P_l (Eq. (2.2)).

$$J_g = \frac{P_{atm} + \rho_b g H_l}{(P_l)\rho_b g} \frac{dP}{dt} \tag{2.2}$$

2.1.2 Gas Holdup (ε_g) sensors

The most common technique for gas holdup measurement in flotation machines is the

capture of a representative aerated slurry volume, as first reported by Jameson and Allum. Gorain et al. (1995) described a sensor to trap the representative volume using a piston – plunger combination. A similar device was described by Yianatos et al. (2001). The most recent version includes pinch valves at the top and bottom of the cylinder (Schwarz and Alexander, 2005). When activated, the pinch valves close, trapping the sample. The volume of slurry is subsequently measured, and by subtraction from the original volume, the gas holdup is calculated. It is assumed that aerated slurry completely fills the chamber.

An alternative approach to ε_g measurement in a laboratory cell was reported by Grau and Heiskanen (2003) where liquid and gas are collected by pumping from a sample location. The collected volumes of both liquid and gas are measured, from which gas holdup is calculated. This technique offers semi-continuous measurement (continuous signals can be obtained for a given period, after which the accumulated air must be discharged), but to date, there is no reference to its use in an industrial setting.

All gas holdup data reported in this thesis are based upon a standard technique of applying Maxwell's fundamental relationship (Maxwell, 1892) between volume fraction of a non-conducting dispersed species and dispersion conductivity (Fan, 1989). Several reviews of the various methods of applying this technique are available (Turner, 1976; Yianatos et al., 1985; Banisi et al., 1993). The appropriate form of the model is Eq. (2.3) where k_{lsg} is conductivity of aerated pulp and k_{ls} is conductivity of de-aerated pulp. Uribe-Salas et al. (1994) verified the model for both gas and solids holdup. Tavera (1996) developed the concept, creating conductivity flow cells that allow the conductivity

of a dispersion to be measured in industrial conditions.

$$\varepsilon_g = \frac{1 - \frac{k_{lsg}}{k_{ls}}}{1 + 0.5\frac{k_{lsg}}{k_{ls}}} \tag{2.3}$$

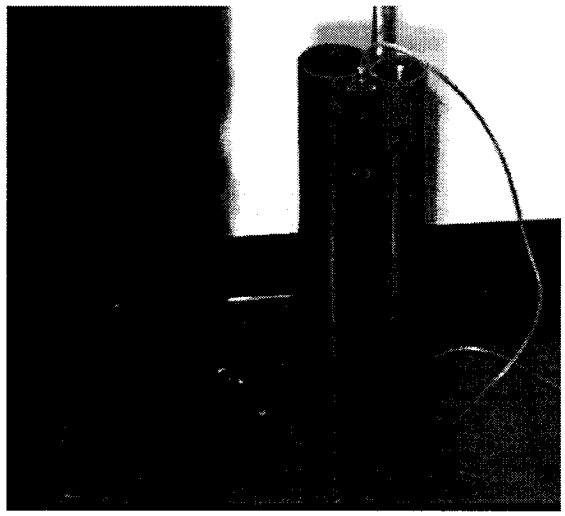

Figure 2.2 – The two conductivity flow cell gas holdup sensor.

Finally, a package 'sensor' comprising two conductivity flow cells (Figure 2.2) for measurement of aerated and de-aerated slurry conductivity was designed and tested (Cortes-Lopez, 1999; Gomez et al., 2003b). This fully continuous sensor allows on-line tracking of gas holdup in a wide variety of flotation environments.

A second conductivity-based technique has been reported by Sanwani et al. (2006). In this case, the sensor consists of a probe with two needles at one end. The conductivity between the two needles is continuously measured. When the tip of the needle is in air, a low conductivity is measured. When the needle tip is in slurry, a higher conductivity is measured. The gas holdup is calculated as the fraction of time during which the probe

measures a low conductivity. Measurements using this technique and the capture technique have correlated well. The deviations between the two techniques were attributed to the difference in sampling area of the two sensors (the sampling space for the 'needle' sensor is 50 mm compared to 500 mm for the capture technique). No reports of industrial tests using this sensor have been found.

Gas holdup measurement in bubble column reactors are reported based on other methods. An acoustic technique was described (Pandit, et al., 1992; Al-Masry et al., 2006) by which gas holdup can be estimated based on an average bubble size determined from pressure waves emitted by impulses associated with bubble oscillations. Techniques have also been used, based on attenuation and transmission time of an incident ultrasonic wave moving through the dispersion (Zheng and Zhang, 2004). These techniques have not been applied in industrial settings.

2.1.3 Bubble Size (D_b) Measurement

As with ε_g and J_g, several techniques have been developed to measure average bubble sizes, or bubble size distributions in flotation systems. As with the other parameters, Jameson and Allum (1984) were first to report bubble size measurements in industrial cells. In that work, bubbles were collected into a sampling tube. The bubbles rose within the sampling tube to a position above the froth into a so-called "viewing chamber" where a camera captured images. Imaged bubbles were compared to a reference object of known size to determine the bubble size distribution. Most of the bubble size measurement techniques employed in flotation systems today are based on this original idea.

An alternative bubble sizing method, the "UCT bubble size analyzer", was described by O'Connor et al. (1989) and with slight modification by Tucker et al. (1994). In this technique, bubbles are collected into a sampling tube. Contained inside the sampling tube is a capillary tube (with a precisely known diameter), which collects some of the sampled bubbles. In the capillary tube bubbles are transformed into cylinders. Detectors monitor changes in light intensity to measure the length of passing bubbles, which can be converted to the equivalent spherical bubble diameter. This technique has been used in industrial settings (Deglon et al., 2000; Yianatos et al., 2001) and has been compared with the imaging technique (Hernandez-Aguilar et al., 2004; Grau and Heiskanen, 2002).

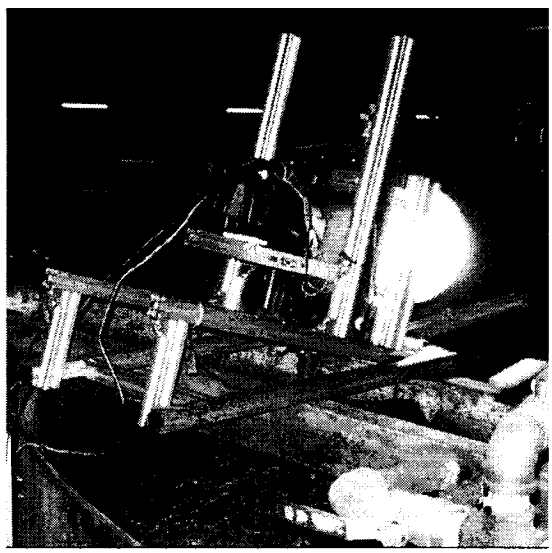

Figure 2.3 – Bubble viewer with inclined viewing chamber.

In recent years, the imaging techniques have become popular (Yianatos et al., 2001; Chen et al., 2001; Grau and Heiskanen, 2002; Hernandez-Aguilar et al., 2002). Yianatos et al. and Chen et al. used an adaptation of the Jameson and Allum (1984) bubble viewer for measurements in an industrial plant. Grau and Heiskanen reported laboratory bubble size measurement using a similar device. Hernandez-Aguilar et al. described a modification,

namely an inclined viewing window (Figure 2.3). The inclined window forces bubbles to spread into a single viewing plane, ensuring that all bubbles photographed are in focus, facilitating automation of the image analysis procedure. All bubble size measurements reported in literature from the McGill mineral processing group since 2002 (including this thesis) are based on the inclined window technique.

2.2 Cell Characterization Techniques

2.2.1 Spatial Variations

In one of the first exercises in individual cell mapping, Gorain et al. (1996) tested the impact of cell design variables on gas dispersion parameters at six locations. Repeatedly, these tests showed significant differences between locations, under the same design and operating conditions. An attempt was made to quantify spatial variation using a dispersion index (DI, Eq. (2.1)) based on gas rate measured at the six locations (where $J_{gcalculated}$ is Q_g/CSA (Eq. 1.1)). The range found was large (0 to 100 %).

$$DI = 100 - 100\left(\frac{J_{g\,measured} - J_{g\,calculated}}{J_{g\,calculated}}\right) \qquad \textbf{(2.1)}$$

Deglon et al. (2000) also reported measurements at six sampling locations, and suggested that air was not distributed evenly throughout machines, particularly at high airflow rates. Cell mapping reported by Yianatos et al. (2001), again citing six sampling locations for each measurement, concluding that the gas dispersion parameters were homogenous across the cross sectional area; however, it is noted that selection of sampling location can have significant impact on the degree of variation between measurements.

In parallel, spatial variations in gas dispersion parameters have been studied under laboratory conditions (Rudolphy et al., 2005; Sanwani et al, 2006), suggesting the presence of spatial variations.

Another example of cell mapping (Dahlke et al., 2001) was carried out at Brunswick Mine, in New Brunswick, Canada (Figure 2.4). It was observed that symmetrically similar points tended to behave in a similar manner. For example, the highest gas rate was recorded at location 1 in Figure 2.4, both left and right of the impeller. Similarly position 2 was second highest, position 5 third highest and, position 3 and 4 recorded the lowest measurements of J_g. It was noted that this trend did not hold for gas holdup measurement, though in both cases the highest ε_g was at position 1.

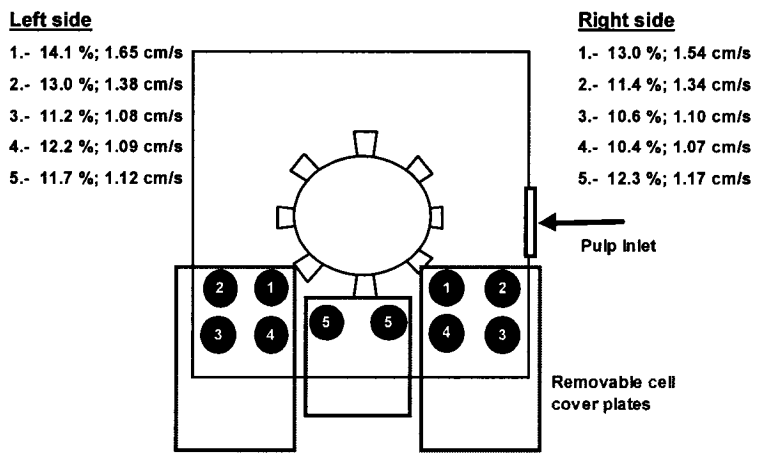

Figure 2.4 - Cell mapping sample point locations, gas holdup (left) and gas velocity (right).

The finding that gas rate tends to be a function of distance from the impeller is expected in a forced air / mechanically agitated flotation machine. However, this test, as with the others cited above, did not measure gas rate at each location simultaneously. So, temporal variation in air delivery rate could report as spatial variations. For example, the

observation that gas rates measured at the left side are not equal to those measured on the right side could simply be an indication of a change in AFR as the sensor was moved and not that air is distributed differently right to left.

2.2.2 Variation of Operating Parameters

A significant body of literature has been devoted to development of relationships between operational variables and gas dispersion parameters. O'Connor et al. (1989) studied the impact of frother on bubble size. A significant decrease in D_b was observed with increasing frother concentrations. Multiple authors have reported similar findings over the years (Klassen and Mokrousov, 1963; Finch and Dobby, 1990; Cho and Laskowski, 2002; Grau et al., 2005; Nesset et al., 2005).

Gorain et al. (1995, 1996, 1997) investigated the impact of the variables impeller type, impeller speed and airflow rate on the gas dispersion parameters in forced air / mechanically agitated machines, finding increased bubble size with decreased impeller speed or increased gas rate. In addition, both gas holdup and bubble surface area flux increased with increasing gas rate and increasing impeller speed. Nesset et al. (2005) performed similar studies in a large variety of industrial flotation machines, confirming an increase in ε_g, D_{10}, D_{32} and S_b with increasing gas rate. Nesset et al. examined the J_g / ε_g relationship at multiple locations in a single machine, demonstrating that spatial variations in the gas dispersion not only exist, but change as a function of operating condition.

Gomez and Finch (2002) presented a comparison between two industrial flotation machines, examining the impact of gas rate on average bubble size (D_{10} and D_{32}) in both.

Both machines demonstrated similar results, confirming the observation of increasing bubble size with increasing gas rate.

Regarding the impact of operating variables on gas dispersion parameters, most test work has been on forced air / mechanically agitated machines. Girgin et al. (2006) examined the relationships in a self-aspirated / mechanically agitated laboratory machine. Gas dispersion parameters were varied by manipulation of frother concentration and impeller speed. It was found that in the self-aerated machine, increases in impeller speed caused increases in J_g and consequently, increases in D_b. It was also found that increases in frother concentrations caused decreases in J_g. The practical implications of these observations is that increased frother concentration and impeller speed (typical actions to increase S_b) may not yield the expected increase in S_b.

2.3 Targeted Improvements

In every case described above, where spatial variations were investigated, the measurements were obtained by moving a single sensor from one point to another. This can take several hours to accomplish. Additionally, there is no guarantee that machine operating conditions were constant throughout the exercise and that the results truly reflect spatial variations. Therefore, there is an incentive to develop mapping procedures where variations with time can be accommodated. Equally, such measurements would indicate operational stability, increasing confidence in the measured spatial variations. In addition to improved mapping procedures, the need for sensor technology capable of simultaneously monitoring multiple locations is clear. A solution to this need is described in the subsequent chapters.

2.4 References

Al-Masry, A.W., Ali, E.M., Aqeel, Y.M., "Effect of antifoam agents on bubble characteristics in bubble columns based on acoustic sound measurements"; Chemical Engineering Science, 61, pp. 3610 – 3622, 2006.

Banisi, S., Finch, J.A., Laplante, A.R., "Electrical conductivity of dispersion: a review"; Minerals Engineering, 6, 4, pp. 369 – 385, 1993.

Burgess, F.L., "OK tank cell operation at Pasminco – Broken Hill"; Minerals Engineering, 10, 7, pp. 723 – 741, 1997.

Chen, F., Gomez, C.O., Finch, J.A., "Technical note: bubble size measurement in flotation machines"; Minerals Engineering, 14, pp. 427 – 432, 2001.

Cho, Y.S., Laskowski, J.S., "Effect of flotation frothers on bubble size and foam stability"; International Journal of Mineral Processing, 64, pp. 69 – 80, 2002.

Cortes-Lopez, F., "Design of a gas holdup sensor for flotation diagnosis"; Masters Thesis, McGill University, Montreal, Quebec, Canada, 1999.

Dahlke, R., Scott, D., Leroux, D., Gomez, C.O., Finch, J.A., "Troubleshooting flotation cell operation using gas velocity measurements"; Proceedings of the 33rd annual Canadian Mineral Processors Conference, Ottawa, Canada, pp. 359 – 370, 2001.

Deglon, D.A., Egya-Mensah, D., Franzidis, J.P., "Review of hydrodynamics and gas dispersion in flotation cells on South African platinum concentrators", Minerals Engineering, 13, 3, pp. 235 – 244, 2000.

Falutsu, M., "Direct measurement of gas rate in a flotation machine"; Minerals Engineering, 7, 12, pp. 1487 – 1494, 1994.

Fan, L.S., Gas-Liquid-Solid Fluidization Engineering; Chapter 2, Butterworths, Boston, 1989.

Finch, J.A., Dobby, G.S., Column Flotation; Pergamon Press, 180 p., 1990.

Girgin, E.H., Do, S., Gomez, C.O., Finch, J.A., "Bubble size as a function of impeller speed in a self-aeration laboratory flotation cell"; Minerals Engineering, 19, 201 – 203, 2006.

Gomez, C.O., Finch, J.A., "Gas dispersion measurements in flotation machines"; CIM Bulletin, Vol 95, N° 1066, pp. 73 – 38, November/December, 2002.

Gomez, C.O., Torrealba-Vargus, J.A., Dahlke, R., Finch, J.A., "Measurement of gas velocity in industrial flotation cells"; International Mineral Processing Congress, Cape Town, South Africa,Vol. 3, pp. 1703 – 1713, 2003a.

Gomez, C.O., Cortés-Lopez, F., Finch, J.A., "Industrial testing of a gas holdup sensor for flotation systems"; Minerals Engineering, 16, pp. 493 – 501, 2003b.

Gorain, B.K., Franzidis, J.P., Manlapig, E.V., "Studies on impeller type, impeller speed and air flow rate in an industrial scale flotation cell. Part 2: effect on gas holdup"; Minerals Engineering, 8, 12, pp 1557-1570, 1995.

Gorain, B.K., Franzidis, J.P., Manlapig, E.V., "Studies on impeller type, impeller speed and air flow rate in an industrial scale flotation cell. Part 3: effect on superficial gas

velocity"; Minerals Engineering, 9, 6, pp. 639 – 654, 1996.

Gorain, B.K., Franzidis, J.P., Manlapig, E.V., "Studies on impeller type, impeller speed and air flow rate in an industrial scale flotation cell. Part 4: effect of bubble surface area flux on flotation performance"; Minerals Engineering, 10, pp. 367-379, 1997.

Grau, R., Heiskanen, K., "Visual techniques for measuring bubble size in flotation machines"; Minerals Engineering, 15, 7, pp. 507 – 513, 2002.

Grau, R.A., Heiskanen, K., "Gas dispersion measurements in a flotation cell"; Minerals Engineering, 16, pp. 1081 – 1089, 2003.

Grau, R.A., Laskowski, J.S., Heiskanen, K., "Effect of frothers on bubble size"; International Journal of Mineral Processing, 76, pp. 225 – 233, 2005.

Hernandez-Aguilar, J.R., Gomez, C.O., Finch, J.A., "A technique for direct measurement of bubble size distributions in industrial flotation cells"; Proceedings of the 34th annual meeting of the Canadian Mineral Processors, pp. 389 – 402, 2002.

Hernandez-Aguilar, J.R., Coleman, R.G., Gomez, C.O., Finch, J.A., "A comparison between capillary and imaging techniques for sizing bubbles in flotation systems"; Minerals Engineering, 17, pp. 53 – 61, 2004.

Jameson, G.J., Allum, P., "A survey of bubble sizes in industrial flotation cells"; Report to AMIRA Ltd., 1984.

Klassen, V.I., Mokrousov, V.A., An Introduction to the Theory of Flotation; Eng. Transl. By J Leja and G.W. Poling, Butterworths, London, 1963.

Maxwell, J.C., A treatise of electricity and magnetism; 3rd edition, vol. 1, part 2, Ch. IX, Oxford University Press, London, pp. 435 – 439, 1892.

Nesset, J.E., Hernandez-Aguilar, J.R., Acuna, C.A., Gomez, C.O., Finch, J.A., "Some gas dispersion characteristics of mechanical flotation machines"; Centenary of Flotation Symposium, Ed. G.J. Jameson, Brisbane, Qld, pp. 243 – 249, 2005.

O'Connor, C.T., Randall, E.W., Goodall, C.M., "Measurement of the effects of physical and chemical variables on bubble size"; International Journal of Mineral Processing, 28, pp. 129 – 139, 1989.

Pandit, A.B., Varley, J., Thorpe, R.B., Davidson, J.F., "Measurement of bubble size distribution: an acoustic technique"; Chemical Engineering Science, 47, 5, pp. 1079 – 1089, 1992.

Rudolphy, L., Grau, R.A., Heiskanen, K., "On-line sensor for measuring gas velocities in laboratory-scale flotation cells"; Centenary of Flotation Symposium, Ed. G.J. Jameson, AusIMM, Brisbane, Qld, June 6 – 9, pp. 573 - 580, 2005.

Sanwani, E., Zhu, Y., Franzidis, J.P., Manlapig, E.V., Wu, J., "Comparison of gas hold-up distribution measurement in a flotation cell using capturing and conductivity techniques"; Minerals Engineering, *Accepted for Publication*, 2006.

Savassi, O.N., Rahal, K.R., Johnson, N.W., Franzidis, J.P., "Mass transfer across the pulp-froth interface in industrial flotation cells. Part1: J_g probe for measurement of air flow rate"; Transactions of the Institution of Mining and Metallurgy-Section C-Mineral Processing, 108, pp. 99 – 102, August, 1999.

Schwarz, S., Alexander, D., "Gas dispersion measurements in industrial flotation cells"; Centenary of Flotation Symposium, Ed. G.J. Jameson, AusIMM, Brisbane, Qld, June 6 – 9, pp. 265 - 269, 2005.

Tavera, F., "Flow cells to measure electrical conductivity: use in estimating gas holdup in flotation systems"; Ph.D. Thesis, McGill University, Montreal, Quebec, Canada, 1996.

Torrealba-Vargas, J.A., Gomez, C.O., Finch, J.A., "Continuous air rate measurement in flotation cells: a step towards gas distribution management"; Minerals Engineering, 17, pp. 761 – 765, 2004.

Torrealba-Vargas, J.A., "Design of a novel gas velocity sensor for flotation systems"; Ph.D. Thesis, McGill University, Montreal, 2004.

Tucker, J.P., Deglon, D.A., Franzidis, J.P., Harris, M.C., O'Connor, C.T., "An evaluation of a direct method of bubble size distribution measurement in a laboratory batch flotation cell"; Minerals Engineering, 7, 5/6, pp. 667 – 680, 1994.

Turner, J.C., "Two phase conductivity: the electrical conductance of liquid-fluidized beds of spheres"; Chemical Engineering Science, 31, pp. 487 – 492, 1976.

Uribe-Salas, A., Gomez, C.O., Finch, J.A., "A conductivity technique for gas and solids holdup determination in three phase reactors"; Chemical Engineering Science, 49, 1, pp. 1 – 10, 1994.

Yianatos, J.B., Laplante, A.R., Finch, J.A., "Estimation of the local holdup in the bubbling and froth zones of a gas liquid column"; Chemical Engineering Science, 40, 10,

pp. 1965 – 1968, 1985.

Yianatos, J.B., Bergh, L., Condori, P., Aguilera, J., "Hydrodynamic and metallurgical characterization of industrial flotation banks for control purposes"; Minerals Engineering, 14, 9, pp. 1033 – 1046, 2001.

Zheng, Y., Zhang, Q., "Simultaneous measurement of gas and solid holdups in multiphase systems using ultrasonic technique"; Chemical Engineering Science, 59, pp. 3505 – 3514, 2004.

Chapter 3 - Characterizing the Impact of Operational Variables on Gas Dispersion Parameters

Abstract

In recent literature, examples of improved metallurgical performance resulting from management of gas dispersion parameters have been reported. At industrial scale, control of gas dispersion parameters (gas rate, gas holdup, bubble size, bubble surface area flux) requires an understanding of the impact of operational variables (airflow rate, frother addition, froth depth...). Tests have been performed to investigate relationships between operational variables and gas dispersion parameters in both forced air and self-aerated mechanical flotation machines. In forced air machines, gas dispersion parameters were manipulated by varying air delivery rate. Manipulation of gas dispersion parameters in self-aerated machines was attempted by varying froth depth, impeller speed, or impeller submergence. In self-aerated machines, in general, it was found that increased froth depth, increased impeller speed and decreased submergence resulted in increased gas rate. When airflow rate was changed in forced air machines, the gas dispersion parameters responded quickly, while, in self-aerated machines, longer periods were required for the operational changes to take effect.

3.1 Introduction

The flotation process is designed to collect hydrophobic minerals on the surfaces of bubbles dispersed throughout a slurry. Theory and experiment suggest that the rate of mineral recovery is dependant on the properties of the bubble swarm (Jameson et al., 1977). Initially, understanding bubble properties was limited due to a lack of

measurement tools, instead relying on machine parameters such as airflow number and power intensity for hydrodynamic control (Arbiter and Steininger, 1965; Arbiter et al., 1976; Harris, 1974). Most conventional flotation machines are designed based on these parameters (Nelson and Lelinski, 2000; Gronstrand et al., 2006).

To facilitate understanding of how the properties of the bubbles can be manipulated for improved metallurgical results, multiple groups have developed sensors (Jameson and Allum, 1984; Yianatos et al., 2001; Gomez and Finch, 2002; Schwarz and Alexander, 2005). The sensors aim to measure gas rate (J_g), gas holdup (ε_g) and bubble size (D_b), based upon which, bubble surface area flux (S_b) is calculated. This set of four parameters has become known as the "gas dispersion parameters". Similarly, the sensors are known as "gas dispersion sensors" recognizing their ability to directly quantify aspects of the bubble population in the dispersion. While most flotation plants continue to operate primarily on operator judgment, reports are starting to emerge linking improved metallurgical performance to management of gas dispersion parameters (Cooper et al., 2004; Gorain, 2005; Pyecha et al., 2005; Hernandez-Aguilar et al., 2006).

A step in the management is determining how the gas dispersion parameters can be manipulated using the available operating variables. One variable is frother addition rate. The effect of frother on bubble size in mechanical flotation machines has been well documented (O'Connor et al., 1989; Cho and Laskowski, 2002; Grau et al., 2005; Nesset et al., 2005). The evidence is that bubble size diminishes rapidly, from > 4 mm at zero frother to a minimum size < 1 mm at concentrations approaching 10 ppm for most commercial frothers. Above this concentration – now called the critical coalescence

concentration (CCC) based on the assumed action of frother – further addition causes little additional decrease in bubble size (there may be effects on froth properties but these are not considered here). One conclusion is it may be advisable to operate at the near-minimum bubble size, i.e., the optimum frother dosage is the CCC. In this way, the maximum impact on flotation recovery rates from bubble size effects is achieved without the bubble size being too sensitive to variations in frother concentration. Industrially, control of frother addition has been hampered by the lack of a frother concentration measurement. Recent work has resulted in the development of an in-plant measurement technique (Gélinas and Finch, 2005).

A second variable for control of gas dispersion parameters is gas rate. It is known that flotation responds to a change in gas rate (Lynch et al., 1981; Deglon et al., 2000; Dahlke et al., 2005). Manipulation of gas rate is considered the prime method of changing properties of the gas dispersion in a controlled manner. Case studies are presented here, demonstrating the impact of gas rate on other gas dispersion parameters. The examples highlight that manipulation of operational variables can be hindered by plant maintenance issues, and can have different impacts in individual cells. Measurement techniques to identify these situations are described.

In self-aerated machines, gas rate cannot be directly manipulated. However, it is recognized that gas rate, and consequently other gas dispersion parameters, can be influenced by varying factors such as impeller speed, froth depth or impeller submergence (Weber et al., 2005; Girgin et al., 2006). One case, demonstrating the challenges of manipulating gas dispersion parameters in self-aerated machines is described. The influence of froth depth, impeller speed and impeller submergence is

reported.

3.2 Measurement Tools

In this chapter, gas dispersion measurements were made using the McGill designed sensors described by Gomez and Finch (2002). Signals from gas rate and gas holdup sensors were monitored using a portable computer running iFIX (control software). Bubble size images were processed off-line using in-house software incorporated in Empix (Northern Eclipse image analysis software).

3.3 Case Studies

3.3.1 Manipulating Gas Dispersion in Forced Air Machines

3.3.1.1 Outokumpu 16 m^3

The first example is an Outokumpu (OK) 16 m^3 machine in BHP Billiton's Leinster operation. The gas dispersion measurements were all taken at the same location and corrected to the pressure at the depth of gas holdup measurement (gas holdup is used as a reference as there is no means to correct for pressure compared to bubble size and gas rate (Gomez and Finch, 2006)). The plant design was such that airflow rate (AFR) could be manipulated by changing the blower settings from the plant control room or by local valves on the machine.

Figure 3.1 shows the results obtained by manipulating the local valves (point A, C) and by control room manipulation of the blower (point B). It is noted that when the local valves were manipulated, only small (almost undetectable) changes in gas rate and gas holdup were found. However, at point B, when the change in the control room was

made, a significant effect was observed in both gas rate and gas holdup. Note that by having at least two independent measurements, J_g and ε_g, the interpretation of an effect is reinforced. This observation suggests a potential maintenance issue with the local valves.

The gas holdup trend shown in Figure 3.1 is essentially that displayed on-screen during the exercise. Initial, only local valve manipulations were planned, but by monitoring the ε_g signal, when no response was observed, alternate plans were formulated.

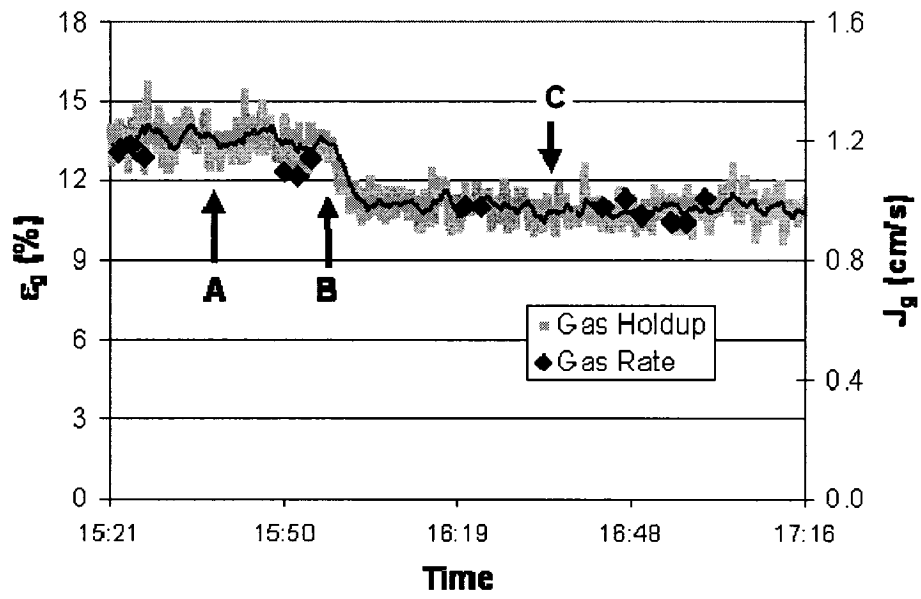

Figure 3.1 – Gas holdup (continuous with 2 min. moving average) and gas rate (periodic measurement) as a function of time. Local valves manipulated at point A and C, control room change at point B.

While it may be intuitive to look to gas rate measurements for detection of changes in airflow rate, experience has shown that gas holdup provides the fastest and most reliable indication of a change. Additionally, gas holdup will respond when any variable changes the properties of the gas dispersion (e.g., a change in frother addition rate).

3.3.1.2 Outokumpu 100 m^3

A similar test was conducted in two OK 100 m^3 machines at BHP Billiton's Escondida (Los Colorados) operation (cell 4 and cell 9 in a row of 10). Airflow rate was manipulated from the plant control system. In both cells, five levels of AFR were used (Figure 3.2, cell 4 and Figure 3.3, cell 9) with gas holdup and gas rate measured at the same location in both cells. This time, bubble size was also measured, not at the same location but at an equal radial distance from the impeller. All gas dispersion parameters were corrected to the pressure at the location of gas holdup measurement as standard protocol. As in the previous case, the gas holdup signal (displayed on-screen) shows clear responses to each change in AFR (Figure 3.2 and Figure 3.3). Similarly, the measured gas rate responds to changes in AFR.

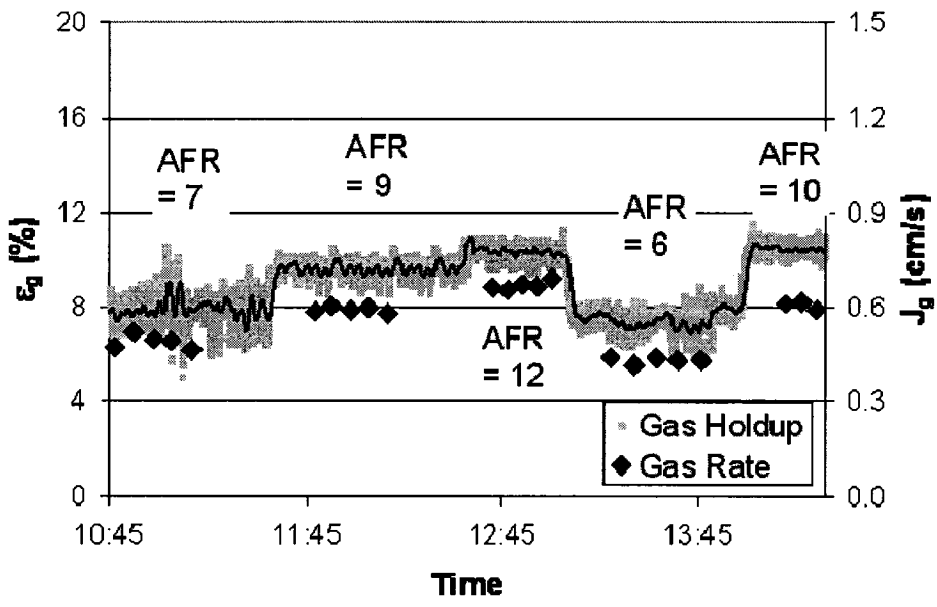

Figure 3.2 – Gas holdup and gas rate response to changes in AFR setting (7, 9, 12, 6 and 10 m^3/min): Cell 4 (of 10).

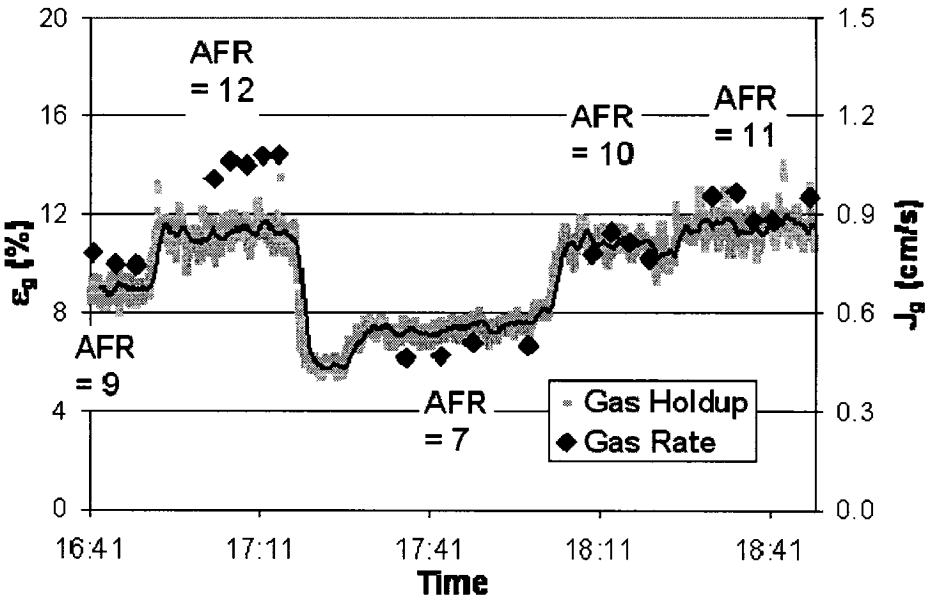

Figure 3.3 - Gas holdup and gas rate response to changes in AFR setting (9, 12, 7, 10, 11 m^3/min): Cell 9 (of 10).

It is noted that the range of gas rates measured in cell 4 was smaller than the range measured in cell 9 (even though the range in AFR was roughly the same). Figure 3.4 shows the relationship between the measured J_g and AFR indicating significant difference between the two cells. From previous experience this may indicate improper calibration of flow meters or insufficient pressure to reach controller set points. (Cell 9 is incidentally closer to J_g calculated as Q_g/CSA.)

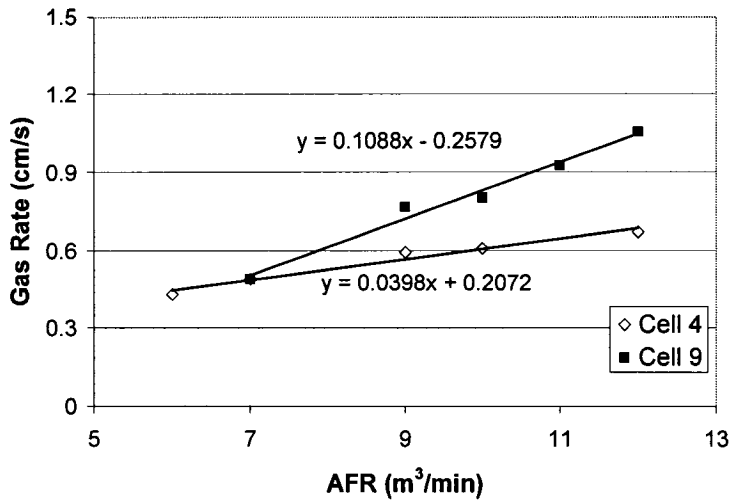

Figure 3.4 – Measured J_g vs. AFR (plant value) in cell 4 and cell 9 showing significant differences.

Figure 3.5 (a, b and c) shows the relationship of gas holdup, bubble size and bubble surface area flux to gas rate for the two cells. While J_g was never as high in cell 4 as it was in cell 9, ε_g in cell 4 demonstrates a higher ε_g (Figure 3.5a). This suggests a smaller bubble size, which was proved to be the case (Figure 3.5b). The end result is a higher S_b is cell 4 (Figure 3.5c). Given that the machine factors controlling bubble generation in these two cells are expected to be identical, it is likely that the difference in bubble size is due to chemical factors, illustrating the potential advantage in combining the measurements with frother concentration measurements (Gélinas et al., 2005).

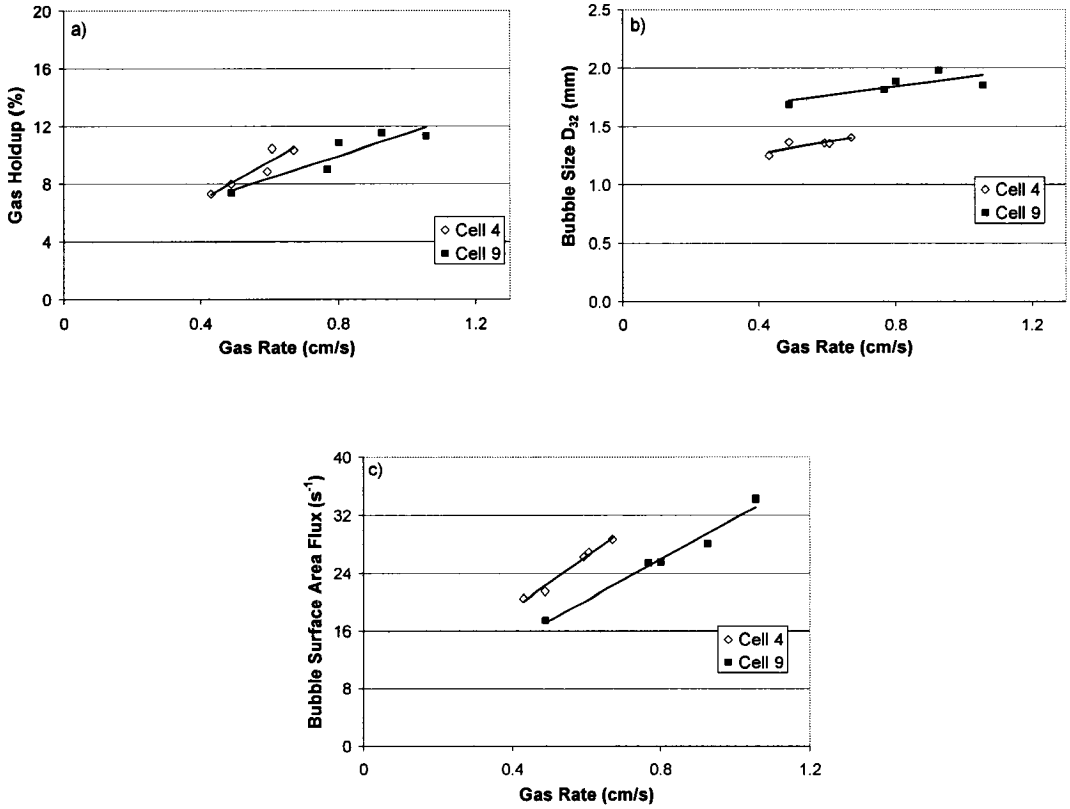

Figure 3.5 – a) Gas holdup, b) bubble size and c) bubble surface area flux as a function of gas rate in the two OK 100 m^3 machines.

The above example demonstrates how relationships can be established between operating variables and gas dispersion parameters. Using these relationships, gas dispersion parameters can be manipulated as desired.

It is noted that in both cells, the gas rate was operated at the lower end of the typical flotation operating range (Dahlke et al., 2005). It was found that further increases in gas rate resulted in excessive water flow into the concentrate causing flooding of the launders.

3.3.2 Manipulation of Gas Dispersion in Self-Aerated Machines

The example is a Wemco 160 m^3 self-aerated flotation machine at BHP Billiton's Escondida (Laguna Seca) operation. Airflow rate in this case must be manipulated indirectly. Tests were run in four machines (A, B, C, D). In cells A and B, froth depth was changed in an attempt to vary the gas dispersion. In cell C, the impeller was run at higher RPM to increase AFR. In cell D, the submergence (defined as distance from the top of the rotor to the top of froth) was increased to decrease AFR based on Weber et al. (2005). In each cell, J_g, ε_g and D_b were measured at the same depth and radial distance from the impeller. All measurements are reported at the pressure of ε_g measurement.

3.3.2.1 Impact of Froth Depth on Gas Dispersion Parameters

Plant practice was to operate with froth depths between 20 and 50 % of the controller range. Froth depth changes can be checked using readings from the J_g sensor and Eq. (3.1), where P_s is the pressure at the sampling location, ρ_b is the bulk density, h_s is the depth of the sampling location, ρ_f is the froth density (estimated as ca. 0.2 ρ_b) and g is the gravitational constant.

$$h_f = \frac{P_s - \rho_b g h_s}{\rho_f g - \rho_b g} \qquad \textbf{(3.1)}$$

Figure 3.6 shows the estimated froth depth plotted against the froth depth set point. A roughly linear relationship was found, however, there were significant cell-to-cell variations.

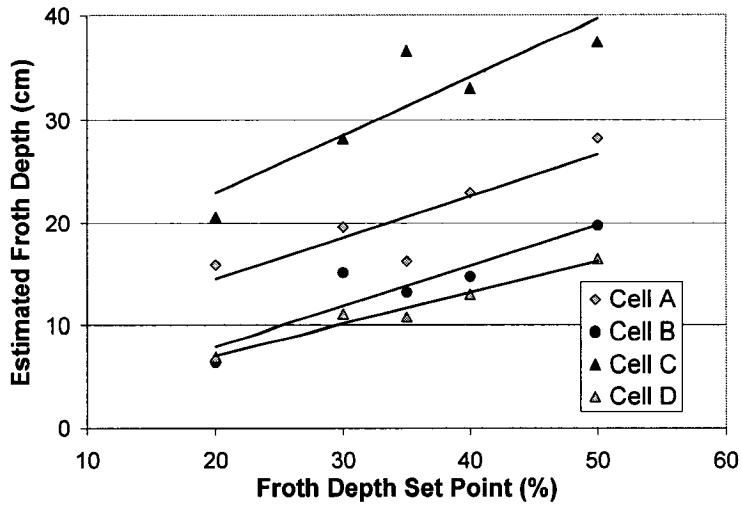

Figure 3.6 – Relationship between estimated froth depth and control system set point for froth depth.

Figure 3.7 shows the detected response in J_g and ε_g as froth depth was varied in cell A. Up until c.a. 11:30, both ε_g and J_g were relatively stable. At 11:30 when the set point in froth depth was changed from 20 % to 30 %, both the gas rate and gas holdup began to increase. With some oscillation, the trend of increasing J_g and ε_g continued as froth depth was stepped up to 50 % from 40 %. At 13:00, when the froth depth set point was decreased to 35 %, J_g and ε_g began to decrease.

Results for cell B (Figure 3.8) are similar to those in cell A, with an increase in J_g and ε_g as froth depth was varied from 20 to 50 %, and the increase stopping when the level set point is reduced to 35 % but not returning to the expected value (i.e., that between the 30 and 40 % setting on the increasing cycle).

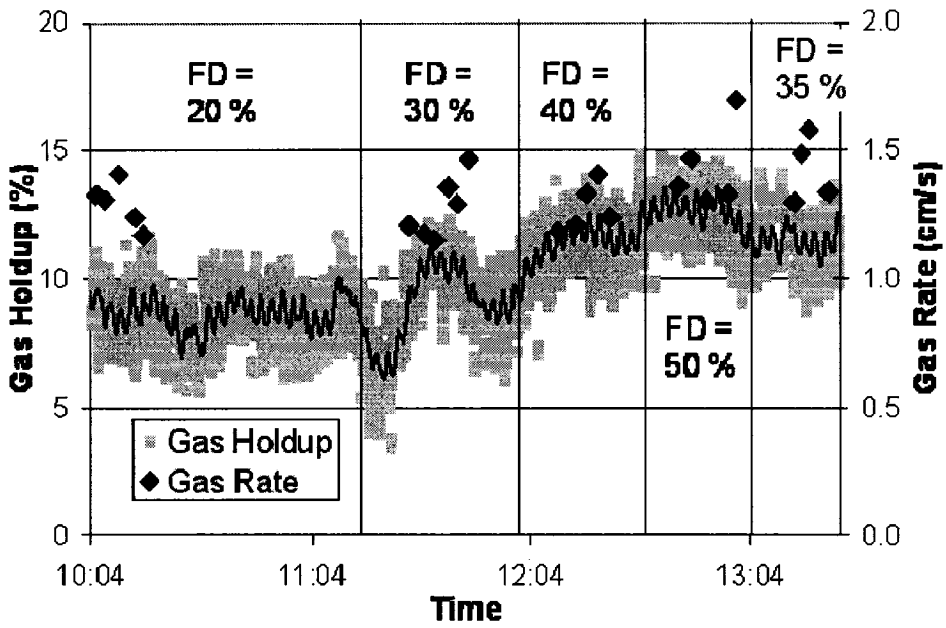

Figure 3.7 – Gas holdup and gas rate in cell A as a function of froth depth (FD) (from 20 to 50 % of the controller range).

It is evident that gas dispersion responds to froth depth changes but steady state values may not have been reached. Given the fast response in forced air cells, this slow response is a system effect (not a sensor effect).

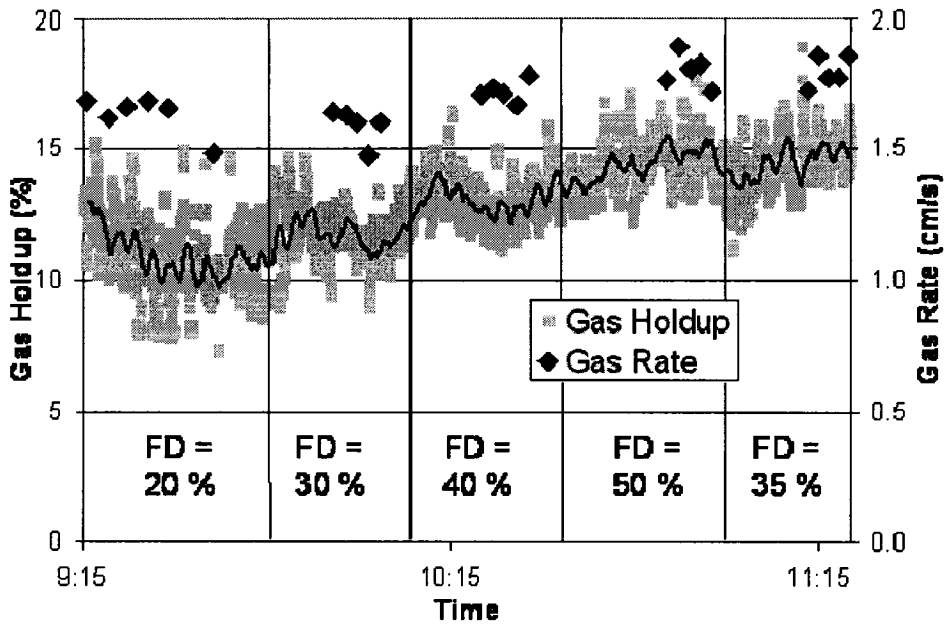

Figure 3.8 - Gas holdup and gas rate in cell B as a function of froth depth (FD) (from 20 to 50 % of the controller range).

A plot of froth depth for cell A as the set point was changed from 50 to 35 % (Figure 3.9) reveals that the froth depth had not reached a steady state value. This oscillatory response explains why gas rate measured at 35 % may be higher than expected.

When results for cell A and B are compared (Figure 3.10) it is revealed that while gas rate is higher in cell B, identical trends were observed as froth depth was varied confirming that gas rate was being manipulated in a similar manner in both cells, suggesting the response may be a property of cell type.

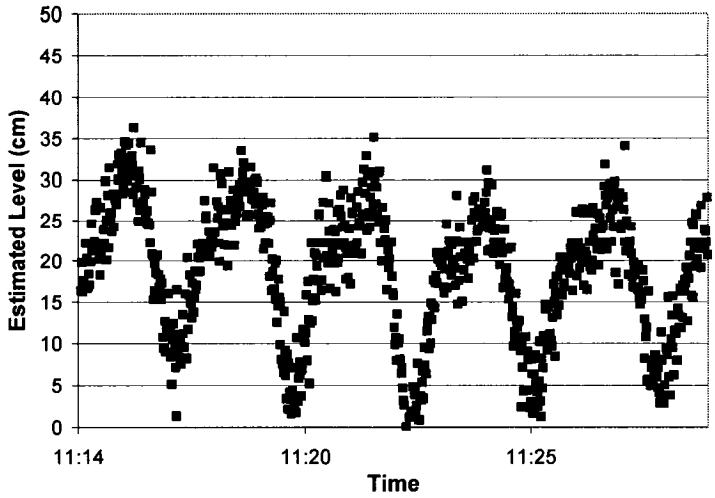

Figure 3.9 – Estimated level when froth depth set point is changed from 50 to 30 % showing unstable system response.

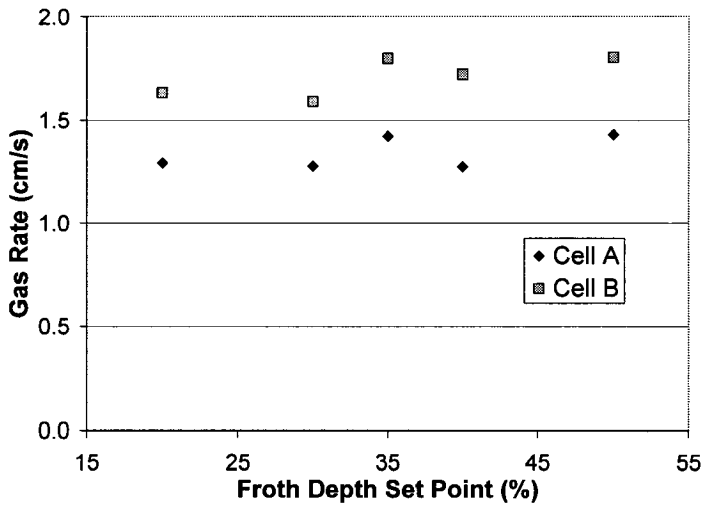

Figure 3.10 – Comparison of J_g in cell A and B as froth depth was varied.

3.3.2.2 Impact of Impeller Speed and Submergence

Before testing began, cell C was set to operate with increased impeller speed and cell D was set to have a larger submergence. It was expected that the increased impeller speed would increase J_g, while an increased submergence would decrease J_g. When gas holdup

is plotted against gas rate for each of the cells (Figure 3.11), it is found that all cells lie on a similar trend line over the range found by Dahlke et al. (2005) for forced air machines (also in line with the Outokumpu machine results presented above cf. Figure 3.5a). It is noted that cell C (increased impeller speed) shows the higher J_g, while cell D (increased submergence) shows the lowest J_g, i.e., both demonstrate the expected trend.

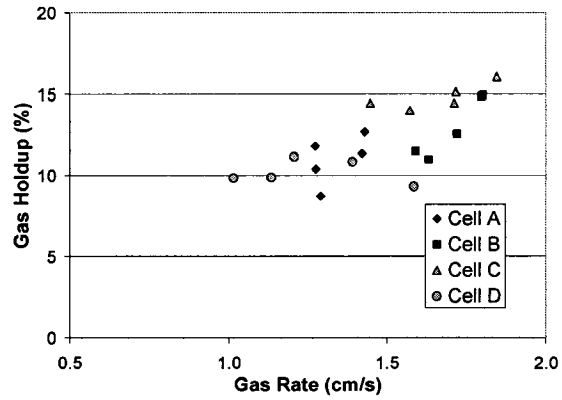

Figure 3.11 – Gas holdup vs. gas rate for four Wemco 160 m^3 machines. Cell A and B under standard conditions, cell C with increased RPM and cell D with increased submergence.

There is a potential complication however. Calculated froth depth based on Eq. (3.1) was largest in cell C and smallest in cell D. The difference in froth depth cell-to-cell may have contributed to increased J_g in cell C and decreased J_g in cell D.

Compared to the forced air machines, manipulation of gas dispersion parameters is more difficult in self-aerated machines. While it appears that level changes can be used to manipulate gas rate, it is apparent that there is a system response time required for cell level (and hence J_g) to reach a new set point.

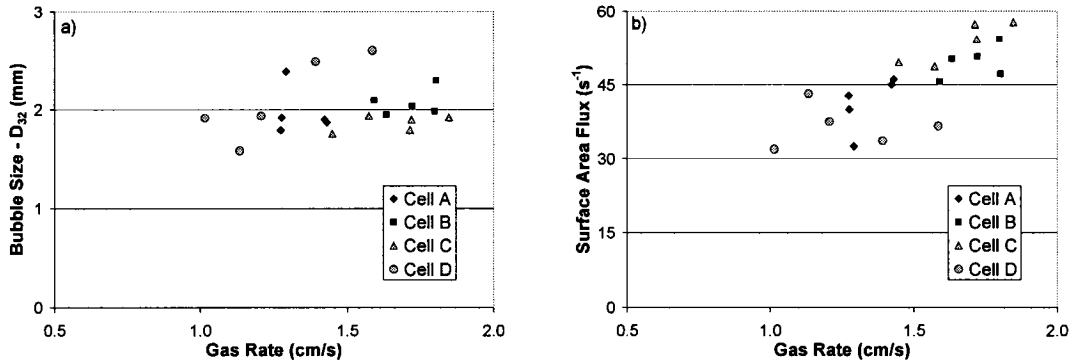

Figure 3.12 – a) Sauter mean bubble size and b) surface area flux vs. gas rate in four Wemco 160 m^3 machines. Cell A and B under standard conditions, cell C with increased RPM and cell D with increased submergence.

By combining changes in froth depth, impeller speed and submergence, bubble surface area generation rate can be manipulated over a range similar to forced air machines (in Figure 3.12b, J_g varies from 1.0 to 1.9 cm/s and S_b from 32 to 58 s^{-1}).

3.4 Conclusions

Control of gas dispersion parameters depends on understanding their relationship to operational variables. The development of gas dispersion sensors has facilitated establishment of these relationships as demonstrated in forced air and self-aerated cell types.

In forced air machines, gas dispersion parameters can be manipulated as a function of airflow rate, but each cell may have individual characteristics. It was also observed that the choice of manipulation route, via local valves or control room, has to be checked.

In self-aerated machines, manipulation of gas dispersion parameters can be achieved by varying froth depth, impeller speed and submergence. When compared to forced air

machines, there is a longer system response time that needs to be considered.

3.5 References

Arbiter, N., Steininger, J., "Hydrodynamics of flotation machines"; In: E. Roberts (Editor), Mineral Processing, Pergamon, New York, pp. 595 – 608, 1965.

Arbiter, N., Harris, C.C., Yap, R.F., "The air flow number in flotation machine scale-up"; International Journal of Mineral Processing, 3, pp. 257 – 280, 1976.

Cho, Y.S., Laskowski, J.S., "Effect of flotation frothers on bubble size and foam stability"; International Journal of Mineral Processing, 64, pp. 69 – 80, 2002.

Cooper, M., Scott, D., Dahlke, R., Gomez, C.O., Finch, J.A., "Impact of air distribution profile on banks in a Zn cleaning circuit"; CIM Bulletin, 97, 1083, pp. 73 – 78, October, 2004.

Dahlke, R., Gomez, C.O., Finch, J.A., "Operating range of a flotation cell determined from gas holdup vs. gas rate"; Minerals Engineering, 18, pp. 977 – 980, 2005.

Deglon, D.A., Egya-Mensah, D., Franzidis, J.P., "Review of hydrodynamics and gas dispersion in flotation cells on South African platinum concentrators"; Minerals Engineering, 13, 3, pp. 235 – 244, 2000.

Gélinas, S., Finch, J.A., "Colorimetric determination of common industrial frothers"; Minerals Engineering, 18, pp. 263 – 266, 2005.

Gélinas, S., Finch, J.A., Cappuccitti, F., "Frother analysis: procedure and plant

experience"; Proceedings of the 37th Annual Meeting of the Canadian Mineral Processors, pp. 569 – 576, 2005.

Girgin, E.H., Do, S., Gomez, C.O., Finch, J.A., "Bubble size as a function of impeller speed in a self-aeration laboratory flotation cell"; Minerals Engineering, 19, 201 – 203, 2006.

Gomez, C.O., Finch, J.A., "Gas dispersion measurements in flotation machines"; CIM Bulletin, Vol 95, N° 1066, pp. 73 – 38, November/December, 2002.

Gomez, C.O., Finch, J.A., "Gas dispersion measurements in flotation cells"; Submitted to the International Journal of Mineral Processing for publication, 2006.

Gorain, B. K., "Optimization of flotation circuits with large flotation cells"; Centenary of Flotation Symposium, Ed. G.J. Jameson, AusIMM, Brisbane, Qld, June 6 – 9, pp. 843 – 851, 2005.

Grau, R.A., Laskowski, J.S., Heiskanen, K., "Effect of frothers on bubble size"; International Journal of Mineral Processing, 76, pp. 225 – 233, 2005.

Gronstrand, S., Niitti, T., Rinne, A., Turenen, J., "Enhancement of flow dynamics of existing flotation cells"; proceedings of the 38th annual meeting of the Canadian mineral processors, Ottawa, Canada, pp. 403 – 422, 2006.

Harris, C.C., "Impeller speed, air and power requirements in flotation machine scale-up.", International Journal of Mineral Processing, 1, pp. 51 – 84, 1974.

Hernandez-Aguilar, J.R., Thorpe, R., Martin, C.J., "Experiences using gas dispersion

measurements to understand and modify metallurgical performance"; Proceedings of the 38th annual Canadian mineral processors conference, pp. 387 – 402, 2006.

Jameson, G.J., Nam, S., and Young, M, "Physical factors affecting recovery rates in flotation"; Mineral Science Engineering, 9, 3, 103 – 118, 1977.

Jameson, G.J., Allum, P., "A survey of bubble sizes in industrial flotation cells"; Report to AMIRA Ltd., 1984.

Lynch, A.J., Johnson, N.W., Manlapig, E.V., Thorne, C.C., Mineral and Coal Flotation Circuits, Their Simulation and Control; Elsevier Publication, 1981.

Nelson, M.G., Lelinski, D., "Hydrodynamic design of self-aerating flotation machines"; Minerals Engineering, 13, 10 – 11, pp. 991 – 998, 2000.

Nesset, J.E., Hernandez-Aguilar, J.R., Acuña, C.A., Gomez, C.O., Finch, J.A., "Some gas dispersion characteristics of mechanical flotation machines."; Centenary of Flotation Symposium, Ed. G.J. Jameson, Brisbane, Qld, pp. 243 – 249, 2005.

O'Connor, C.T., Randall, E.W., Goodall, C.M., "Measurement of the effects of physical and chemical variables on bubble size"; International Journal of Mineral Processing, 28, pp. 129 – 139, 28, 1989.

Pyecha, J., Sims, S., Lacouture, B., Hope, G., Stradling, A., "Evaluation of a Microcel™ sparger in the Red Dog column flotation cells"; In G.J. Jameson (Ed), AusIMM, Centenary of Flotation Symposium, Brisbane, Qld, pp. 1017 – 1025, 2005.

Schwarz, S., Alexander, D., "Gas dispersion measurements in industrial flotation cells";

Centenary of Flotation Symposium, Ed. G.J. Jameson, AusIMM, Brisbane, Qld, June 6 – 9, pp. 265 - 269, 2005.

Weber, A., Meadows, D., Villanueva, F., Polamo, R., Prado, S., "Development of the world's largest flotation machine"; Centenary of Flotation Symposium, Ed. G.J. Jameson, Brisbane, AusIMM, Qld, pp. 285 - 291, 2005.

Yianatos, J.B., Bergh, L., Condori, P., Aguilera, J., "Hydrodynamic and metallurgical characterization of industrial flotation banks for control purposes; Minerals Engineering, 14 (9), pp. 1033 – 1046, 2001.

Chapter 4 - Sample Point Selection for Down-the-Bank Optimization of Gas Dispersion Parameters

Abstract

Several reports cite the benefits of managing gas dispersion parameters in flotation for improved metallurgical performance. In the case of down-the-bank optimization, this depends on selection of a sampling point, at which gas dispersion parameters can be measured in each cell. Evaluating a single cell to select a sampling point has been a lengthy procedure and as a result is often not done. To facilitate selection, a set-up was developed to measure gas rate (J_g) simultaneously at multiple locations (multi-Jg sensor). The selection of a sample point is faster and more reliable as time variations are allowed for. Specifications and operational experience using the multi-Jg sensor are presented. Three in-plant case studies are described. Recommendations on sample point selection are discussed.

4.1 Introduction

The froth flotation process involves a complex interaction between many variables, from chemistry to economics. Central is the production of gas bubbles to collect and transport particles. The ability of a flotation machine to form bubbles of a given size, at a given gas flow-rate will determine the bubble surface available for bubble-mineral contact. Despite the obvious importance of gas dispersion in flotation (Fewings et al., 1981), limited progress incorporating these properties into plant optimization has been made due primarily to a lack of measurement tools. The pioneering hydrodynamic work of Arbiter, Harris and co-workers (Arbiter and Steininger, 1965; Arbiter et al., 1976; Harris, 1974;

Harris, 1976) for instance, did not include parameters specific to the dispersion of bubbles (bubble size, bubble surface area flux). Given the benefits apparent to understanding how to control the properties of the gas dispersion, several groups have developed measurement instruments. In general, three main properties of the gas dispersion are measured, namely: superficial gas velocity (gas rate, J_g), gas holdup (ε_g) and bubble size (D_b). Using these parameters, the bubble surface area flux (S_b) is calculated. This area of study has been termed "gas dispersion" referring to the dispersion of bubbles in slurry, and the set of four parameters (J_g, ε_g, D_b, S_b) have become known as the "gas dispersion parameters".

Jameson and Allum (1984) appear to be the first to have developed sensors to measure gas dispersion parameters in industrial flotation machines. Subsequently, development has been underway at the Julius Kruttschnitt Mineral Research Centre, University of Cape Town and McGill University (Gorain et al., 1995[a,b], 1996, 1997; Cortes-Lopez, 1999; Deglon et al., 2000; Torrealba-Vargas et al., 2004; Hernandez-Aguilar et al., 2004), initially independently and now under the AMIRA P9 project, as a collaborative effort, the Helsinki University of Technology (Grau and Heiskanen, 2003) and at Santa Maria University (Yianatos et al., 2001).

Reports of metallurgical benefit achieved by managing the gas phase in flotation are now beginning to emerge. Some of these reports incorporate gas dispersion parameters into flotation circuit models that predict how plant metallurgy will respond when operational variables are manipulated (Alexander et al., 2005). More directly, exercises in gas management via gas rate profiling across banks of flotation machines have resulted in

metallurgical gains (Cooper et al., 2004; Gorain, 2005).

In the above examples, gas dispersion parameters were measured in multiple cells across flotation circuits requiring the selection of sampling points for measurement. The technique of sample point determination, is known as cell mapping. The technique was lengthy and could not easily allow for possible variations in time. To speed up the process and increase reliability, a technique employing a multi sensor unit (known as the multi-Jg sensor), capable of measuring gas rate simultaneously at multiple locations, has been developed.

This chapter presents details of the technique and the sensor. Three industrial trials of the technique are reported. Each demonstrates benefits of the technique. Recommendations regarding the selection of sampling points for measurement of gas dispersion parameters during down-the-bank optimization exercises are offered.

4.2 Previous Cell Mapping Procedure

A procedure, more formally known as radial cell mapping, has been commonly used to investigate spatial variation in gas dispersion parameters (usually gas rate) as a function of distance from the impeller (Gorain et al., 1996; Deglon et al., 2000; Yianatos et al., 2001; Dahlke et al., 2001). Typically, this procedure consists of sequentially installing a sensor at selected points in a cell, resulting in a relatively time consuming exercise.

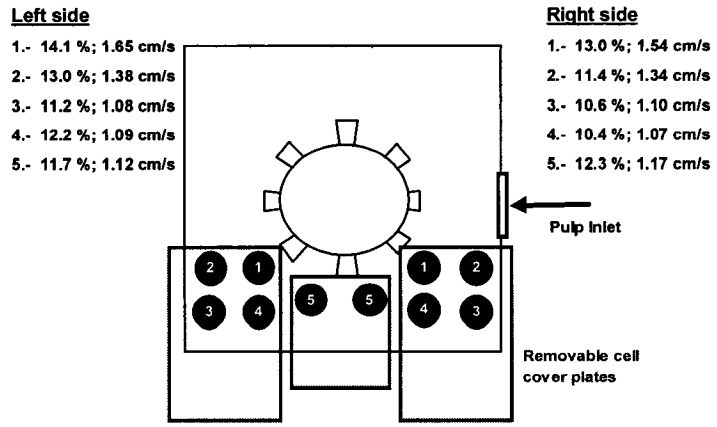

Figure 4.1 – Example of typical cell mapping results showing sample locations, gas holdup (%) and gas rate (cm/s).

Figure 4.1 shows the results of radial mapping reported by Dahlke et al. (2001). In general, gas rate and gas holdup increased towards the centre of the flotation machine. While results between the left side and right side of the flotation machine are similar, certain differences can be observed, e.g., location five on the left exhibited the second lowest gas holdup, while location five on the right exhibited the second highest gas holdup. Given the fact that the measurements were taken by moving a single sensor from point to point, significant time would have elapsed between measurements at location five on the right and location five on the left. Therefore, it is possible that some of the results presented in Figure 4.1 are not reflective of spatial variations, but fluctuations with time. This uncertainty in outcome, combined with the time requirements, were the motivation to develop the multi-Jg sensor unit.

4.3 The Multi-Jg Sensor

The McGill J_g sensor[2] functions by measuring pressure inside a probe inserted in the pulp zone of a flotation cell. The multi-Jg sensor is a package including multiple probes, dedicated electronics and computer software that facilitate simultaneous measurements at multiple locations.

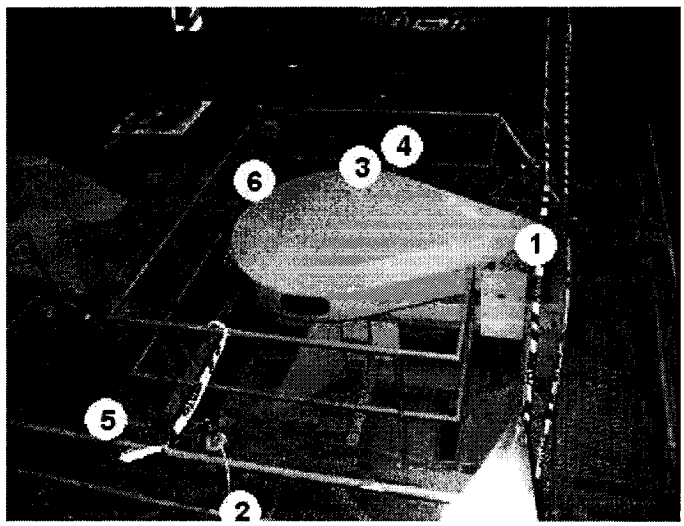

Figure 4.2 – Wemco flotation machine with J_g sensors installed in six locations as part of a radial mapping exercise.

The multi-sensor electronics incorporates eight 12-bit Dutec modules to convert the analog 4-20 mA pressure signals from up to eight J_g probes into digital signals. These digital signals are then converted into RS-232 (serial communication) and transferred to a laptop computer. The serial communication signals are processed by iFIX, a commercial control software, which contains in-house programming to calculate J_g on-line. The software stores data to the computer hard drive for later off-line analysis. With a

---

[2] There are two versions of the J_g sensor, the so-called on-off and continuous (Gomez et al., 2003; Torrealba-Vargas et al., 2004). Measurements presented in this thesis used the on-off version.

standard quality laptop computer (Pentium 3, 256 Mb RAM), two eight-sensor units can be run simultaneously, meaning that gas rate can be measured in up to sixteen locations. For cell mapping tests, this is usually sufficient (access limitations frequently keep the number below ten).

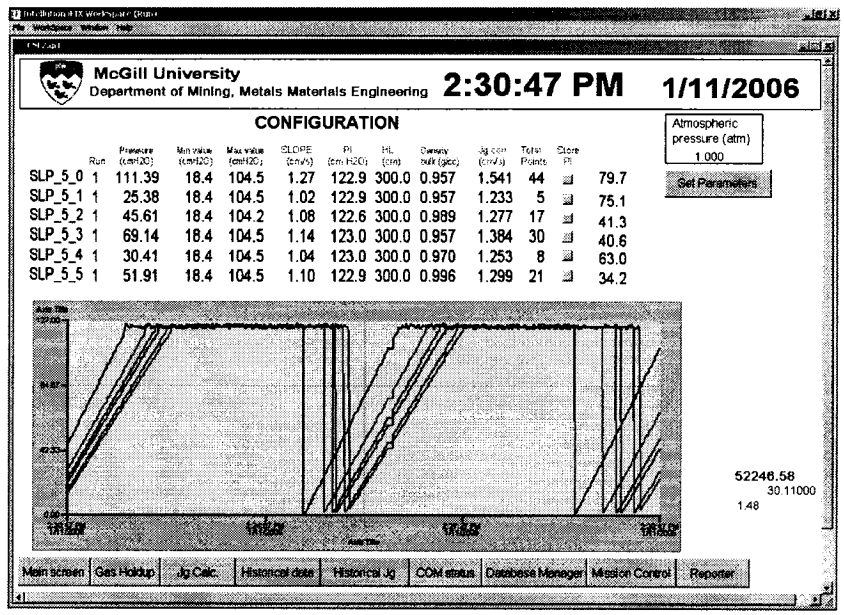

Figure 4.3 – Sample of on-line computer display with simultaneous J_g measurement at six locations using multi-Jg sensor package.

4.4 Plant Trials with Multi-Jg Sensor

The multi-Jg sensor is now used routinely for cell mapping as part of standard McGill gas dispersion campaigns. In addition, other industrial groups have been trained and are using Multi-Jg technology. The following are three examples of industrial mapping tests using the multi-Jg package carried out by the author.

4.4.1 Mapping a Wemco 45 m^3 Cell

Multi-Jg technology was used for cell mapping as part of a two-week campaign at

Codelco's El-Salvador concentrator in northern Chile. The cell under investigation was a Wemco 45 m^3 (self-aerated / mechanically agitated) machine. In this case, gas rate was measured at six locations (Figure 4.2). The mapping test was repeated on two consecutive days.

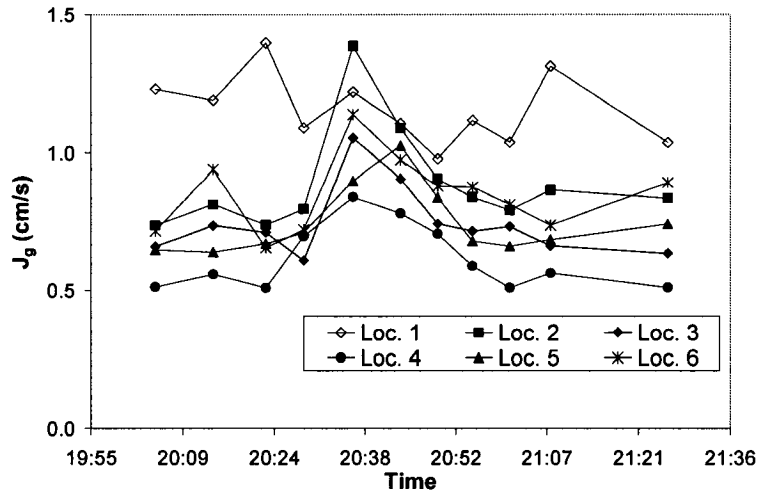

Figure 4.4 – Results from mapping test on day 1.

Using the multi-Jg sensor 11 gas rate measurements at each of the 6 locations were completed in just over one hour (Figure 4.4). Five of the sensors detected an increase in gas rate at c.a. 20:30. A change in gas rate, for a self-aerated flotation machine, could be caused by fluctuations in froth depth, or varying feed density. The transient airflow rates demonstrate two features of the multi-Jg mapping test design. The first is that changes in airflow rates can be distinguished from experimental error (not all five sensors can be in "error"). In the previous, single sensor method, a sudden measurement spike may have been attributed to sensor malfunction. The second feature is that variations with location can be distinguished from variations with time. Consider mapping the cell in question by moving a single sensor from point to point. If J_g were measured at location 4 at 20:09 it

would be concluded that this location had an intermediate superficial gas velocity. Had the same location been sampled at 20:38, it would have been concluded that the superficial gas velocity at this location was particularly high. Because each location was measured simultaneously, the high J_g measurements at 20:38 can be attributed to changes in airflow rates with time and not spatial variations.

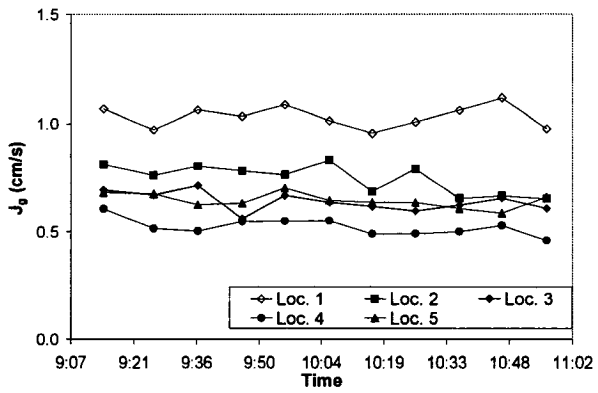

Figure 4.5 – Results from mapping test on day 2.

Results from the mapping test on day two are shown in Figure 4.5, revealing a significantly more stable operation. It is noted however, that on both days the general distribution of air within the machine seems to be constant, i.e., highest gas rate remained at location 1, lowest gas rate at location 4.

On further inspection it is determined that on both days, not only was J_g at location 1 considerably higher than other locations, but J_g in location 1 does not respond in the same way as other positions in the cell. Location 1 is relatively near to the feed inlet from the previous cell. It is hypothesized that the gas rate at location 1 is influenced by air entrained from the previous cell. Because the gas dispersion at location 1 does not seem to reflect the gas dispersion within the bulk of the cell, location 1 is eliminated as a viable

sampling point.

4.4.2 Mapping an Outokumpu 70 m^3 Cell

A mapping test was run in an Outokumpu (OK) 70 m^3 (forced air / mechanically agitated) flotation machine in Anglo-Platinum's Waterval concentrator in South Africa. In this case, eight sensors were placed in the cell. Four positions were selected at a constant distance from the impeller. At each position, J_g was measured at depths of 1 m and 1.5 m below the cell lip. Figure 4.6 shows the top view of an OK 70 m^3 with sampling locations marked. Gas rate was measured continually for a period of three hours.

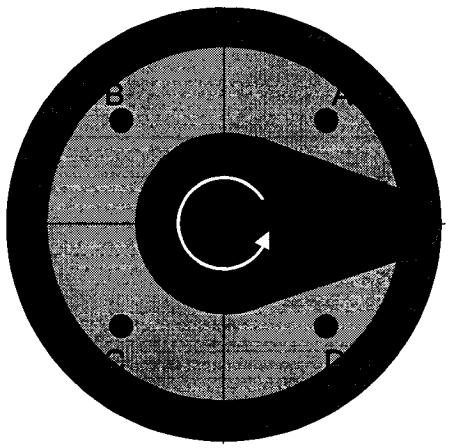

Figure 4.6 – Diagram of the top view of an OK 70 m^3 showing J_g sampling locations.

Gas rate plotted against time (Figure 4.7) reveals no obvious variation between the sampling locations. Given the symmetry of the machine and the equal distance from the centre, the similarity between J_g at each location is expected.

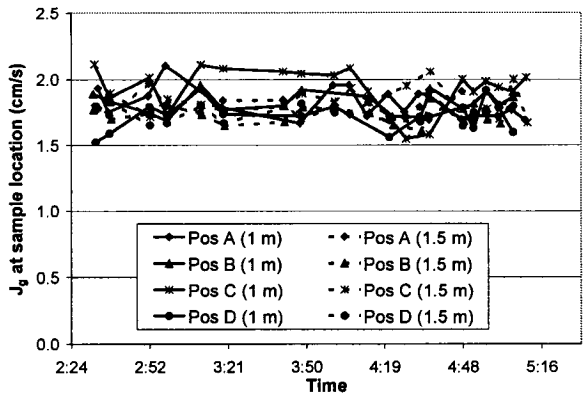

Figure 4.7 – Gas rate vs. time at 8 different locations in an OK 70 tank cell.

When results are compared more closely, some variation in J_g can be observed between the locations. Figure 4.8 shows the average J_g at each of the four locations at a depth0 of 1 m with error bars representing the standard deviation of the 20 measurements, revealing that average J_g at location C was higher than at the other points. The equivalent plot (Figure 4.9) for the deeper measurements (1.5 m) again show the highest average J_g at location C.

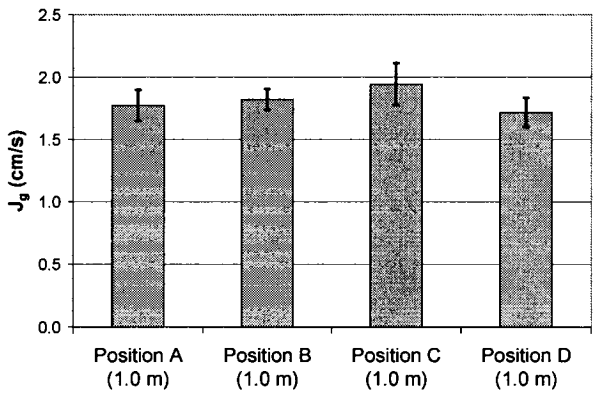

Figure 4.8 – Average J_g at four locations (1.0 m below the cell lip) in an OK 70 with error bars representing the standard deviation in 20 measurements.

During the mapping test, gas holdup was also measured at locations C and location D

(16.9 % and 16.5% respectively). The three measurements comparing location C and D, (J_g at 1.0 m, at 1.5 m and ε_g at 1.5 m), each indicated that more air is being delivered to location C than location D. While in each case the difference is small, the consistent agreement supports the validity of the measurements.

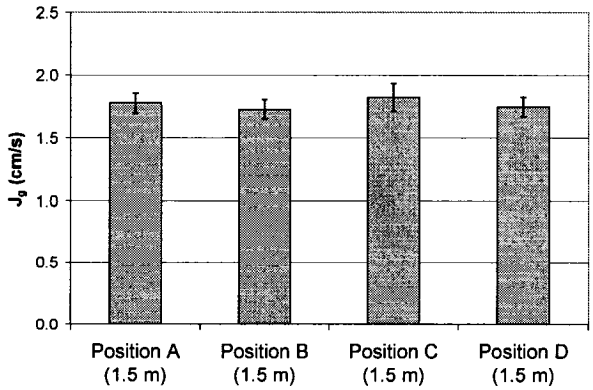

Figure 4.9 - Average J_g at four locations (1.5 m below the cell lip) in an OK 70 with error bars representing the standard deviation in 20 measurements.

Ideally, during down-the-bank optimization exercises, gas dispersion parameters should be sampled in the same location in each cell. The variation in gas rate between locations C and D is noteworthy as during down-the-bank optimization there is often a temptation to substitute one location for another of equal distance from the impeller. This example shows that locations at equal radial positions in cylindrical machines can exhibit different gas dispersion parameters, probably a result of asymmetric flow impediments such as discharge valve supports.

4.4.3 Mapping an Outokumpu 50 m^3 Cell

A mapping test was run in an OK 50 (forced air/mechanically agitated) with a U-shaped tank at Inmet's Troilus operation 120 km north of Chibougamau, Canada. Gas rate was

measured in five positions in cell 1 of the rougher bank. Figure 4.10 shows the approximate locations. The airflow rate was set at four values (4, 6, 8, 12 m^3/min) to determine the impact of gas rate on the distribution of gas within the machine. Dividing these flow rates by the cell cross sectional area, J_g is estimated to be 0.49, 0.73, 0.97 and 1.46 cm/sec, respectively.

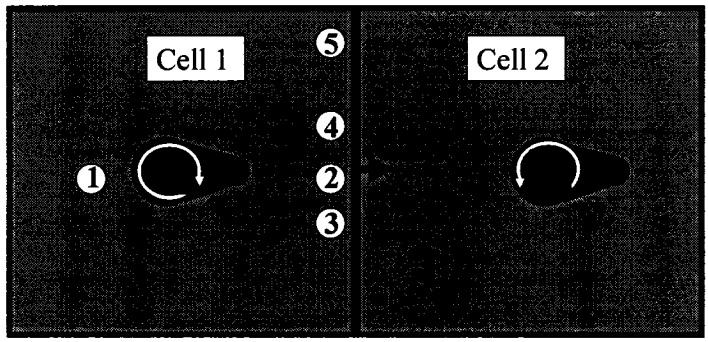

Figure 4.10 – Sketch of the OK 50 U showing the five J_g measurement locations.

The measured J_g at each of the locations is plotted against J_g calculated on the basis of airflow rate and cross sectional area (Figure 4.11).

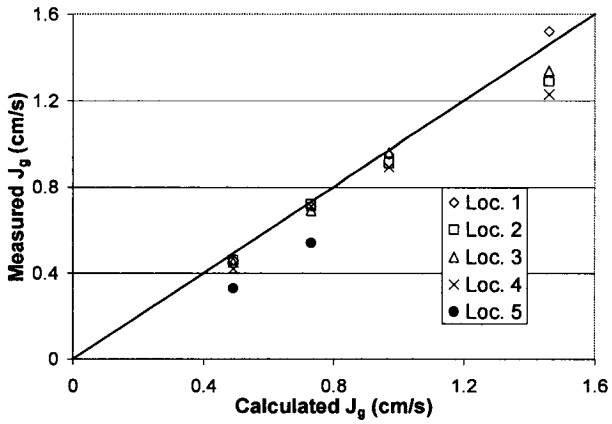

Figure 4.11 – Measured compared to calculated (Q/A) gas rate at five locations in an OK U shaped machine.

Figure 4.11 shows that the measured J_g at locations 2, 3 and 4 tend to be similar across the operating range of the machine. Gas rate at location 1 was similar to other locations until the highest air flow rate, at which point J_g in location 1 was measured to be significantly higher. This is probably caused by the fact that at high airflow rates, it is more difficult for the mixing mechanism to disperse the gas throughout the cell. Consequently more gas was detected at the location closer to the point of air delivery (through the impeller). It is also noted that at the highest aeration rate, J_g measured at locations 2, 3 and 4 dropped below the calculated value of J_g, confirming that less air was reaching these locations.

Although measurements at location 5 were only taken at the two lowest airflow rates it is observed that J_g at location five was lower than at the other locations. This finding is expected, given the large distance from the impeller.

One stated approach for down-the-bank optimization exercises is to sample gas dispersion parameters in the same geometric location in each cell (Dahlke et al., 2001; Cooper et al., 2004). The Troilus example demonstrates that in practice, selecting or defining the same location in each cell is not trivial. Examination of Figure 4.10 shows that the impeller is not centred in the cell. As such, there can be debate as to whether the sample locations should kept at the same location with respect to impeller location and rotation, or the same location with respect to cell walls, or the same location with respect to the downstream direction. The mapping results demonstrate a relationship between gas rate at a particular location and distance from the impeller. This is most significant at high airflow rates, or at large distances from the impeller (location 5). Therefore, the mapping results suggest that the distance between sampling point and impeller should be

kept constant in each cell.

4.5 Discussion on Sample Point Selection

Based on the mapping tests and field observations, a hierarchy of criteria for down-the-bank sample point selection has been established.

The most important consideration is what locations are available in each cell. These will be limited by obstacles (launders, level measurement devices, unmoveable grating) or safety concerns (lack of suitable guard rails, proximity to a motor). This aspect most often dictates the initial selection of locations.

Once the potential locations are established, the next step is to eliminate locations that do not give the same response as other cell locations. For example, location 1 in Figure 4.4 was eliminated because when most locations detected an increase in gas rate, the sensor in location 1 did not.

Thirdly, mapping results should be examined to determine how the "same" location in each cell can be identified across the bank. In most cases, for mechanically agitated machines, the most important consideration is distance from the impeller. While a trivial concern for circular cross-section machines, it may be more involved for rectangular or U-shaped machines, particularly when the impeller is not located in the centre of the machine.

Additionally, consideration should be given to: a) the location of physical obstacles that could affect the path of bubbles (e.g., internal launders, froth crowders or shrouds) and b) changes in impeller direction or grating configuration across the bank. Care should be

taken to ensure that these factors have the same impact on gas dispersion parameters in each cell at the selected sampling location.

Choosing a location where measured J_g is equal to the calculated (Q/A) J_g or where J_g is most responsive to changes in operating variables may be considered. However, these locations are often challenging to locate, and are rarely equally accessible in each cell across the bank. The final selection, between points that satisfy the above criteria, is essentially arbitrary, but once chosen, the location must be well documented and respected for all subsequent campaigns.

4.6 Conclusions

Down-the-bank gas rate (J_g) profiling exercises have produced improvements in the metallurgical performance of a flotation plant. Cell mapping of J_g is an essential precursor to these optimization campaigns. Once lengthy, the development and application of a multi-Jg sensor package has greatly reduced the time requirements for cell mapping and increased reliability by allowing for variations in time.

Results of testing the multi-Jg mapping technique at three industrial sites have been presented. These case studies demonstrate how the technique can be used to help select the sampling point for measurement. A hierarchy of criteria for sample point selection has been offered.

4.7 References

Alexander, D.J., Bilney, T., Schwarz, S., "Flotation performance improvement at Placer

Dome Kanowna Belle Gold Mine"; Proceedings of the 37th Annual Canadian Mineral Processors Conference, Ottawa, Canada, pp. 171 – 201, 2005.

Arbiter, N., Steininger, J., "Hydrodynamics of flotation machines"; In: E. Roberts (Editor), Mineral Processing, Pergamon, New York, pp. 595 – 608, 1965.

Arbiter, N., Harris, C.C., Yap, R.F., "The air flow number in flotation machine scale-up"; International Journal of Mineral Processing, 3, pp. 257 – 280, 1976.

Cooper, M., Scott, D., Dahlke, R., Gomez, C.O., Finch, J.A., "Impact of air distribution profile on banks in a Zn cleaning circuit"; CIM Bulletin, 97, 1083, pp. 761 – 765, October, 2004.

Cortes-Lopez, F., "Design of a gas holdup sensor for flotation diagnosis"; Masters Thesis, McGill University, Montreal, Quebec, Canada, 1999.

Dahlke, R., Scott, D., Leroux, D., Gomez, C.O., Finch, J.A., "Troubleshooting flotation cell operation using gas velocity measurements"; Proceedings of the 33rd Annual Canadian Mineral Processors Conference, Ottawa, Canada, pp. 359 – 370, 2001.

Deglon, D.A., Egya-Mensah, D., Franzidis, J.P., "Review of hydrodynamics and gas dispersion in flotation cells on South African platinum concentrators"; Minerals Engineering, 13, 3, pp. 235 – 244, 2000.

Fewings, J.H., Slaughter P.J., Manlapig, E.V., Lynch, A.J., "The dynamic behaviour and automation control of the chalcopyrite flotation circuit at Mount Isa Mines Limited"; Developments in Mineral Processing, pp. 1541 – 1575, 1981.

Gomez, C.O., Torrealba-Vargas, J.A., Dahlke, R., Finch, J.A., "Measurement of gas velocity in industrial flotation cells"; International Mineral Processing Conference, 3, pp. 1703 – 1713, 2003.

Gorain, B.K., Franzidis, J.P., Manlapig, E.V., "Studies on impeller type, impeller speed and air flow rate in an industrial scale flotation cell. Part 1: Effect on bubble size distribution"; Minerals Engineering, 8, 6, pp. 615-635, 1995[a].

Gorain, B.K., Franzidis, J.P., Manlapig, E.V., "Studies on impeller type, impeller speed and air flow rate in an industrial scale flotation cell. Part 2: effect on gas holdup"; Minerals Engineering, 8, 12, pp. 1557 – 1570, 1995[b].

Gorain, B.K., Franzidis, J.P., Manlapig, E.V., "Studies on impeller type, impeller speed and air flow rate in an industrial scale flotation cell. Part 3: effect on superficial gas velocity"; Minerals Engineering, 9, 6, pp. 639 – 654, 1996.

Gorain, B.K., Franzidis, J.P., Manlapig, E.V., "Studies on impeller type, impeller speed and air flow rate in an industrial scale flotation cell. Part 4: effect of bubble surface area flux on flotation performance"; Minerals Engineering, 10, pp. 367 – 379, 1997.

Gorain, B. K., "Optimization of flotation circuits with large flotation cells"; Centenary of Flotation Symposium, Ed. G.J. Jameson, AusIMM, Brisbane, Qld, June 6 – 9, pp. 843 – 851, 2005.

Grau, R.A., Heiskanen, K., "Gas dispersion measurements in a flotation cell"; Minerals Engineering, 16, pp. 1081 – 1089, 2003.

Harris, C.C., "Impeller speed, air and power requirements in flotation machine scale-up"; International Journal of Mineral Processing, 1, pp. 51 – 84, 1974.

Harris, C.C., "Flotation machines"; in Flotation, A.M. Gaudin Memoprial Volume, Vol. 2, Ed. M.C. Fuerstenau, AIME, New York, pp. 753 – 815, 1976.

Hernandez-Aguilar, J.R., Coleman, R.G., Gomez, C.O., Finch, J.A., "A comparison between capillary and imaging techniques for sizing bubbles in flotation systems"; Minerals Engineering, 17, pp. 53 – 61, 2004.

Jameson, G.J., Allum, P., "A survey of bubbles sizes in industrial flotation cells"; Report to AMIRA Ltd, 22 August, 1984.

Torrealba-Vargas, J.A., Gomez, C.O., Finch, J.A., "Continuous air rate measurement in flotation cells: a steps towards gas distribution management"; Minerals Engineering, 17, pp. 761 – 765, 2004.

Yianatos, J.B., Bergh, L., Condori, P., Aguilera, J., "Hydrodynamic and metallurgical characterization of industrial flotation banks for control purposes"; Minerals Engineering, 14 (9), pp. 1033 – 1046, 2001.

Chapter 5 - Measurement and Interpretation of Axial Pressure Profiles in Mechanically Agitated Flotation Machines

Abstract

In the mid nineties, a technique was developed to investigate axial bulk density variations in flotation columns (axial profiles). The technique, based upon pressure measurement with increasing depth (pressure profiles), was used to identify axial variations in gas holdup and to estimate froth depth for level control.

Large tank cells, typically 4 – 5 meters deep, offer a similar opportunity to use axial pressure profiling to probe the cell contents. The measurement device, mounted on a rigid support to resist the turbulence of mechanical cells, is described. Examples of profiles from different flotation plants around the world are presented. A methodology was developed to predict the shape of the profiles and identify axial variations in gas and solid holdup. It was found that pressure profiles from similar machine types show significant differences. Conversely, pressure profiles measured in multiple cells down a bank tend to be similar. It is therefore concluded that the shape of an axial pressure profile depends more on operational mode than machine type.

5.1 Introduction

Gas dispersion and hydrodynamic parameters are commonly identified as important for control of the flotation process (Arbiter and Steininger, 1965; Harris, 1974; Finch and Dobby, 1990). While it is accepted that within flotation machines local variations exist, in most cases, cells are characterized by parameters obtained overall or at a single

location. Experience has shown that potentially useful diagnostic information can be revealed by examination of spatial variations in gas dispersion parameters.

One technique to investigate variations in the axial direction is to measure axial pressure profiles (APP), i.e., the plot of hydrostatic pressure as a function of depth in a flotation machine. Hydrostatic pressure at any point within the machine is a function of gas, liquid and solid holdup, therefore axial pressure profiles can be used to identify variations in these parameters with depth.

Several studies have used axial pressure profiles to investigate flotation columns, which can be over 15 m in height. Gomez et al. (1995), using fixed pressure tapping points in laboratory and pilot columns, reported that gas holdup (ε_g) doubled over a height of 8 to 10 m. This increase was greater than could be attributed to bubble expansion and the origin was not fully explained.

Yianatos et al. (1995) measured pressure profiles in industrial columns using a portable pressure sensor to evaluate the effect of operating variables such as pulp density, gas flow-rate and interface level. Again, a significant increase in gas holdup (comparable to Gomez et al.) was observed from bottom to top. Relationships were established between the machine operating conditions and the shape of the axial pressure profile.

Gomez et al. (1997) used axial pressure measurements in columns to establish and control the position of the froth/pulp interface. They reported that the interface could be located by the point of change in the slope of the pressure vs. depth curve.

Garibay et al. (2002) studied the effect of percent solids on axial gas holdup profiles in

columns, finding that solid content could have a dramatic impact. Above a certain solid concentration, the gas holdup profile reversed and gas holdup decreased with height.

In the past 30 years, the capacity of mechanical flotation machines has increased significantly, some machines now exceeding 250 m^3 with heights of 5 m or more. Consequently, there is opportunity to transfer the axial profiling technology from columns. A sensor was developed by the candidate to measure axial pressure profiles, which is described in this chapter. Experiments performed by the candidate using the APP sensor have been performed in flotation plants in Canada, the United States, Chile, Australia and South Africa. Results from four plants are presented and interpreted.

In general, axial pressure profiles measured in flotation columns tended to be approximately linear. In certain cases, profiles measured in mechanical machines show significant deviations from linearity. In order to resolve the origins of the observed non-linearity, a methodology incorporating volumetric gas expansion and the drift flux model was developed to predict the shape of axial pressure profiles. Details of this procedure are discussed.

5.2 The Axial Pressure Profile Sensor

The sensor is an adaptation of the McGill gas rate (J_g) sensor (Gomez et al., 2003[a]; Torrealba-Vargas et al., 2004). The working principle of the APP sensor is that in a submerged tube full of air with the top sealed, the pressure is equal to the hydrostatic pressure above the tube opening (Figure 5.1).

The J_g sensor requires tube diameters of 3 to 4 inches to ensure representative bubble sampling (Torrealba-Vargas, 2005). Since sampling is not an issue in the APP sensor, the diameter of the tubes used can be reduced. In most cases tubes with a diameter of 2 inches are employed. This diameter could be further reduced but at a cost of tube rigidity.

It is a key requirement of the APP sensor to be sufficiently rigid to withstand the turbulent flows in the mixing zone of mechanical machines. Typically, PVC tubes less than 2 inches in diameter tend to flex when subjected to these forces. To provide additional support, the sensor is attached to sections of galvanized steel rod that form a rigid frame. The steel sections extend 4 – 5 meters above the APP sensor allowing it to be lowered to near the bottom of the largest cells.

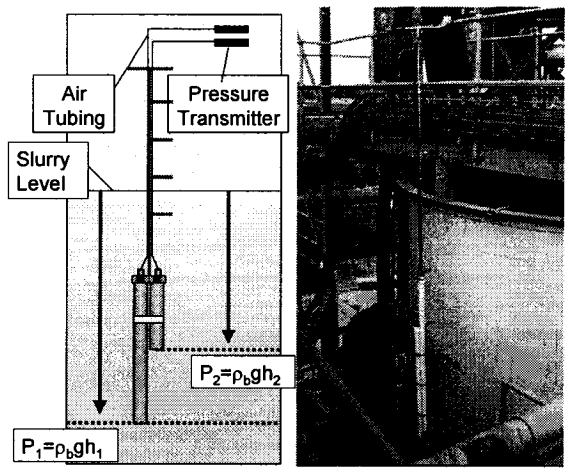

Figure 5.1– Schematic and in-plant photograph of the axial pressure profile sensor.

As with the J_g sensor, the pressure inside the APP sensor is measured using Wika piezo-electric pressure transmitters. Typically, multiple pressure transmitters with appropriate ranges are used (0 – 127 cm up to 0 - 700 cm H_2O) to accommodate the wide range in

pressures to be measured. The analog pressure transmitter signals are converted by 12 bit analog/digital modules and directed to a laptop computer via RS-232 serial communication. The data is stored and displayed using iFIX 3.5 (GE Fanuc Automation).

In all cases, two tubes are used (see Figure 5.1) allowing simultaneous pressure measurement at 2 locations. Consequently, measured pressure profiles comprise two independent data sets producing overlaying curves, increasing confidence in the profile results.

5.3 Experimental Procedure

The sensor is submerged below the pulp/froth interface and fixed in position for 5 minutes, pressure measurements being saved at intervals of 1 second. After the 5 minutes, the sensor is lowered, typically 50 cm, and a further set of 300 points is collected. This procedure is repeated to cover the vertical distance of the machine.

When the sensor descends, pressure causes compression of the gas inside the tube. As a result, some pulp could enter the tube making the pressure measured by the instrument slightly less than the hydrostatic head at the bottom of the tube. In most cases however, the air present in the machine (i.e., bubbles) quickly re-fills the tube, restoring measurement. Concern arises when the probe enters a zone void of gas where the bias will not be eliminated. A solution would be to implement a system to replenish air from the surface, ensuring the tubes are always filled.

5.4 Model to Predict Pressure Profile

A calculation procedure (model) was developed to predict the shape of a pressure profile under various conditions and has been used to interpret results. The procedure aims to determine how gas dispersion and hydrodynamic parameters influence the shape of the pressure profile. As a starting point, calculations assume that the cell is well-mixed and therefore, that slurry density (ρ_{sl}) is uniform throughout the machine. Hence, the only variable is the gas holdup. Using a Visual Basic routine incorporated into an Excel spreadsheet, a procedure (model) to calculate changes in gas content with depth was developed.

The model requires that gas holdup, gas velocity and slurry density (de-aerated) be known at a particular depth and pressure. Since the APP sensor is typically used in conjunction with the standard McGill gas dispersion sensors (Gomez and Finch; 2002), values of gas holdup, superficial gas velocity and bulk density are available. Based on measurements of gas holdup and bulk density, the slurry density can be estimated using equation (1) where ρ_b is the bulk density (air, liquid, solid).

$$\rho_{sl} = \frac{\rho_b}{(1-\varepsilon_g)} \qquad \textbf{(5.1)}^3$$

Using ρ_{sl}, ε_g and J_g, bubble size (D_b) can be estimated using drift flux analysis (Wallis, 1969; Masliyah, 1979; Yianatos et al., 1988).

Assuming that over a small increment in depth, there is no variation in ρ_b, the change in

---

[3] Equation 1 is a simplified equation considering that the density of gas is negligible.

J_g and D_b can be calculated using Boyle's law. Subsequently, using the new J_g and D_b, a new value of ε_g can be predicted using the drift flux model and a new value of ρ_b can be calculated based on the ε_g. With the new value of ρ_b, the change in J_g and D_b can be calculated for a new small increment in depth. This procedure is repeated as required to generate a theoretical axial pressure profile. (Generation of a profile by the above procedure, across 10 meters at intervals of 5 cm, can be completed in less than 1 second.)

To validate, the calculation was tested against an experimental axial pressure profile reported in Gomez et al. (1995). The profile was measured in a pilot column, 12 m in height, operating with only air and water (i.e., ρ_{sl} = 1 g/cm^3). Starting values of J_g and ε_g were taken at a depth of 1 m based on data from the paper. The calculation agrees with the experimental results (Figure 5.2).

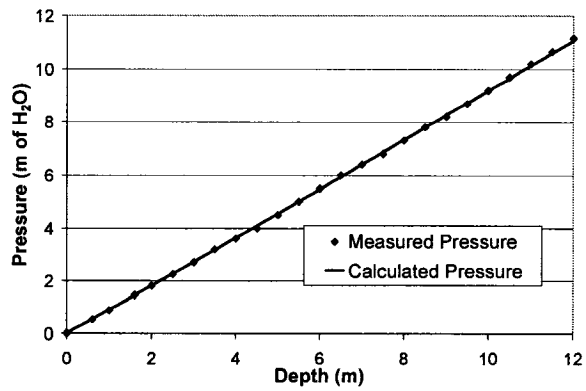

Figure 5.2 – Calculated pressure profile in a 2-phase pilot column compared to the measured pressure profile.

A detailed explanation of the model is attached as Appendix 1.

5.5 Case Studies

Using the APP sensor, measurements of axial pressure profiles have been performed in a variety of mechanical flotation machines. In this chapter, results from four plants are presented. The calculation procedure is used to help interpret the measured profiles. The case studies demonstrate the effect of froth depth, gas holdup, solid content, cell geometry and gas deficient zones on the shape of a pressure profile.

5.5.1 Case 1 – Outokumpu 70 m^3

Axial pressure profiles were measured in four Outokumpu (OK) 70 m^3 cells from the same bank in Anglo-Platinum's Waterval concentrator. Results are displayed in Figure 5.3. It can be noted that the shape is significantly different from the 2-phase result in Figure 5.2 (the profile from the pilot column was linear while the profile from the OK 70 has an increasing slope). It is also noted that the measured pressure profiles are all similar across the bank. The curves for cell 2, 3 and 5 lie directly on top of each other. The curve for cell 1 demonstrates a similar shape, but is shifted to the left, likely indicative of a different froth depth in the cell (Yianatos et al., 1995).

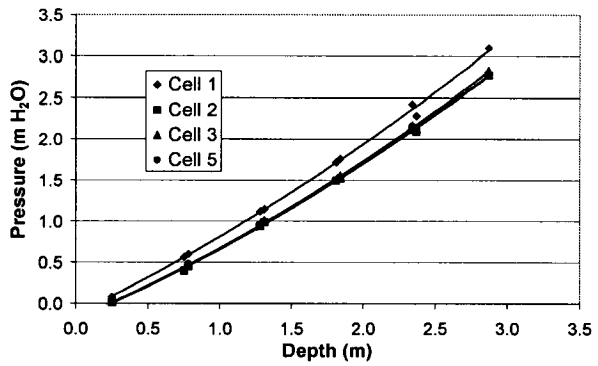

Figure 5.3 – Pressure profiles measured in 4 OK-70 cells across a flotation bank.

The similarity among the profiles in the four cells helps establish that conditions are not changing during the test. For example, the increasing gradient in Figure 5.3 could be caused by a gradual decrease in froth depth as the sensor is submerged. Because the same curvature is observed in each cell, it is unlikely that identical changes would have occurred in each of the cells.

The calculation procedure was used to examine the shape of the pressure profile. The factors considered include: froth depth, gas holdup, solid content and cell geometry. The calculated results were compared to the measurements from cell 2 as representative of the four. In this cell, gas holdup data were available at 150 and 200 cm below the top of the froth and gas rate was measured at 130 and 200 cm below the top of froth. The calculation is initiated based on the gas holdup at 150 cm and the gas rate at 130 cm, corrected to the hydrostatic pressure at 150 cm. This location was selected because the cross sectional area of the flotation machine was known at this depth. The first calculations were performed assuming a uniform slurry density throughout with depth.

5.5.1.1 Froth Depth

Figure 5.4 compares the experimental results with calculations performed assuming 3 froth depths. The froth depth impacts the axial pressure profile by shifting it either right (more froth) or left (less froth) as froth depth changes the volume of the cell occupied by low density material.

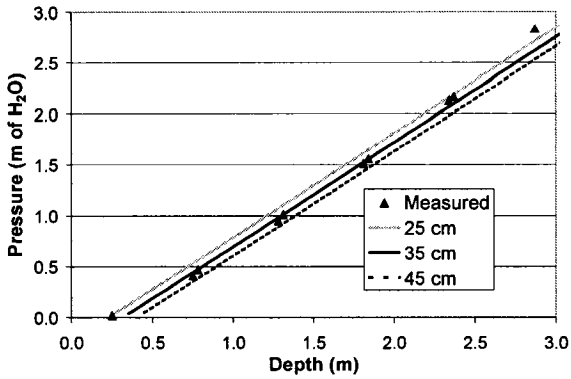

Figure 5.4 – Experimental results compared to calculation at selected froth depths (OK 70 cell)

Figure 5.4 shows that a froth depth of 35 cm gives the best fit to the experimental data (which, incidentally, matched the plant control room value). However, it is noted that the experimental points at 2.4 and 2.9 meters lie above the calculated curve. The implication is that towards the bottom of the machine, the contents (gas + liquid + solid) are more dense than predicted.

5.5.1.2 Gas Holdup

The possibility of an error in the measured gas holdup at 150 cm was considered. The calculations (Figure 5.5) show that changes in gas holdup impact the slope of the axial pressure profile, but will not cause any significant change in curvature. By varying ε_g and froth depth, it is possible to fit sections of the experimental data, but it is not possible to fit across the whole range.

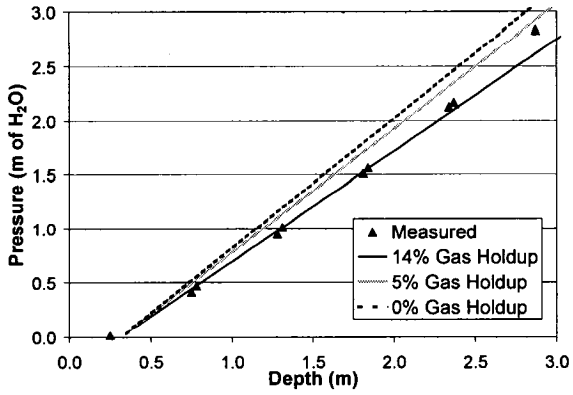

Figure 5.5 – Experimental results compared to calculations at selected gas holdups (OK-70 cell).

5.5.1.3 Slurry Density

Calculations were performed at various slurry densities to investigate if this parameter could account for the curvature in the experimental data.

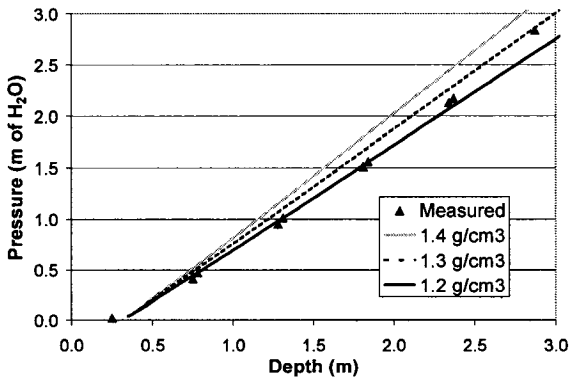

Figure 5.6 – Experimental results compared to calculated results at selected slurry densities.

Similar to the case of varying gas holdup, changes in pulp density cause changes in slope of the pressure profile but have little impact on its curvature.

5.5.1.4 Cell Geometry

One parameter that can cause curvature in the axial pressure profile is cell geometry. All

calculations presented above assumed a constant cross sectional area (CSA) with depth in the machine.

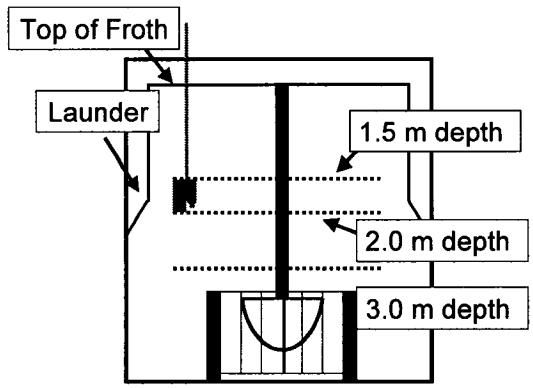

Figure 5.7 – Sketch of an OK 70 illustrating changes in cross sectional area.

In reality there is a change in CSA at around 2 m in the cell caused by the presence of an internal launder (Figure 5.7). As a consequence, variations in ε_g and J_g around the bottom of the launder are expected. To confirm, ε_g measurements were taken at 1.5 and 2.0 m using the McGill gas holdup sensor (Gomez et al., 2003[b]), which revealed the expected decrease in gas holdup as CSA increases with depth (Figure 5.8).

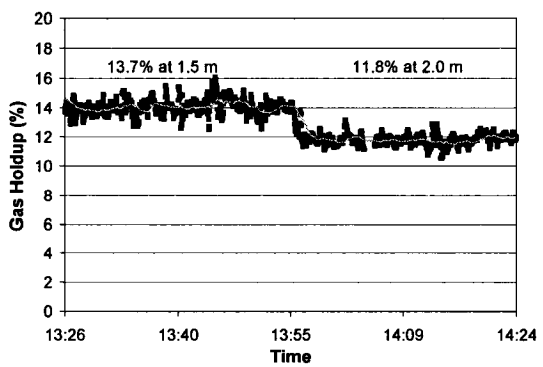

Figure 5.8 – Gas holdup signals at two depths: note the lower gas holdup at 2.0 m expected as CSA is greater than at 1.5 m.

The calculation procedure was repeated considering the changes in cross sectional area.

Figure 5.9 shows the calculated gas holdup and gas rate profiles, considering both a constant and variable CSA, compared to the experimental data. It was found that the changes in CSA reasonably accounted for the measured changes in gas holdup and gas rate. The effect was a closer fit to the measured axial pressure profile (Figure 5.10).

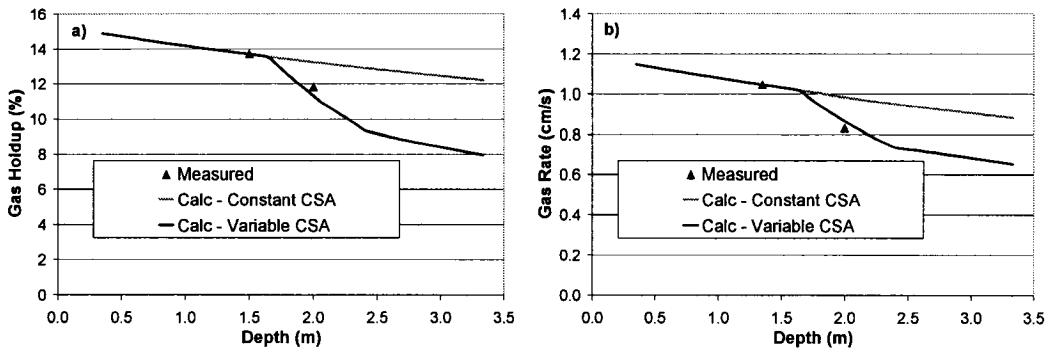

Figure 5.9– Comparison between a) measured and calculated gas holdup profiles and b) measured and calculated gas rate profiles considering constant and variable CSA.

While the fit to the curvature is closer, there is still a lack of fit at 2.9 meters where the measured pressure remains higher than predicted. This means that the density of material (indicated by the slope of the pressure profile) between 2.0 and 3.0 m was greater than accounted for by the model. Increased bulk density can be due to either increased solid holdup or decreased gas holdup.

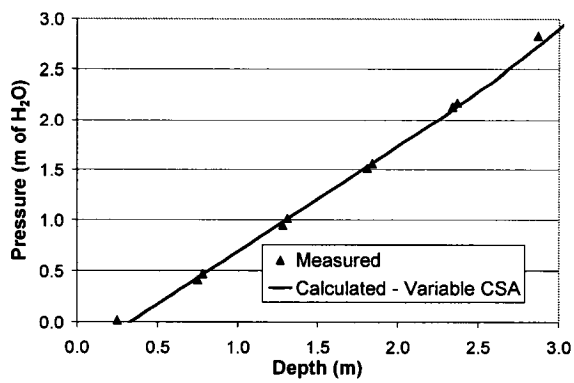

Figure 5.10 – Calculated pressure profile considering a variable cross sectional area.

Calculation shows that even if the area were completely void of air, the change in the shape of the pressure profile would still not account for the experimental results (and it is unlikely from the cell design that air is absent at 3 m). Therefore, the most likely explanation of the higher than expected density between 2 and 3 m is a concentration of solids towards the bottom of the cell, a hypothesis consistent with these machines (Gronstrand et al., 2006).

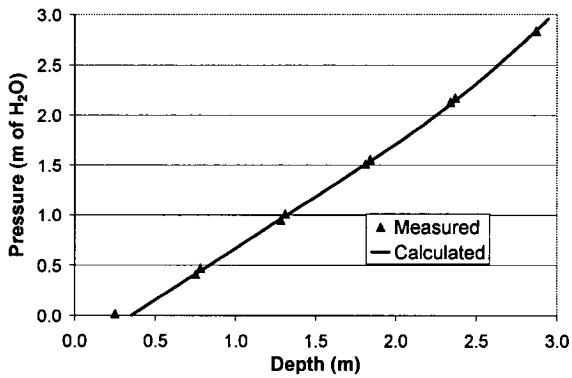

Figure 5.11 – Calculation results considering a linear increase in pulp density.

To examine if this offers a realistic explanation, the effect of a linear slurry density increase from 1.2 to 2 g/cm^3 from the top to the bottom of the machine was considered. The calculation fits the experimental results (Figure 5.11). Assuming a solid density of 3 g/cm^3, this gives a percent solids (by mass) of 75 % at 3 m. This is feasible. The increasing slope of the axial pressure profile may be a warning that sanding is occurring.

5.5.2 Case 2 – Outokumpu 100 m^3

Pressure profiles were measured in four OK 100 flotation machines in a bank of six at

Mount Keith operation in Western Australia (now BHP Billiton, formerly WMC). Similar to the case above, the profiles all demonstrated upward trends (Figure 5.12).

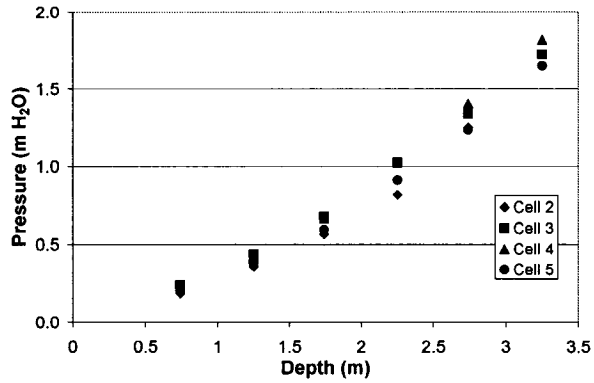

Figure 5.12 – Pressure profiles measured in four OK 100 flotation machines.

The results in cell 2 were used in the exercise. The first observation (Figure 5.13) is the change in slope now apparent at a depth of ca. 2 m. Recalling that the slope of the pressure vs. depth curve is the bulk density, in this case the bulk density in the top 2 m was approximately 0.4 g/cm^3. Typical experience has been that bulk densities in flotation pulp zones range from 0.9 to 1.1 g/cm^3. Even a decrease in solid content to zero can not account for such a low bulk density; the only factor that could explain the low density is an elevated gas holdup, in the order of 60 - 70 %.

The bulk density at depths greater than 2 m was about 0.8 g/cm^3, i.e., close to the expected range. The inference is that the density change is most likely associated with a change in gas holdup; i.e., that there is an "interface" located at approximately 1.9 m where density changes.

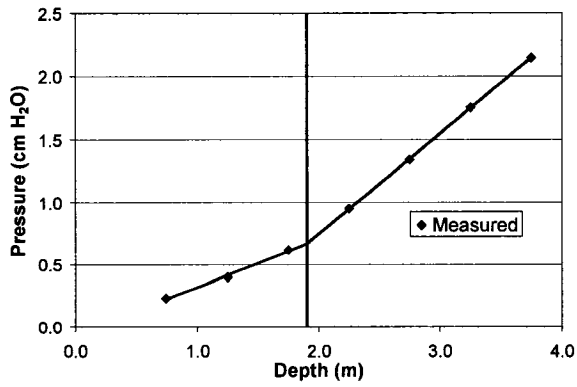

Figure 5.13 – Axial pressure profile measured in cell 2 of 6 showing apparent interface at ca. 1.9 m.

Other research groups have previously reported, without comment, similarly high values of gas holdup (Schwarz and Alexander, 2005). The axial pressure profile here supports that this can occur and, further, identifies a change in gas holdup with depth inside the machine.

The origin of the high gas holdup remains unknown. Typical froths have gas holdups > 80 % (Tavera et al., 1998) thus this zone above 2 m is not froth in that sense, and further, froth depth was controlled at 30 cm (measured using a float device), a value supported by the initial surveys. One hypothesis is that the phase down to 2 m is froth that is more dense than the floating device, thus causing a measurement error. A second hypothesis is that the material is a 'third phase', one between froth and pulp. Existence of 'third phase', low shear, high gas fraction zones below the froth have been previously suggested (Jameson, 2005). While the cause of the low density region above 2 m is not known, a possible explanation is that the pulp chemistry in this particular plant tends to facilitate small bubble production and high froth stability.

An alternate possibility for the formation of the high gas phase was the presence of a

froth cone at the top of the machine. By restricting the effective area through which gas is passing, the gas holdup will increase. Dimensions of froth cones used in Outokumpu machines tend to vary from plant to plant. Calculations were performed to determine the impact of froth cones of different diameter on the APP, assigning a cone depth of 1.6 m.

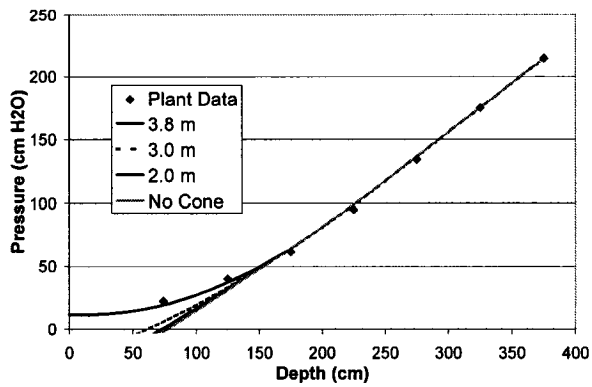

Figure 5.14 – Calculated axial pressure profiles with different size froth cones.

Figure 5.14 demonstrates that below 3 m in diameter, the predicted impact of a froth cone on the pressure profile is minor. In this case, a froth cone of 3.8 m in diameter could account for the shape of the pressure profile.

5.5.3 Case 3 – Outokumpu 100 m^3

Two cases have been presented in which the axial pressure profile measured in a large OK flotation machine demonstrated significant curvature. In case 3, measurements taken in an OK 100 cell (BHP Billiton's Escondida (Los Colorados)) operation yield a profile that appears more linear (Figure 5.15).

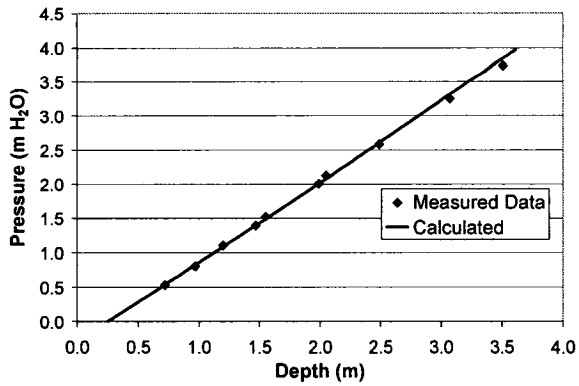

Figure 5.15 – Axial pressure profile from an OK 100 in Chile.

The model prediction is in reasonable agreement with the measured data. There is slight disagreement at the largest depths (> 3m). Given that in this case, a profile was measured in only 1 cell, it is difficult to establish that the lower than expected value between 3 and 4 m is not due to a process change (e.g., increase in froth depth) during the experiments. The plant control room tends to support this possibility as level oscillations were detected. An alternate explanation could be a bias in the measurement technique. As noted earlier, if the sensor is placed in a region void of air, pressure measurements will be lower than the true value.

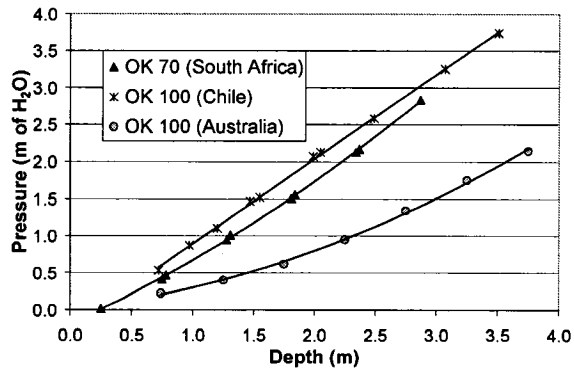

Figure 5.16 – Comparison of axial pressure profiles measured in three OK flotation machines.

Comparison of the three Outokumpu type cells shows that similar machines can demonstrate significantly different axial pressure profiles (Figure 5.16). Since profiles for cells in the same bank are similar, axial pressure profiles seem to be more indicative of the operational mode, and less a function of machine type.

5.5.4 Case 4 – Wemco 90 m^3

An axial pressure profile was measured in a Wemco 90 m^3 machine (Rio Tinto's Kennecott operation) where, in addition, axial gas holdup and gas rate measurements were made.

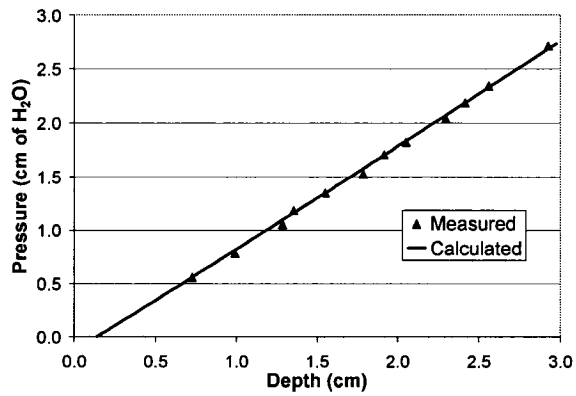

Figure 5.17 – Axial pressure profile measured in a Wemco 90.

Based upon the ε_g and J_g measured at 1.5 m, model calculations were compared to the experimental data (Figure 5.17). While the calculated pressure profile showed reasonable agreement, the calculated ε_g and J_g profiles did not (Figure 5.18). Given the design of Wemco machines, it is reasonable to expect a decrease in gas holdup and gas rate with increasing depth. This expectation was confirmed by the measurements. In this region it is also expected that the majority of the air present is entrained by the fluid streamlines, i.e., small bubbles with less buoyancy would make up a large fraction of the bubble

population.

A second calculation was performed assuming a linear decrease in gas rate below 1.7 m, to determine the impact on the shape of the pressure profile. A comparison between measured and calculated ε_g and J_g employing this assumption is shown to fit the gas rate and gas holdup data in Figure 5.18. The corresponding calculated axial pressure profile is shown in Figure 5.19.

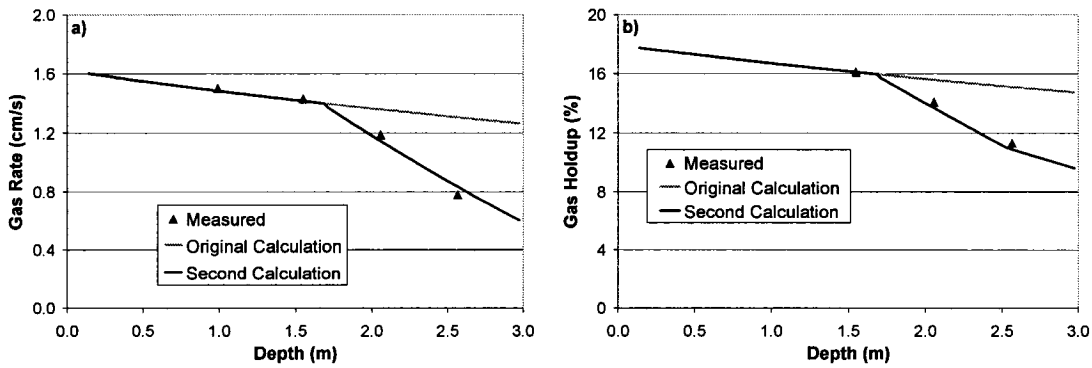

Figure 5.18– Measured a) J_g and b) ε_g profiles compared to calculations assuming constant air (original) and diminishing air with depth (second).

From Figure 5.19 it is noted that the assumption of diminishing air content had a relatively small impact on the calculated axial pressure profile. Since bulk density is proportional to gas holdup and the slope of the axial pressure profile is equal to the bulk density this means that a 5 percent change in gas holdup corresponds roughly to a 5% change in slope. The result is that even large changes in gas holdup tend to have a relatively small effect on the shape of the axial pressure profile.

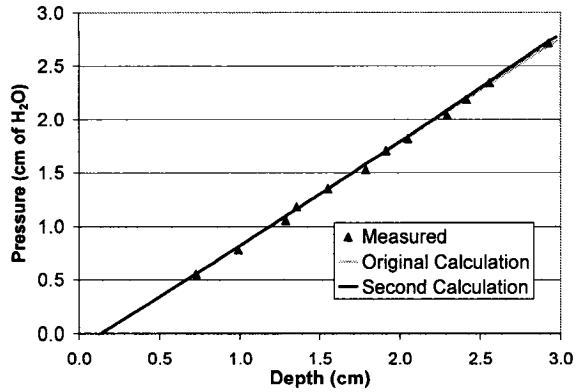

Figure 5.19 – Comparison of measured axial pressure profile and calculated profile considering linear decrease in gas rate with depth.

It should be noted that the calculations here consider constant slurry density with depth. It is likely that there is an increase in solid content, and therefore slurry density, with depth in any flotation machine.

As a note, since the McGill J_g and ε_g sensor measurements are dependant on sampling rising bubbles, with depth a sampling error may be introduced as bubble flow becomes more random because of the turbulence due to proximity of the impeller in mechanical machines. At this stage, the magnitude of any error is unknown (note that this error does not apply to the APP sensor).

5.6 Conclusions

The technique of axial pressure profiling, originally developed to investigate column flotation performance, can be applied to the new generation of large mechanical flotation cells.

The technique has been tested in a variety of flotation machines. It is found that the

shape of the axial pressure profile tends to be dependant on the operational conditions of the machine rather than machine type. Across a bank, machines tend to demonstrate similar pressure profiles while machines of similar type performing different duties can demonstrate significantly different profiles.

A model prediction routine was developed that facilitated off-line interpretation of the axial pressure profiles. Examples were presented pointing to increases in solid content (% solids) with depth and the impact of cell geometry. One case apparently identifying a high gas holdup region (a 'third phase') was described.

The axial pressure profiling technique, combined with the computational analysis, provides a way to investigate the nature of axial gas dispersion and hydrodynamic parameter variation within large mechanical flotation machines.

5.7 References

Arbiter, N., Steininger, J., "Hydrodynamics of flotation machines"; In: E. Roberts (Editor), Mineral Processing, Pergamon, New York, pp. 595 – 608, 1965.

Finch, J.A., Dobby, G.S., Column Flotation; Pergamon Press, 1990.

Garibay, R.P., Gallegos, P.M., Uribe-Salas, A., Nava, F.A., "Effect of collection zone height and operating variables on recovery of overload flotation columns"; Minerals Engineering, 15, pp. 325 – 331, 2005.

Gomez, C.O., Uribe-Salas, A., Finch, J.A., Huls, B.J., "Axial gas holdup profiles in the collection zones of flotation columns"; Minerals and Metals Processing, February, pp. 16

– 23, 1995.

Gomez, C.O., Fernandez, J., Finch, J.A., "Observations on level measurement in flotation columns from pressure readings"; 36th annual conference of metallurgists of CIM, Processing of Complex Ores: Mineral Processing and the Environment, Sudbury, Ontario, August 17-19, pp. 21 – 32, 1997.

Gomez, C.O., Finch, J.A., "Gas dispersion measurements in flotation machines", CIM Bulletin, October/November, pp. 73 – 78, 2002.

Gomez, C.O., Torrealba-Vargas, J.A, Dahlke, R., Finch, J.A., "Measurement of gas velocity in industrial flotation cells"; International Mineral Processing Conference, Vol. 3, pp. 1703 – 1713, 2003[a].

Gomez, C. O., Cortés-Lopez, F., Finch, J.A., "Industrial testing of a gas holdup sensor for flotation systems"; Minerals Engineering, 16, pp. 493 – 501, 2003[b].

Gronstrand, S., Niitti, T., Rinne, A., Turenen, J., "Enhancement of flow dynamics of existing flotation cells"; proceedings of the 38th annual meeting of the Canadian mineral processors, Ottawa, Canada, pp. 403 – 422, 2006.

Harris, C.C., "Impeller speed, air and power requirements in flotation machine scale-up.", International Journal of Mineral Processing, 1, pp. 51 – 84, 1974.

Masliyah, J.H., "Hindered settling in a multispecies particle system"; Chemical Engineering Science, 39 (4), pp. 1166 – 1168, 1979.

Jameson, G.J., "Flotation of coarse and ultrafine particles"; Centenary of Flotation

Symposium, Ed. G.J. Jameson, AusIMM, Brisbane, Qld, p. 33, 2005.

Schwarz, S., Alexander, D., "Gas dispersion measurements in industrial flotation cells"; Centenary of Flotation Symposium, Ed. G.J. Jameson, AusIMM, Brisbane, Qld, June 6 – 9, pp. 265 - 269, 2005.

Tavera, F.J., Gomez, C.O., Finch, J.A., "Estimation of gas holdup in froths by electrical conductivity: application of the standard addition method"; Minerals Engineering, 11, 10, pp. 941 – 947, 1998.

Torrealba-Vargas, J.A., Gomez, C.O., Finch, J.A., "Continuous air rate measurement in flotation cells: a step towards gas distribution management"; Minerals Engineering, 17, pp. 761 – 765, 2004.

Torrealba-Vargas, J.A., PhD Thesis; McGill University, Montreal, Quebec, Canada, 2005.

Wallis, G.B., One-Dimensional Two Phase Flow; McGraw-Hill, New York, 1969.

Yianatos, J.B., Finch, J.A., Dobby, G.S., Xu, M., "Bubble size estimation in a bubble swarm"; Journal of colloid and interface science, 126 (1), pp. 37 - 44, 1988.

Yianatos, J.B., Bergh, L.G., Sepulveda, C., Nunez, R., "Measurement of axial pressure profiles in large-size industrial flotation columns"; Minerals Engineering, 8(1/2), pp. 101-109, 1995.

Chapter 6 - General Conclusions

6.1 Concept of Cell Characterization

Gas dispersion, defined as the suspension of gas bubbles in slurry, can be quantified by a set of so-called gas dispersion parameters. These parameters include superficial gas velocity (gas rate, J_g), gas holdup (ε_g), bubble size (D_b) and bubble surface area flux (S_b). Measurement of these parameters is facilitated by the development of a set of tools, known as gas dispersion sensors.

Cell characterization is a term used frequently in the application of gas dispersion parameters. In this thesis it is used to describe tests that employ sensors to assess the gas dispersion in a particular flotation machine. These tests include identifying relationships between operating variables and gas dispersion parameters, and investigating spatial variations in the gas dispersion.

6.2 Manipulation of Gas Dispersion Parameters via Operating Variables

It has been demonstrated that manipulation of gas dispersion parameters can yield improved metallurgical performance. For controlled manipulation of gas dispersion parameters, it is important to have an understanding of the relationships between operation variables and the resulting gas dispersion.

Case studies are presented, showing how gas dispersion parameters can be manipulated in forced air and self-aerated mechanical flotation machines.

In forced-air machines, airflow rate (AFR) can be used to manipulate gas dispersion

parameters. It was noted that relationships between J_g and AFR can vary from cell-to-cell across a bank. Investigating these relationships can identify malfunctioning components. Measured gas holdup vs. gas rate (ε_g vs. J_g) and Sauter mean bubble size vs. gas rate (D_{32} vs. J_g) are presented as key relationships that characterize the ability of a machine to form a gas dispersion. It is shown that identical machines in a bank can demonstrate different ε_g vs. J_g and D_{32} vs. J_g relationships. These differences usually are attributable to chemical factors (e.g., different frother concentration).

In self-aerated machines, manipulation of gas dispersion parameters was found to be more complicated, and to require more time for the cell to reach a steady state. However, it was demonstrated that the gas dispersion parameters in a self-aerated machine can be manipulated by variation in froth depth, impeller speed and impeller submergence. It was found that increases in froth depth and impeller speed resulted in increased gas rate and gas holdup, while increases in submergence resulted in a decrease in gas rate.

6.3 Sample Point Selection via Multi-Jg Radial Mapping

Radial mapping is a test designed to investigate variation in gas dispersion parameters as a function of distance from the impeller axis. In prior exercises this was done by moving a single gas rate sensor from location to location. In an industrial setting, the operating parameters of a machine can vary and as a result, when a single sensor is moved from one location to another, there is a possibility that properties of the gas dispersion will change. Therefore, the resulting "map" of gas rate my not be solely a function of location, but also a function of time. The development of a multi-Jg sensor that is capable of measuring gas rate simultaneously at multiple locations has facilitated the elimination of

time as a variable, so that the generated "map" of gas rate is purely a function of location. An additional impact of the multi-Jg sensor is that mapping tests can be completed more quickly (minutes rather than hours). These capabilities of the multi-sensor unit have been demonstrated in plant environments.

Down-the-bank optimization routines have been proven capable of increasing the metallurgical performance of a flotation bank. It is suggested that careful selection of the cell sampling point is a key step towards success of the exercise. A methodology, applying the multi-Jg sensor, is offered as a way to select the sampling point for down-the-bank metallurgical optimization.

6.4 Axial Pressure Profiling using an Axial Pressure Profile Sensor

A technique known as axial pressure profiling was originally developed to investigate axial variation in flotation columns. The new generation of large tank cells offer a similar opportunity to investigate axial pressure profiles.

A sensor capable of measuring axial pressure profiles was developed and tested in industrial machines. The experience from four plants was described. In general it was found that axial profiles in machines of similar type could differ significantly. However, it was noted that across a bank, machines tended to show similar axial profiles. As a result, it is concluded that axial pressure profiles depend more on the operating conditions rather than machine type.

A model prediction routine was developed that facilitated the off-line interpretation of the axial pressure profiles. Examples were presented pointing to variations in solid and gas

holdup. The axial pressure profiling technique combined with the computational analysis, provides a way to investigate the nature of axial gas dispersion and hydrodynamic parameter variation within large mechanical flotation machines.

6.5 General Conclusions

The components of cell characterization presented in this thesis, including investigation of spatial variations in dispersion parameters and measuring the impact of operating variables on the gas dispersion, do not in themselves result in metallurgical improvements for a flotation plant. Rather, these procedure provide the knowledge that will facilitate plant trouble shooting, stability evaluation and successful down-the-bank optimization routines.

Appendix 1 – Model for Pressure Profile Determination

The following is the calculation procedure used to predict axial pressure profiles. The procedure was developed in order that the calculation could be performed using Microsoft Excel and Visual Basic. Sample numbers are included in the explanation.

Initial Measured Parameters

Before the calculation is run, J_g, ρ_b and ε_g are measured at a particular depth and pressure. For this example, consider at a depth of 1.0 m and a pressure of 100 cm H_2O (P_l), J_g was measured to be 1.2 cm/s, bulk density (ρ_b) 1.0 g/cm^3 and ε_g 10 %. We will consider that atmospheric pressure (P_{atm}) is 1033 cm H_2O. Slurry viscosity (μ_{sl}) will be taken as 0.01002 Pa·s. Density of the bubble particle aggregate (ρ_{bp}) will be taken as 0.02 g/cm^3. A constant slurry temperature within the machine is assumed. The axial liquid velocity (J_l) will be considered to be 0. The froth depth will also be considered to be 0. The diameter of the flotation machine is taken as 5.0 meters.

Determination of Slurry Density

Slurry density (ρ_{sl}) is calculated using Equation (1).

$$\rho_{sl} = \frac{\rho_b}{(1-\varepsilon_g)} \qquad \text{---------- (1)}$$

In this case, slurry density is calculated to be 1.11 g/cm^3. Bubble size at this depth is calculated by the drift flux model using the following strategy.

Calculation of Initial Bubble Size Using Drift Flux Model and Excel

Bubble size (D_b) is assumed to be 0.1 cm and the single bubble Reynolds number (Re_b) is assumed to be 100. The assumption values are not critical; they will be manipulated throughout the calculation. Using these assumptions, the bubble terminal velocity ($U_{t(mas)}$) is calculated using the Masliyah equation (2). In Equation (2), g is the gravitational constant (980.6 cm/s^2).

$$U_{t(mas)} = \frac{gD_b^2(\rho_{sl} - \rho_{bp})}{18\mu_{sl}(1 + 0.15\mathrm{Re}_b^{0.687})} \qquad \text{---------- (2)}$$

From the value of $U_{t(mas)}$ a value of Re_b is calculated using Equation (3).

$$\mathrm{Re}_b = \frac{\rho_{sl} U_{t(mas)} D_b}{\mu_{sl}} \qquad \text{---------- (3)}$$

At this stage, when using Excel, the value calculated using Equation (3) can be inserted into Equation (2) to generate a new value of $U_{t(mas)}$. In most computers, when Re_b from Equation (3) is inserted into Equation (2), Excel will give a warning that a circular reference has been created. By selecting "Options" in the "Tools" menu, and then selecting the "Calculations" tab, Excel can be set to perform iterations (i.e., repeats calculation 2 and 3 until the values of $U_{t(mas)}$ are not changing). When this is set, Excel will rapidly converge upon a value for Re_b. For this example, if D_b is assumed to be 0.1 cm, then Re_b should converge to 164 and $U_{t(mas)}$ should be 12.9 cm/s.

Subsequently, a value for the parameter m is determined using Equation (4), (5) or (6). In Equation (4), D_c is the diameter of the flotation machine which in industry, is significantly larger than the bubble size, effectively reducing Equation (4) to Equation (5). In the case of this example, m is calculated as 2.68.

$$if\,(\mathrm{Re}_b) \le 200 \rightarrow m = (4.45 + 18\frac{D_b}{D_c})\mathrm{Re}_b^{-0.1} \quad \text{---------- (4)}$$

$$if\,200 < (\mathrm{Re}_b) <= 500 \rightarrow m = 4.45\mathrm{Re}_b^{-0.1} \quad \text{---------- (5)}$$

$$if\,(\mathrm{Re}_b) \ge 500 \rightarrow m = 2.39 \quad \text{---------- (6)}$$

Simultaneously the drift flux bubble swarm velocity ($U_{bs(d)}$) is calculated using Equation (7) and used to calculated the bubble swarm Reynolds number (Equation (8)).

$$U_{bs(d)} = \frac{J_g}{\varepsilon_g} + \frac{J_l}{1-\varepsilon_g} \quad \text{---------- (7)}$$

$$\mathrm{Re}_{bs} = \frac{\rho_{sl} U_{bs(d)} D_b (1-\varepsilon_g)}{\mu_{sl}} \quad \text{---------- (8)}$$

Using the value of Re_{bs} from Equation (8), the Masliyah bubble swarm velocity ($U_{bs(mas)}$) is calculated from Equation (9).

$$U_{bs(mas)} = \frac{gD_b^2(\rho_{sl} - \rho_{bp})(1-\varepsilon_g)^{(m-1)}}{18\mu_{sl}(1+0.15\mathrm{Re}_b^{0.687})} \quad \text{---------- (9)}$$

There will be an initial disagreement between the values of $U_{bs(d)}$ and $U_{bs(mas)}$. If $U_{bs(d)}$ is greater than $U_{bs(mas)}$ then the estimate of D_b was too small. The reverse is true if $U_{bs(d)}$ is smaller than $U_{bs(mas)}$. Using a Visual Basic routine, bubble size can be manipulated until the magnitude of the difference between $U_{bs(d)}$ and $U_{bs(mas)}$ is reduced to below 0.01 cm/s. In this case, it is found that the two values of U_{bs} converge at 12.0 cm/s when D_b is equal 0.11 cm.

Parameter Correction to Top of Slurry Zone

Once a value of D_b has been determined, both the values of J_g and D_b must be corrected to the pressure at the top of the slurry zone. In this example, as there is no froth depth, the pressure at the top of the slurry zone is equal to atmospheric. The new J_g and D_b values are calculated by Equations (10) and (11) where $J_{g(t)}$ and $D_{b(t)}$ correspond to the parameter values at the top of the slurry zone and $J_{g(m)}$ and $D_{b(m)}$ correspond to parameters at the measured pressure. Note that in Equations (10) and (11), the units of pressure should be cm H_2O, the froth density (ρ_f) should be in g/cm^3 and the froth depth should be expressed in cm.

$$J_{g(t)} = \frac{J_{g(m)}(P_{atm} + P_l)}{(P_{atm} + \rho_f \cdot f_d)} \qquad \text{---------- (10)}$$

$$D_{b(t)} = D_{b(m)}\left[\frac{(P_{atm} + P_l)}{(P_{atm} + \rho_f \cdot f_d)}\right]^{\frac{1}{3}} \qquad \text{---------- (11)}$$

In this case, $J_{g(t)}$ is 1.32 cm/s and $D_{b(t)}$, 0.12 cm.

Determining ε_g at Top of Collection Zone

The drift flux model is used to determine the value of ε_g at the top of the slurry zone ($\varepsilon_{g(t)}$) based on $J_{g(t)}$ and $D_{b(t)}$. The following portion of the procedure is driven using a Visual Basic routine.

The first step is to calculate the single bubble terminal velocity (U_t). To start this calculation, Re_b is assumed to be 100. U_t is calculated by Equation (12).

$$U_t = \frac{\mathrm{Re}_b \mu_{sl}}{\rho_{sl} D_b} \qquad \text{---------- (12)}$$

U_t is subsequently calculated using the Masliyah equation (Equation (13)).

$$U_{t(mas)} = \frac{g D_b^2 (\rho_{sl} - \rho_{bp})}{18 \mu_{sl} (1 + 0.15 \mathrm{Re}_b^{0.687})} \qquad \text{---------- (13)}$$

Based on the results from Equation (13), a new value of Re_b is calculated by re-arranging Equation (12) to get Equation (14).

$$\mathrm{Re}_b = \frac{\rho_{sl} U_{t(mas)} D_b}{\mu_{sl}} \qquad \text{---------- (14)}$$

Re_b calculated by Equation (14) is returned into Equation (13) to generate a new value of $U_{t(mas)}$. This procedure is repeated, and with each iteration, the change in the value of $U_{t(mas)}$ becomes smaller. When the value of $U_{t(mas)}$ converges to the solution (difference in the value of $U_{t(mas)}$ between iterations is less than 0.001 cm/s) the iterations stop. For the current example, $U_{t(mas)}$ was found to be 13.3 cm/s and Re_b equal to 174.

Subsequently, the value of m is determined using Equation (4), (5) or (6). The value of $\varepsilon_{g(t)}$ is assumed to be 0.5%. $U_{bs(d)}$ is calculated by Equation (7), Re_{bs} by Equation (8) and $U_{bs(mas)}$ by Equation (9). Let this set of values be called "set A".

If the magnitude of the difference between $U_{bs(mas)}$ and $U_{bs(d)}$ is greater than 0.01 then the value of $\varepsilon_{g(t)}$ is increased and $U_{bs(d)}$, Re_{bs} and $U_{bs(mas)}$ are calculated again. These values become "set B". The magnitude of the difference between $U_{bs(mas)}$ and $U_{bs(d)}$ for "set B" is calculated.

Using a linear estimation following (Equation (15)), the difference between $U_{bs(mas)}$ and $U_{bs(d)}$ for both set "A" and "B" determines the next value of $\varepsilon_{g(t)}$ that should be tested (ε_g^*). In Equation (15), Δ_A and Δ_B are the differences between $U_{bs(mas)}$ and $U_{bs(d)}$ for set "A" and "B" respectively.

$$\varepsilon_g^* = \frac{\varepsilon_{gA}\Delta_B - \varepsilon_{gB}\Delta_A}{\Delta_B - \Delta_A} \qquad \text{---------- (15)}$$

This procedure is repeated until the magnitude of the difference between $U_{bs(mas)}$ and $U_{bs(d)}$ is smaller than 0.01 cm/s. The resulting value of ε_g is stored as $\varepsilon_{g(t)}$ (in this case, 10.72 %).

Bulk Density at Top of Slurry Zone

The bulk density ($\rho_{b(t)}$) is calculated at the top of the collection zone using Equation (16).

$$\rho_{b(t)} = \rho_{sl}(1 - \varepsilon_{g(t)}) \qquad \text{---------- (16)}$$

In our case, $\rho_{b(t)}$ is 0.991 g/cm^3.

Stepping Downward

The next stage in the calculation procedure assumes that over a short distance (3 – 5 cm) the bulk density can be considered constant. Therefore, using the bulk density at the top of the collection zone ($\rho_{b(t)}$), new values of J_g and D_b, slightly deeper in the machine can be determined using Equation (17) and (18), where $J_{g(t+1)}$ and $D_{b(t+1)}$ are gas rate and bubble size a small distance below the top of collection zone, P_t is the pressure at the top of the collection zone and δh is the change in depth.

$$J_{g(t+1)} = \frac{J_{g(t)}(P_{(t)})}{(P_{(t)} + \rho_{b(t)}\delta h)} \qquad \text{---------- (17)}$$

$$D_{b(t+1)} = D_{b(t)}\left[\frac{(P_{(t)})}{(P_{(t)} + \rho_{b(t)}\delta h)}\right]^{\frac{1}{3}} \qquad \text{---------- (18)}$$

At this stage, there is sufficient information to determine gas holdup and bulk density at a small depth below the top of the collection zone following the above procedure. By repeating, over increments of depth the calculated axial pressure profile can be constructed.

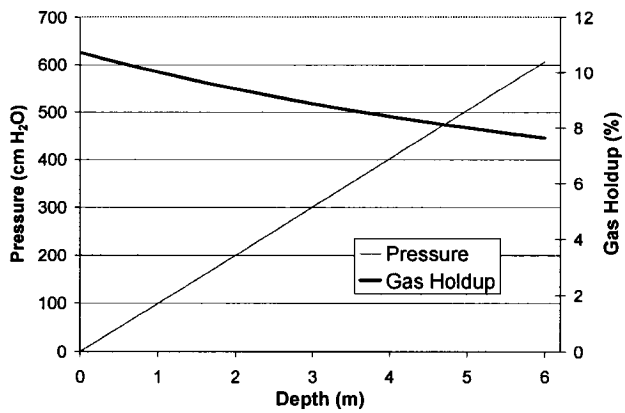

Figure A.1 - Calculated pressure and gas holdup profiles.

Appendix 2 – Supporting Data Tables

Table 1 – Data for Figure 3.1

Measurement	Bulk Density (g/cm^3)	Slope dP/dt (cm/s)	HL (cm)	H0 (cm)	J_g (cm/s) at L
F3.1 - J_g1	0.97	0.96	300	207	1.16
F3.1 - J_g2	0.97	0.98	300	207	1.18
F3.1 - J_g3	0.97	0.94	300	207	1.14
F3.1 - J_g4	0.99	0.91	300	207	1.09
F3.1 - J_g5	0.99	0.90	300	207	1.08
F3.1 - J_g6	0.99	0.95	300	207	1.14
F3.1 - J_g7	1.03	0.85	300	207	0.98
F3.1 - J_g8	1.03	0.84	300	207	0.98
F3.1 - J_g9	1.05	0.86	300	207	0.98
F3.1 - J_g10	1.05	0.88	300	207	1.00
F3.1 - J_g11	1.05	0.83	300	207	0.95
F3.1 - J_g12	1.05	0.81	300	207	0.92
F3.1 - J_g13	1.05	0.81	300	207	0.92
F3.1 - J_g14	1.05	0.88	300	207	1.00

Table 2 – Data for Figure 3.2

Measurement	Bulk Density (g/cm^3)	Slope dP/dt (cm/s)	HL (cm)	PI (cm H_2O)	J_g (cm/s) corr	AFR m^3/min
F3.2 - J_g1	1.11	0.37	300	109	0.47	7
F3.2 - J_g2	1.11	0.41	300	109	0.52	7
F3.2 - J_g3	1.11	0.39	300	109	0.50	7
F3.2 - J_g4	1.11	0.39	300	109	0.49	7
F3.2 - J_g5	1.11	0.37	300	109	0.46	7
F3.2 - J_g6	1.09	0.46	300	115	0.59	9
F3.2 - J_g7	1.09	0.48	300	115	0.60	9
F3.2 - J_g8	1.09	0.47	300	115	0.59	9
F3.2 - J_g9	1.09	0.47	300	115	0.60	9

F3.2 - J_g10	1.09	0.46	300	115	0.58	9
F3.2 - J_g11	1.07	0.52	300	118	0.66	12
F3.2 - J_g12	1.07	0.51	300	118	0.66	12
F3.2 - J_g13	1.07	0.53	300	118	0.67	12
F3.2 - J_g14	1.07	0.52	300	118	0.67	12
F3.2 - J_g15	1.07	0.54	300	118	0.69	12
F3.2 - J_g16	1.09	0.35	300	120	0.44	6
F3.2 - J_g17	1.09	0.33	300	120	0.42	6
F3.2 - J_g18	1.09	0.35	300	120	0.44	6
F3.2 - J_g19	1.09	0.34	300	120	0.43	6
F3.2 - J_g20	1.09	0.34	300	120	0.43	6
F3.2 - J_g21	1.06	0.48	300	125	0.61	10
F3.2 - J_g22	1.06	0.48	300	125	0.62	10
F3.2 - J_g23	1.06	0.46	300	125	0.59	10
F3.2 - J_g24	1.06	0.46	300	125	0.57	10
F3.2 - J_g25	1.06	0.49	300	125	0.54	10

Table 3 – Data for Figure 3.3

Measurement	Bulk Density (g/cm^3)	Slope dP/dt (cm/s)	HL (cm)	PI (cm H_2O)	J_g (cm/s) corr.	AFR m^3/min
F3.3 - J_g1	1.13	0.59	300	116	0.74	9
F3.3 - J_g2	1.13	0.65	300	116	0.81	9
F3.3 - J_g3	1.13	0.63	300	116	0.78	9
F3.3 - J_g4	1.13	0.63	300	116	0.78	9
F3.3 - J_g5	1.13	0.61	300	116	0.75	9
F3.3 - J_g6	1.13	0.60	300	116	0.75	9
F3.3 - J_g7	1.10	0.80	300	121	1.01	12
F3.3 - J_g8	1.10	0.85	300	121	1.06	12
F3.3 - J_g9	1.10	0.84	300	121	1.05	12
F3.3 - J_g10	1.10	0.86	300	121	1.08	12
F3.3 - J_g11	1.10	0.86	300	121	1.08	12
F3.3 - J_g12	1.17	0.38	300	111	0.47	7
F3.3 - J_g13	1.17	0.39	300	111	0.47	7
F3.3 - J_g14	1.17	0.42	300	111	0.51	7
F3.3 - J_g15	1.17	0.41	300	111	0.50	7

F3.3 - J_g16	1.12	0.62	300	113	0.78	10
F3.3 - J_g17	1.12	0.68	300	113	0.84	10
F3.3 - J_g18	1.12	0.65	300	113	0.82	10
F3.3 - J_g19	1.12	0.61	300	113	0.77	10
F3.3 - J_g20	1.11	0.76	300	117	0.95	11
F3.3 - J_g21	1.11	0.77	300	117	0.97	11
F3.3 - J_g22	1.11	0.70	300	117	0.88	11
F3.3 - J_g23	1.11	0.70	300	117	0.88	11
F3.3 - J_g24	1.11	0.76	300	117	0.95	11

Table 4 – Data for Figure 3.5

Measurement	AFR (m^3/min)	J_g (cm/s)	Gas Holdup (%)	D_{32} (mm)	S_b (s^{-1})
F3.5 - Cell 4 - AFR 1	7	0.49	7.96	1.36	21.5
F3.5 - Cell 4 - AFR 2	9	0.59	8.85	1.35	26.3
F3.5 - Cell 4 - AFR 3	12	0.67	10.35	1.40	28.7
F3.5 - Cell 4 - AFR 4	6	0.43	7.29	1.25	20.6
F3.5 - Cell 4 - AFR 5	10	0.61	10.44	1.35	26.9
F3.5 - Cell 9 - AFR 1	9	0.77	8.99	1.81	25.4
F3.5 - Cell 9 - AFR 2	12	1.06	11.31	1.85	34.3
F3.5 - Cell 9 - AFR 3	7	0.49	7.36	1.68	17.5
F3.5 - Cell 9 - AFR 4	10	0.80	10.83	1.88	25.5
F3.5 - Cell 9 - AFR 5	11	0.93	11.54	1.98	28.1

Table 5 – Data for Figure 3.6

Measurement	FD set point (%)	Ps (cm H_2O)	Bulk Density (g/cm^3)	Hs (cm)	FD calc (mm)
F3.6 Cell A FD1	20.00	107.4	1.00	120	15.9
F3.6 Cell A FD2	30.00	108.0	1.04	120	19.6
F3.6 Cell A FD3	40.00	100.8	0.99	120	22.9

F3.6 Cell A FD4	50.00	94.2	0.97	120	28.2
F3.6 Cell A FD5	35.00	96.8	0.90	120	16.3
F3.6 Cell B FD1	20.00	123.5	1.07	120	6.40
F3.6 Cell B FD2	30.00	112.3	1.04	120	15.16
F3.6 Cell B FD3	40.00	110.9	1.02	120	14.76
F3.6 Cell B FD4	50.00	105.7	1.01	120	19.74
F3.6 Cell B FD5	35.00	116.5	1.06	120	13.20
F3.6 Cell C FD1	20.00	106.1	1.02	120	20.57
F3.6 Cell C FD2	30.00	97.4	1.00	120	28.20
F3.6 Cell C FD3	40.00	93.1	0.99	120	33.02
F3.6 Cell C FD4	50.00	87.3	0.97	120	37.43
F3.6 Cell C FD5	35.00	87.5	0.96	120	36.59
F3.6 Cell D FD1	20.00	116.1	1.01	120	6.91
F3.6 Cell D FD2	30.00	110.6	1.00	120	11.07
F3.6 Cell D FD3	40.00	105.4	0.96	120	13.03
F3.6 Cell D FD4	50.00	98.8	0.93	120	16.53
F3.6 Cell D FD5	35.00	102.9	0.92	120	10.78

Table 6 – Data for Figure 3.7

Measurement	Bulk Density (g/cm^3)	Slope dP/dt (cm/s)	HL (cm)	PI (cm H_2O)	J_g (cm/s) corr	FD (%)
F3.7 - J_g1	1.00	1.04	300	107	1.33	20
F3.7 - J_g2	1.00	1.02	300	107	1.31	20
F3.7 - J_g3	1.00	1.10	300	107	1.41	20
F3.7 - J_g4	1.00	0.97	300	107	1.24	20
F3.7 - J_g5	1.00	0.92	300	107	1.17	20
F3.7 - J_g6	1.04	0.97	300	108	1.21	30
F3.7 - J_g7	1.04	0.94	300	108	1.18	30
F3.7 - J_g8	1.04	0.92	300	108	1.15	30
F3.7 - J_g9	1.04	1.08	300	108	1.35	30
F3.7 - J_g10	1.04	1.04	300	108	1.29	30
F3.7 - J_g11	1.04	1.17	300	108	1.46	30

F3.7 - J_g12	0.99	0.91	300	101	1.18	40
F3.7 - J_g13	0.99	0.93	300	101	1.21	40
F3.7 - J_g14	0.99	1.03	300	101	1.33	40
F3.7 - J_g15	0.99	1.08	300	101	1.40	40
F3.7 - J_g16	0.99	0.95	300	101	1.24	40
F3.7 - J_g17	0.97	1.02	300	94	1.36	50
F3.7 - J_g18	0.97	1.10	300	94	1.47	50
F3.7 - J_g19	0.97	0.98	300	94	1.31	50
F3.7 - J_g20	0.97	1.00	300	94	1.33	50
F3.7 - J_g21	0.97	1.27	300	94	1.69	50
F3.7 - J_g22	0.90	0.94	300	97	1.30	35
F3.7 - J_g23	0.90	1.07	300	97	1.48	35
F3.7 - J_g24	0.90	1.14	300	97	1.58	35
F3.7 - J_g25	0.90	0.96	300	97	1.34	35
F3.7 - J_g26	0.90	1.02	300	97	1.42	35

Table 7 – Data for Figure 3.8

Measurement	Bulk Density (g/cm^3)	Slope dP/dt (cm/s)	HL (cm)	PI (cm H_2O)	J_g (cm/s) corr	FD (%)
F3.8 - J_g1	1.02	1.39	300	106	1.69	20
F3.8 - J_g2	1.02	1.33	300	106	1.62	20
F3.8 - J_g3	1.02	1.37	300	106	1.66	20
F3.8 - J_g4	1.02	1.39	300	106	1.69	20
F3.8 - J_g5	1.02	1.36	300	106	1.66	20
F3.8 - J_g6	1.02	1.22	300	106	1.48	20
F3.8 - J_g7	1.00	1.31	300	97	1.64	30
F3.8 - J_g8	1.00	1.31	300	97	1.63	30
F3.8 - J_g9	1.00	1.28	300	97	1.60	30
F3.8 - J_g10	1.00	1.18	300	97	1.47	30
F3.8 - J_g11	1.00	1.29	300	97	1.60	30
F3.8 - J_g12	0.99	1.36	300	93	1.71	40
F3.8 - J_g13	0.99	1.38	300	93	1.73	40

F3.8 - J_g14	0.99	1.36	300	93	1.71	40
F3.8 - J_g15	0.99	1.33	300	93	1.67	40
F3.8 - J_g16	0.99	1.42	300	93	1.78	40
F3.8 - J_g17	0.97	1.37	300	87	1.76	50
F3.8 - J_g18	0.97	1.47	300	87	1.89	50
F3.8 - J_g19	0.97	1.40	300	87	1.81	50
F3.8 - J_g20	0.97	1.41	300	87	1.83	50
F3.8 - J_g21	0.97	1.33	300	87	1.72	50
F3.8 - J_g22	0.96	1.33	300	87	1.72	35
F3.8 - J_g23	0.96	1.43	300	87	1.86	35
F3.8 - J_g24	0.96	1.37	300	87	1.77	35
F3.8 - J_g25	0.96	1.37	300	87	1.77	35
F3.8 - J_g26	0.96	1.43	300	87	1.86	35

Table 8 – Data for Figure 3.11

Measurement	J_g (cm/s) corr	Conductivity (mS/cm)			Gas Holdup (%)	D_{32} (mm)	S_b (s^{-1})
		Open Cell	Syphon Cell	# of measurements			
F3.11 Cell A 20	1.29	6.87	7.86	780	8.69	2.39	32.47
F3.11 Cell A 30	1.28	6.60	7.75	960	10.36	1.92	39.93
F3.11 Cell A 40	1.27	6.52	7.83	840	11.79	1.79	42.69
F3.11 Cell A 50	1.43	6.44	7.84	900	12.67	1.86	46.06
F3.11 Cell A 35	1.42	6.67	7.95	780	11.35	1.90	44.96
F3.11 Cell B 20	1.02	6.68	7.77	1200	9.81	1.91	31.87
F3.11 Cell B 30	1.13	6.56	7.63	720	9.86	1.58	43.12
F3.11 Cell B 40	1.39	6.75	7.98	660	10.83	2.49	33.55
F3.11 Cell B 50	1.21	6.40	7.61	780	11.14	1.93	37.44
F3.11 Cell B 35	1.59	6.84	7.89	840	9.29	2.60	36.56
F3.11 Cell C 20	1.63	6.93	8.21	1260	10.96	1.95	50.31
F3.11 Cell C 30	1.59	6.59	7.87	480	11.49	2.09	45.66
F3.11 Cell C 40	1.72	6.44	7.83	420	12.56	2.03	50.80
F3.11 Cell C 50	1.80	6.27	7.92	420	14.91	2.29	47.18
F3.11 Cell C 35	1.80	6.32	7.97	420	14.85	1.98	54.45

F3.11 Cell D 20	1.45	6.50	8.15	720	14.45	1.75	49.55
F3.11 Cell D 30	1.57	6.54	8.13	540	13.99	1.94	48.74
F3.11 Cell D 40	1.72	6.51	8.25	540	15.13	1.89	54.41
F3.11 Cell D 50	1.85	6.50	8.37	780	16.04	1.92	57.73
F3.11 Cell D 35	1.71	6.64	8.32	780	14.46	1.79	57.35

Table 9 – Data for Figure 4.4

Measurement	Bulk Density (g/cm^3)	Slope dP/dt (cm/s)	HL (cm)	H0 (cm)	J_g (cm/s) at L
F4.4 - Loc 1 - # 1	1.07	1.06	300	218	1.23
F4.4 - Loc 1 - # 2	1.07	1.03	300	218	1.19
F4.4 - Loc 1 - # 3	1.07	1.21	300	218	1.40
F4.4 - Loc 1 - # 4	1.07	0.94	300	218	1.09
F4.4 - Loc 1 - # 5	1.07	1.05	300	218	1.22
F4.4 - Loc 1 - # 6	1.07	0.95	300	218	1.11
F4.4 - Loc 1 - # 7	1.07	0.84	300	218	0.98
F4.4 - Loc 1 - # 8	1.07	0.97	300	218	1.12
F4.4 - Loc 1 - # 9	1.07	0.90	300	218	1.04
F4.4 - Loc 1 - # 10	1.07	1.13	300	218	1.31
F4.4 - Loc 1 - # 11	1.07	0.90	300	218	1.04
F4.4 - Loc 2 - # 1	1.07	0.64	300	218	0.74
F4.4 - Loc 2 - # 2	1.07	0.70	300	218	0.81
F4.4 - Loc 2 - # 3	1.07	0.64	300	218	0.74
F4.4 - Loc 2 - # 4	1.07	0.69	300	218	0.80
F4.4 - Loc 2 - # 5	1.07	1.20	300	218	1.39
F4.4 - Loc 2 - # 6	1.07	0.94	300	218	1.09
F4.4 - Loc 2 - # 7	1.07	0.78	300	218	0.91
F4.4 - Loc 2 - # 8	1.07	0.72	300	218	0.84
F4.4 - Loc 2 - # 9	1.07	0.68	300	218	0.79
F4.4 - Loc 2 - # 10	1.07	0.75	300	218	0.87
F4.4 - Loc 2 - # 11	1.07	0.72	300	218	0.84
F4.4 - Loc 3 - # 1	1.07	0.57	300	218	0.66

F4.4 - Loc 3 - # 2	1.07	0.64	300	218	0.74
F4.4 - Loc 3 - # 3	1.07	0.61	300	218	0.71
F4.4 - Loc 3 - # 4	1.07	0.53	300	218	0.61
F4.4 - Loc 3 - # 5	1.07	0.91	300	218	1.05
F4.4 - Loc 3 - # 6	1.07	0.78	300	218	0.91
F4.4 - Loc 3 - # 7	1.07	0.64	300	218	0.74
F4.4 - Loc 3 - # 8	1.07	0.62	300	218	0.72
F4.4 - Loc 3 - # 9	1.07	0.63	300	218	0.73
F4.4 - Loc 3 - # 10	1.07	0.57	300	218	0.66
F4.4 - Loc 3 - # 11	1.07	0.55	300	218	0.63
F4.4 - Loc 4 - # 1	1.07	0.44	300	218	0.51
F4.4 - Loc 4 - # 2	1.07	0.48	300	218	0.56
F4.4 - Loc 4 - # 3	1.07	0.44	300	218	0.51
F4.4 - Loc 4 - # 4	1.07	0.60	300	218	0.70
F4.4 - Loc 4 - # 5	1.07	0.73	300	218	0.84
F4.4 - Loc 4 - # 6	1.07	0.67	300	218	0.78
F4.4 - Loc 4 - # 7	1.07	0.61	300	218	0.71
F4.4 - Loc 4 - # 8	1.07	0.51	300	218	0.59
F4.4 - Loc 4 - # 9	1.07	0.44	300	218	0.51
F4.4 - Loc 4 - # 10	1.07	0.49	300	218	0.56
F4.4 - Loc 4 - # 11	1.07	0.44	300	218	0.51
F4.4 - Loc 5 - # 1	1.07	0.56	300	218	0.65
F4.4 - Loc 5 - # 2	1.07	0.55	300	218	0.64
F4.4 - Loc 5 - # 3	1.07	0.58	300	218	0.67
F4.4 - Loc 5 - # 4	1.07	0.61	300	218	0.71
F4.4 - Loc 5 - # 5	1.07	0.78	300	218	0.90
F4.4 - Loc 5 - # 6	1.07	0.89	300	218	1.03
F4.4 - Loc 5 - # 7	1.07	0.72	300	218	0.84
F4.4 - Loc 5 - # 8	1.07	0.59	300	218	0.68
F4.4 - Loc 5 - # 9	1.07	0.57	300	218	0.66
F4.4 - Loc 5 - # 10	1.07	0.59	300	218	0.68
F4.4 - Loc 5 - # 11	1.07	0.64	300	218	0.74
F4.4 - Loc 6 - # 1	1.07	0.62	300	218	0.72
F4.4 - Loc 6 - # 2	1.07	0.81	300	218	0.94
F4.4 - Loc 6 - # 3	1.07	0.57	300	218	0.66
F4.4 - Loc 6 - # 4	1.07	0.62	300	218	0.72

F4.4 - Loc 6 - # 5	1.07	0.98	300	218	1.14
F4.4 - Loc 6 - # 6	1.07	0.84	300	218	0.97
F4.4 - Loc 6 - # 7	1.07	0.76	300	218	0.88
F4.4 - Loc 6 - # 8	1.07	0.76	300	218	0.88
F4.4 - Loc 6 - # 9	1.07	0.70	300	218	0.81
F4.4 - Loc 6 - # 10	1.07	0.64	300	218	0.74
F4.4 - Loc 6 - # 11	1.07	0.77	300	218	0.89

Table 10 – Data for Figure 4.5

Measurement	Bulk Density (g/cm^3)	Slope dP/dt (cm/s)	HL (cm)	H0 (cm)	J_a (cm/s) at L
F4.5 - Loc 1 - # 1	1.07	0.92	300	218	1.07
F4.5 - Loc 1 - # 2	1.07	0.84	300	218	0.97
F4.5 - Loc 1 - # 3	1.07	0.92	300	218	1.06
F4.5 - Loc 1 - # 4	1.07	0.89	300	218	1.03
F4.5 - Loc 1 - # 5	1.07	0.94	300	218	1.09
F4.5 - Loc 1 - # 6	1.07	0.88	300	218	1.01
F4.5 - Loc 1 - # 7	1.07	0.82	300	218	0.95
F4.5 - Loc 1 - # 8	1.07	0.87	300	218	1.01
F4.5 - Loc 1 - # 9	1.07	0.92	300	218	1.06
F4.5 - Loc 1 - # 10	1.07	0.97	300	218	1.12
F4.5 - Loc 1 - # 11	1.07	0.84	300	218	0.98
F4.5 - Loc 2 - # 1	1.07	0.70	300	218	0.81
F4.5 - Loc 2 - # 2	1.07	0.66	300	218	0.76
F4.5 - Loc 2 - # 3	1.07	0.69	300	218	0.80
F4.5 - Loc 2 - # 4	1.07	0.67	300	218	0.78
F4.5 - Loc 2 - # 5	1.07	0.66	300	218	0.76
F4.5 - Loc 2 - # 6	1.07	0.72	300	218	0.83
F4.5 - Loc 2 - # 7	1.07	0.59	300	218	0.69
F4.5 - Loc 2 - # 8	1.07	0.68	300	218	0.79
F4.5 - Loc 2 - # 9	1.07	0.57	300	218	0.66
F4.5 - Loc 2 - # 10	1.07	0.58	300	218	0.67
F4.5 - Loc 2 - # 11	1.07	0.56	300	218	0.65
F4.5 - Loc 3 - # 1	1.07	0.60	300	218	0.69
F4.5 - Loc 3 - # 2	1.07	0.58	300	218	0.67
F4.5 - Loc 3 - # 3	1.07	0.62	300	218	0.71
F4.5 - Loc 3 - # 4	1.07	0.48	300	218	0.56
F4.5 - Loc 3 - # 5	1.07	0.58	300	218	0.67
F4.5 - Loc 3 - # 6	1.07	0.55	300	218	0.63
F4.5 - Loc 3 - # 7	1.07	0.53	300	218	0.62

F4.5 - Loc 3 - # 8	1.07	0.51	300	218	0.60
F4.5 - Loc 3 - # 9	1.07	0.54	300	218	0.62
F4.5 - Loc 3 - # 10	1.07	0.57	300	218	0.66
F4.5 - Loc 3 - # 11	1.07	0.53	300	218	0.61
F4.5 - Loc 4 - # 1	1.07	0.52	300	218	0.61
F4.5 - Loc 4 - # 2	1.07	0.44	300	218	0.51
F4.5 - Loc 4 - # 3	1.07	0.43	300	218	0.50
F4.5 - Loc 4 - # 4	1.07	0.47	300	218	0.55
F4.5 - Loc 4 - # 5	1.07	0.47	300	218	0.55
F4.5 - Loc 4 - # 6	1.07	0.48	300	218	0.55
F4.5 - Loc 4 - # 7	1.07	0.42	300	218	0.49
F4.5 - Loc 4 - # 8	1.07	0.42	300	218	0.49
F4.5 - Loc 4 - # 9	1.07	0.43	300	218	0.50
F4.5 - Loc 4 - # 10	1.07	0.46	300	218	0.53
F4.5 - Loc 4 - # 11	1.07	0.40	300	218	0.46
F4.5 - Loc 5 - # 1	1.07	0.59	300	218	0.68
F4.5 - Loc 5 - # 2	1.07	0.58	300	218	0.67
F4.5 - Loc 5 - # 3	1.07	0.54	300	218	0.62
F4.5 - Loc 5 - # 4	1.07	0.55	300	218	0.63
F4.5 - Loc 5 - # 5	1.07	0.61	300	218	0.70
F4.5 - Loc 5 - # 6	1.07	0.56	300	218	0.65
F4.5 - Loc 5 - # 7	1.07	0.55	300	218	0.64
F4.5 - Loc 5 - # 8	1.07	0.55	300	218	0.64
F4.5 - Loc 5 - # 9	1.07	0.52	300	218	0.61
F4.5 - Loc 5 - # 10	1.07	0.51	300	218	0.59
F4.5 - Loc 5 - # 11	1.07	0.57	300	218	0.66

Table 11 – Data for Figure 4.6

Measurement	Bulk Density (g/cm^3)	Slope dP/dt (cm/s)	HL (cm)	H0 (cm)	J_g (cm/s) at L
F4.6 - Loc A - # 1	0.97	1.53	300	200	1.93
F4.6 - Loc A - # 2	0.97	1.39	300	200	1.75
F4.6 - Loc A - # 3	0.97	1.49	300	200	1.87
F4.6 - Loc A - # 4	0.97	1.67	300	200	2.11
F4.6 - Loc A - # 5	0.97	1.41	300	200	1.78
F4.6 - Loc A - # 6	0.97	1.32	300	200	1.66
F4.6 - Loc A - # 7	0.97	1.55	300	200	1.96
F4.6 - Loc A - # 8	0.97	1.55	300	200	1.96
F4.6 - Loc A - # 9	0.97	1.36	300	200	1.72
F4.6 - Loc A - # 10	0.97	1.50	300	200	1.89
F4.6 - Loc A - # 11	0.97	1.39	300	200	1.75
F4.6 - Loc A - # 12	0.97	1.50	300	200	1.89
F4.6 - Loc A - # 13	0.97	1.49	300	200	1.88

F4.6 - Loc A - # 14	0.97	1.34	300	200	1.70
F4.6 - Loc A - # 15	0.97	1.36	300	200	1.72
F4.6 - Loc A - # 16	0.97	1.36	300	200	1.72
F4.6 - Loc A - # 17	0.97	1.40	300	200	1.76
F4.6 - Loc A - # 18	0.97	1.34	300	200	1.69
F4.6 - Loc A - # 1	0.97	1.48	300	150	1.78
F4.6 - Loc A - # 2	0.97	1.43	300	150	1.72
F4.6 - Loc A - # 3	0.97	1.63	300	150	1.97
F4.6 - Loc A - # 4	0.97	1.49	300	150	1.79
F4.6 - Loc A - # 5	0.97	1.45	300	150	1.74
F4.6 - Loc A - # 6	0.97	1.52	300	150	1.84
F4.6 - Loc A - # 7	0.97	1.52	300	150	1.84
F4.6 - Loc A - # 8	0.97	1.39	300	150	1.68
F4.6 - Loc A - # 9	0.97	1.49	300	150	1.80
F4.6 - Loc A - # 10	0.97	1.43	300	150	1.73
F4.6 - Loc A - # 11	0.97	1.51	300	150	1.82
F4.6 - Loc A - # 12	0.97	1.42	300	150	1.72
F4.6 - Loc A - # 13	0.97	1.41	300	150	1.71
F4.6 - Loc A - # 14	0.97	1.48	300	150	1.79
F4.6 - Loc A - # 15	0.97	1.40	300	150	1.69
F4.6 - Loc A - # 16	0.97	1.58	300	150	1.91
F4.6 - Loc A - # 17	0.97	1.38	300	150	1.66
F4.6 - Loc A - # 18	0.97	1.47	300	150	1.77
F4.6 - Loc B - # 1	0.98	1.51	300	200	1.89
F4.6 - Loc B - # 2	0.98	1.46	300	200	1.83
F4.6 - Loc B - # 3	0.98	1.39	300	200	1.74
F4.6 - Loc B - # 4	0.98	1.34	300	200	1.68
F4.6 - Loc B - # 5	0.98	1.56	300	200	1.96
F4.6 - Loc B - # 6	0.98	1.41	300	200	1.77
F4.6 - Loc B - # 7	0.98	1.44	300	200	1.80
F4.6 - Loc B - # 8	0.98	1.53	300	200	1.92
F4.6 - Loc B - # 9	0.98	1.49	300	200	1.86
F4.6 - Loc B - # 10	0.98	1.37	300	200	1.72
F4.6 - Loc B - # 11	0.98	1.37	300	200	1.71
F4.6 - Loc B - # 12	0.98	1.54	300	200	1.93
F4.6 - Loc B - # 13	0.98	1.41	300	200	1.77
F4.6 - Loc B - # 14	0.98	1.45	300	200	1.81
F4.6 - Loc B - # 15	0.98	1.52	300	200	1.91
F4.6 - Loc B - # 16	0.98	1.44	300	200	1.80
F4.6 - Loc B - # 17	0.98	1.49	300	200	1.86
F4.6 - Loc B - # 1	0.98	1.47	300	150	1.77
F4.6 - Loc B - # 2	0.98	1.42	300	150	1.70
F4.6 - Loc B - # 3	0.98	1.45	300	150	1.74
F4.6 - Loc B - # 4	0.98	1.50	300	150	1.80
F4.6 - Loc B - # 5	0.98	1.44	300	150	1.73
F4.6 - Loc B - # 6	0.98	1.37	300	150	1.65
F4.6 - Loc B - # 7	0.98	1.40	300	150	1.68
F4.6 - Loc B - # 8	0.98	1.49	300	150	1.79

F4.6 - Loc B - # 9	0.98	1.45	300	150	1.74
F4.6 - Loc B - # 10	0.98	1.38	300	150	1.65
F4.6 - Loc B - # 11	0.98	1.34	300	150	1.61
F4.6 - Loc B - # 12	0.98	1.55	300	150	1.85
F4.6 - Loc B - # 13	0.98	1.40	300	150	1.68
F4.6 - Loc B - # 14	0.98	1.44	300	150	1.73
F4.6 - Loc B - # 15	0.98	1.41	300	150	1.69
F4.6 - Loc B - # 16	0.98	1.39	300	150	1.66
F4.6 - Loc B - # 17	0.98	1.58	300	150	1.89
F4.6 - Loc C - # 1	0.95	1.65	300	200	2.12
F4.6 - Loc C - # 2	0.95	1.45	300	200	1.86
F4.6 - Loc C - # 3	0.95	1.57	300	200	2.01
F4.6 - Loc C - # 4	0.95	1.34	300	200	1.72
F4.6 - Loc C - # 5	0.95	1.65	300	200	2.12
F4.6 - Loc C - # 6	0.95	1.62	300	200	2.08
F4.6 - Loc C - # 7	0.95	1.61	300	200	2.06
F4.6 - Loc C - # 8	0.95	1.59	300	200	2.05
F4.6 - Loc C - # 9	0.95	1.58	300	200	2.03
F4.6 - Loc C - # 10	0.95	1.63	300	200	2.09
F4.6 - Loc C - # 11	0.95	1.49	300	200	1.91
F4.6 - Loc C - # 12	0.95	1.21	300	200	1.55
F4.6 - Loc C - # 13	0.95	1.23	300	200	1.58
F4.6 - Loc C - # 14	0.95	1.56	300	200	2.00
F4.6 - Loc C - # 15	0.95	1.48	300	200	1.90
F4.6 - Loc C - # 16	0.95	1.55	300	200	1.98
F4.6 - Loc C - # 17	0.95	1.51	300	200	1.94
F4.6 - Loc C - # 18	0.95	1.48	300	200	1.90
F4.6 - Loc C - # 1	0.95	1.57	300	200	2.01
F4.6 - Loc C - # 2	0.95	1.45	300	150	1.78
F4.6 - Loc C - # 3	0.95	1.54	300	150	1.89
F4.6 - Loc C - # 4	0.95	1.40	300	150	1.72
F4.6 - Loc C - # 5	0.95	1.50	300	150	1.85
F4.6 - Loc C - # 6	0.95	1.47	300	150	1.81
F4.6 - Loc C - # 7	0.95	1.43	300	150	1.75
F4.6 - Loc C - # 8	0.95	1.46	300	150	1.79
F4.6 - Loc C - # 9	0.95	1.54	300	150	1.89
F4.6 - Loc C - # 10	0.95	1.49	300	150	1.83
F4.6 - Loc C - # 11	0.95	1.57	300	150	1.93
F4.6 - Loc C - # 12	0.95	1.48	300	150	1.82
F4.6 - Loc C - # 13	0.95	1.59	300	150	1.95
F4.6 - Loc C - # 14	0.95	1.67	300	150	2.06
F4.6 - Loc C - # 15	0.95	1.37	300	150	1.69
F4.6 - Loc C - # 16	0.95	1.40	300	150	1.72
F4.6 - Loc C - # 17	0.95	1.44	300	150	1.77
F4.6 - Loc C - # 18	0.95	1.38	300	150	1.70
F4.6 - Loc C - # 19	0.95	1.63	300	150	2.00
F4.6 - Loc C - # 20	0.95	1.36	300	150	1.67
F4.6 - Loc D - # 1	0.95	1.21	300	150	1.52

F4.6 - Loc D - # 2	0.95	1.26	300	150	1.59
F4.6 - Loc D - # 3	0.97	1.42	300	200	1.79
F4.6 - Loc D - # 4	0.97	1.37	300	200	1.73
F4.6 - Loc D - # 5	0.97	1.52	300	200	1.93
F4.6 - Loc D - # 6	0.97	1.37	300	200	1.73
F4.6 - Loc D - # 7	0.97	1.36	300	200	1.72
F4.6 - Loc D - # 8	0.97	1.42	300	200	1.79
F4.6 - Loc D - # 9	0.97	1.23	300	200	1.56
F4.6 - Loc D - # 10	0.97	1.36	300	200	1.71
F4.6 - Loc D - # 11	0.97	1.35	300	200	1.71
F4.6 - Loc D - # 12	0.97	1.41	300	200	1.78
F4.6 - Loc D - # 13	0.97	1.29	300	200	1.63
F4.6 - Loc D - # 14	0.97	1.52	300	200	1.91
F4.6 - Loc D - # 15	0.97	1.41	300	200	1.78
F4.6 - Loc D - # 16	0.97	1.26	300	200	1.59
F4.6 - Loc D - # 1	0.97	1.49	300	150	1.80
F4.6 - Loc D - # 2	0.97	1.52	300	150	1.83
F4.6 - Loc D - # 3	0.97	1.36	300	150	1.65
F4.6 - Loc D - # 4	0.97	1.38	300	150	1.67
F4.6 - Loc D - # 5	0.97	1.49	300	150	1.80
F4.6 - Loc D - # 6	0.97	1.38	300	150	1.67
F4.6 - Loc D - # 7	0.97	1.50	300	150	1.81
F4.6 - Loc D - # 8	0.97	1.44	300	150	1.74
F4.6 - Loc D - # 9	0.97	1.40	300	150	1.69
F4.6 - Loc D - # 10	0.97	1.39	300	150	1.68
F4.6 - Loc D - # 11	0.97	1.58	300	150	1.91
F4.6 - Loc D - # 12	0.97	1.36	300	150	1.64
F4.6 - Loc D - # 13	0.97	1.44	300	150	1.74
F4.6 - Loc D - # 14	0.97	1.44	300	150	1.74
F4.6 - Loc D - # 15	0.97	1.47	300	150	1.78
F4.6 - Loc D - # 16	0.97	1.49	300	150	1.80

Table 12 – Data for Figure 4.7

Measurement	Num Slopes	J_g (cm/s) at L
F4.7 Loc 1 AFR1	5	0.46
F4.7 Loc 1 AFR2	5	0.71
F4.7 Loc 1 AFR3	5	0.95
F4.7 Loc 1 AFR4	5	1.52
F4.7 Loc 2 AFR1	5	0.46
F4.7 Loc 2 AFR2	5	0.72

F4.7 Loc 2 AFR3	5	0.91
F4.7 Loc 2 AFR4	5	1.29
F4.7 Loc 3 AFR1	5	0.45
F4.7 Loc 3 AFR2	5	0.69
F4.7 Loc 3 AFR3	5	0.96
F4.7 Loc 3 AFR4	5	1.34
F4.7 Loc 4 AFR1	5	0.42
F4.7 Loc 4 AFR2	5	0.71
F4.7 Loc 4 AFR3	5	0.89
F4.7 Loc 4 AFR4	5	1.23
F4.7 Loc 5 AFR1	5	0.33
F4.7 Loc 5 AFR2	5	0.54

Table 13 – Data for Figure 5.2

Measurement	Depth (m)	Pressure (m H_2O)	Points	Stdev (m H2O)
F5.2 C1 P1	0.25	0.07	300	0.02
F5.2 C1 P2	0.75	0.56	300	0.02
F5.2 C1 P3	0.78	0.60	300	0.02
F5.2 C1 P4	1.28	1.12	300	0.04
F5.2 C1 P5	1.31	1.14	300	0.02
F5.2 C1 P6	1.81	1.72	300	0.03
F5.2 C1 P7	1.84	1.76	220	0.05
F5.2 C1 P8	2.34	2.43	220	0.02
F5.2 C1 P9	2.37	2.28	310	0.04
F5.2 C1 P10	2.87	3.10	310	0.01
F5.2 C2 P1	0.25	0.01	300	0.03
F5.2 C2 P2	0.75	0.40	300	0.01
F5.2 C2 P3	0.78	0.44	300	0.03
F5.2 C2 P4	1.28	0.93	300	0.04
F5.2 C2 P5	1.31	0.99	300	0.03
F5.2 C2 P6	1.81	1.49	300	0.04
F5.2 C2 P7	1.84	1.52	300	0.05

F5.2 C2 P8	2.34	2.11	300	0.03
F5.2 C2 P9	2.37	2.09	300	0.06
F5.2 C2 P10	2.87	2.77	300	0.03
F5.2 C3 P1	0.25	0.02	250	0.05
F5.2 C3 P2	0.75	0.41	250	0.01
F5.2 C3 P3	0.78	0.47	300	0.05
F5.2 C3 P4	1.28	0.95	300	0.05
F5.2 C3 P5	1.31	1.01	300	0.05
F5.2 C3 P6	1.81	1.51	300	0.06
F5.2 C3 P7	1.84	1.56	300	0.07
F5.2 C3 P8	2.34	2.17	300	0.05
F5.2 C3 P9	2.37	2.13	300	0.07
F5.2 C3 P10	2.87	2.83	300	0.03
F5.2 C4 P1	0.25	0.01	265	0.02
F5.2 C4 P2	0.75	0.42	265	0.00
F5.2 C4 P3	0.78	0.48	250	0.01
F5.2 C4 P4	1.28	0.96	250	0.03
F5.2 C4 P5	1.31	1.01	300	0.02
F5.2 C4 P6	1.81	1.52	300	0.04
F5.2 C4 P7	1.84	1.54	300	0.04
F5.2 C4 P8	2.34	2.16	300	0.01
F5.2 C4 P9	2.37	2.12	260	0.05
F5.2 C4 P10	2.87	2.81	260	0.01

Table 14 – Data for Figure 5.12

Measurement	Depth (m)	Pressure (m H_2O)	Points	Stdev (m H2O)
F5.12 C1 P1	1.25	0.35	260	0.005
F5.12 C1 P2	2.25	0.81	260	0.002
F5.12 C1 P3	3.25	1.65	105	0.005
F5.12 C1 P4	0.74	0.18	105	0.003
F5.12 C1 P5	1.74	0.56	220	0.023

F5.12 C1 P6	2.74	1.25	220	0.019
F5.12 C2 P1	1.25	0.44	250	0.005
F5.12 C2 P2	2.25	1.02	250	0.004
F5.12 C2 P3	3.25	1.72	155	0.013
F5.12 C2 P4	0.74	0.24	155	0.008
F5.12 C2 P5	1.74	0.68	120	0.016
F5.12 C2 P6	2.74	1.34	120	0.013
F5.12 C3 P1	1.25	0.42	105	0.007
F5.12 C3 P2	2.25	1.02	105	0.004
F5.12 C3 P3	3.25	1.82	150	0.007
F5.12 C3 P4	0.74	0.22	150	0.003
F5.12 C3 P5	1.74	0.67	120	0.016
F5.12 C3 P6	2.74	1.40	120	0.016
F5.12 C4 P1	1.25	0.38	180	0.010
F5.12 C4 P2	2.25	0.91	180	0.008
F5.12 C4 P3	3.25	1.65	110	0.010
F5.12 C4 P4	0.74	0.20	110	0.003
F5.12 C4 P5	1.74	0.59	80	0.012
F5.12 C4 P6	2.74	1.23	80	0.009

Table 15 – Data for Figure 5.15

Measurement	Depth (m)	Pressure (m H_2O)	Points	Stdev (m H2O)
F5.15 C1 P1	1.5	1.5	180	0.026
F5.15 C1 P2	2.1	2.2	180	0.020
F5.15 C1 P3	2.5	2.7	240	0.048
F5.15 C1 P4	3.1	3.3	240	0.015
F5.15 C1 P5	3.5	3.8	240	0.056
F5.15 C1 P6	1.0	0.9	240	0.028
F5.15 C1 P7	1.6	1.6	120	0.045
F5.15 C1 P8	2.0	2.1	120	0.012
F5.15 C1 P9	1.2	1.1	120	0.020

F5.15 C1 P10	0.7	0.5	120	0.031

Table 16 – Data for Figure 5.17

Measurement	Depth (m)	Pressure (m H_2O)	Points	Stdev (m H2O)
F5.17 C1 P1	2.56	2.34	80	0.04
F5.17 C1 P2	2.05	1.82	80	0.02
F5.17 C1 P3	1.55	1.35	80	0.03
F5.17 C1 P4	0.99	0.78	80	0.09
F5.17 C1 P5	2.92	2.71	80	0.03
F5.17 C1 P6	2.41	2.19	80	0.02
F5.17 C1 P7	1.91	1.71	80	0.08
F5.17 C1 P8	1.35	1.18	80	0.03
F5.17 C1 P9	2.30	2.04	80	0.05
F5.17 C1 P10	1.79	1.53	80	0.13
F5.17 C1 P11	1.29	1.05	80	0.06
F5.17 C1 P12	0.73	0.56	80	0.75